VISCOUS STRATIFIED FLOW TOWARDS A LINE SINK

Thesis by

Robert Ching-yee Koh

In Partial Fulfillment of the Requirements

for the Degree of

Doctor of Philosophy

California Institute of Technology

Pasadena, California

1964

ACKNOWLEDGEMENTS

The writer would like to express his gratitude for the guidance and advice offered by Professor Norman H. Brooks throughout the course of this investigation.

He is also indebted to Professors Donald R. F. Harleman and Vito A. Vanoni for valuable criticisms of many aspects of the research.

The financial assistance received from the following fellowships by the writer during his period of graduate study is gratefully acknowledged: 1961-62 (academic year), Corning Glass Works Foundation Fellowship in Engineering; 1962 (summer), Woodrow Wilson Fellowship; 1963-64 (first term), Gillette Paper-Mate Fellowship in Engineering.

The laboratory investigation was supported from September, 1962 through 1963 by Research Grant WP-00428 from the National Institute of Health, United States Public Health Service. The experiments were carried out in the William M. Keck Laboratory of Hydraulics and Water Resources at the California Institute of Technology.

For their invaluable help in the design and construction of the laboratory equipment, the writer wishes to thank Mr. Elton F. Daly and Mr. Robert L. Greenway.

For his help both in the laboratory and in analysing the data, the writer wishes to express his gratitude to Mr. Loh-nien Fan.

ABSTRACT

A theoretical and experimental investigation has been made for the problem of two-dimensional viscous, incompressible, steady, slightly-stratified flow towards a line sink. The analytical solution was obtained from the Navier Stokes equations, the continuity equation, and the diffusion equation by first making a boundary-layer-type assumption and then using a small perturbation technique based on a perturbation parameter proportional to the sink strength q. The effects of the viscosity, the diffusivity, and the gravity have been included while the inertia effect is neglected in the zeroth order solution. The solution indicates that there exists a withdrawal layer which grows in thickness with the distance x from the sink at the rate $x^{1/3}$ and that the velocity distributions $u(y)$ are similar from one station x to another.

Twenty-five tank experiments were performed using water stratified by means of either salt or temperature. Detailed measurements of the velocity field were made by means of photographs of vertical dye lines. The experiments verify the shape of the velocity profiles as well as their similarity in x as predicted by the theory.

Except for scale, this is very similar to the problem of selective withdrawal from a reservoir.

TABLE OF CONTENTS

Chapter		Page
1.	INTRODUCTION	1
	1-1 Selective Withdrawal	1
	1-2 An Important Property of Stratified Flow	2
	1-3 Two-Layer Systems	6
	1-4 Continuously Stratified Systems	6
	1-5 Purpose and Scope of the Present Investigation	13
2.	ANALYTICAL CONSIDERATIONS	15
	2-1 The Basic Equations	15
	2-2 A Boundary-Layer-Type Assumption and the Reduced Equations	22
	2-3 Normalized Equations	27
	2-4 The Boundary Conditions	29
	2-5 A Perturbation Scheme	30
	2-6 Solution to the Zeroth Order Equations	33
	2-7 The Density Field	40
	2-8 The Withdrawal Layer	45
	2-9 Summary	50
3.	APPARATUS AND PROCEDURE	51
	3-1 General Description of the Procedure	51
	3-2 The Experimental Reservoir	54
	3-3 The Conductivity Probes and the Sanborn Recorder	54
	3-4 Dye Particles	58
	3-5 Photography	60
	3-6 Filling the Reservoir	60
	3-7 Measurements of Conductivity Profiles and Temperature Profiles	66
	3-8 Measurement of Discharge	67
	3-9 Measurement of Velocity Profiles	70
	3-10 Measurement of Time between Pictures	71
4.	EXPERIMENTAL RESULTS	72
	4-1 Basic Data for the Experiments	72

Chapter Page

4-2 Measurement and Calculation of Data from Velocity Profiles 76

4-3 Similarity in the Velocity Profiles 78

4-4 An Extension of the Zeroth Order Solution 109

4-5 The Experimental Parameter $\chi = \alpha/\alpha_0$ 111

4-6 Summary 111

5. DISCUSSION OF RESULTS 119

5-1 Discussion of the Finite Length and Depth of the Experimental Tank 119

5-2 The Effect of the Finite Width; the Sidewall Effect 121

5-3 The Effect of the Transient 129

5-4 Summary of Experimental Errors 131

5-5 Discussion of the Validity of the Theoretical Solutions 131

5-6 The General Problem of Selective Withdrawal 133

5-7 Discussion of the Role of Diffusion in the Theoretical Solution 134

5-8 Discussion of the Practical Applicability of the Solution 136

6. SUMMARY OF CONCLUSIONS 137

APPENDIX. Summary of Notations 139

REFERENCES 142

LIST OF FIGURES

Fig. No.	Title	Page No.
1-1	The phenomenon of withdrawal. (A) Withdrawal from full depth in a homogeneous fluid (B) Selective withdrawal in a stratified fluid	3
1-2	Definition sketch.	4
1-3	The forward wake due to a slowly moving two-dimensional object in a stably stratified fluid.	4
1-4	Yih's solution for F = 0.35. Lines shown are streamlines (from Yih (6)).	9
1-5	Kao's method of solution (Kao (7)).	9
2-1	Viscous stratified flow towards a line sink: the withdrawal layer.	24
2-2	The non-dimensional stream function and its derivatives.	44
2-3	The non-dimensional density function and its first derivative.	49
3-1	Typical time lapse photographs of dye lines. (Run N-50-0.5) (A) at time $t = t_o$ (B) at time $t \cong t_o + 55$ sec (C) at time $t \cong t_o + 110$ sec	53
3-2A	Schematic drawing of the experimental reservoir.	55
3-2B	Photograph of the reservoir used in the experiments.	56
3-3	The conductivity probes.	57
3-4	The bridge circuit used in conjunction with the Sanborn recorder for the measurement of the conductivity.	59
3-5	The photographic setup.	61
3-6	The camera and camera stand in use.	62
3-7	Filling the reservoir in layers to produce continuous density stratifications.	64

Fig. No.	Title	Page No.
3-8	The filling device.	65
3-9	Typical measured density profile.	68
3-10	Measuring the conductivity profile with the conductivity probe and the Sanborn recorder.	69
4-1	Definition sketch.	77
4-2	Complete velocity profiles at various stations for run N-12-4.4.	80
4-3	Complete velocity profiles at various stations for run N-25-5.	81
4-4	Complete velocity profiles at various stations for run N-50-3.	82
4-5	Complete velocity profiles at various stations for run T-10-5.	83
4-6	Velocity profiles at various stations for run N-8-1.7.	84
4-7	Velocity profiles at various stations for run N-8-3.5.	85
4-8	Velocity profiles at various stations for run N-8-11.7.	86
4-9	Velocity profiles at various stations for run N-12-0.15.	87
4-10	Velocity profiles at various stations for run N-12-0.3.	88
4-11	Velocity profiles at various stations for run N-12-0.9.	89
4-12	Velocity profiles at various stations for run N-12-2.3.	90
4-13	Velocity profiles at various stations for run N-12-4.4.	91
4-14	Velocity profiles at various stations for run N-12-10.	92
4-15	Velocity profiles at various stations for run N-25-0.04.	93
4-16	Velocity profiles at various stations for run N-25-0.2.	94
4-17	Velocity profiles at various stations for run N-25-0.5.	95
4-18	Velocity profiles at various stations for run N-25-1.5.	96
4-19	Velocity profiles at various stations for run N-25-5.	97
4-20	Velocity profiles at various stations for run N-25-9.	98

Fig. No.	Title	Page No.
4-21	Velocity profiles at various stations for run N-50-0.13	99
4-22	Velocity profiles at various stations for run N-50-0.5.	100
4-23	Velocity profiles at various stations for run N-50-1.	101
4-24	Velocity profiles at various stations for run N-50-3.	102
4-25	Velocity profiles at various stations for run N-50-6.	103
4-26	Velocity profiles at various stations for run N-50-11.7.	104
4-27	Velocity profiles at various stations for run T-16-0.6.	105
4-28	Velocity profiles at various stations for run T-18-2.	106
4-29	Velocity profiles at various stations for run T-21-4.	107
4-30	Velocity profiles at various stations for run T-10-5.	108
4-31	Variation of $\chi=\frac{\alpha}{\alpha_o}$ with $q_f/D\alpha_o x^{2/3}$ for the N-8-series runs.	112
4-32	Variation of $\chi=\frac{\alpha}{\alpha_o}$ with $q_f/D\alpha_o x^{2/3}$ for the N-12-series runs.	113
4-33	Variation of $\chi=\frac{\alpha}{\alpha_o}$ with $q_f/D\alpha_o x^{2/3}$ for the N-25-series runs.	114
4-34	Variation of $\chi=\frac{\alpha}{\alpha_o}$ with $q_f/D\alpha_o x^{2/3}$ for the N-50-series runs.	115
4-35	Variation of $\chi=\frac{\alpha}{\alpha_o}$ with $q_f/D\alpha_o x^{2/3}$ for the T-series runs.	116
4-36	Variation of $\chi=\frac{\alpha}{\alpha_o}$ with $q_f/D\alpha_o x^{2/3}$.	117
5-1	Typical variation of local unit forward discharge q_f with x.	122
5-2	Velocity distribution in the z-direction for the investigation of the sidewall effect.	124
5-3	Photograph taken from atop the tank showing the dye lines for the investigation of the side wall effect.	125
5-4	Comparison of $\partial^2 u/\partial y^2$ with $\partial^2 u/\partial z^2$ to demonstrate that sidewall effects are negligible.	127

Fig. No.	Title	Page No.
5-5	Comparison of first and second sets of dye line measurements to demonstrate that the transient has subsided.	130

LIST OF TABLES

Table No.	Title	Page No.
2-1	The Non-dimensional Stream Function $f_0(\zeta)$ and its Derivatives. $f_0(\zeta) = \psi(x,y)/q$ $\zeta = \frac{\alpha_0 y}{x^{1/3}}$, $\alpha_0 = \left(\frac{\epsilon q}{\mathcal{D}\nu}\right)^{1/6}$	41
2-2	The Non-dimensional Density Function $h_0(\zeta)$ and its Derivative. $h_0(\zeta) = \xi^{1/3}\sigma(\xi,\eta) = \frac{S}{\rho_0 \epsilon}\frac{\mathcal{D}}{q}\alpha_0^2 x^{1/3}$ $\zeta = \frac{\alpha_0 y}{x^{1/3}}$, $\alpha_0 = \left(\frac{\epsilon q}{\mathcal{D}\nu}\right)^{1/6}$	46
4-1	Summary of Basic Experimental Parameters for Each Run.	73

CHAPTER 1

INTRODUCTION

In large bodies of water such as lakes or oceans, the density of the water often varies slightly from one level to another. This density variation can be caused by seasonal changes in atmospheric temperature and solar radiation, or the intrusion of saline or muddy water into fresh water reservoirs. Such density stratifications also exist in the atmosphere.

Stratified flow may be defined as the flow of fluid with a density stratification. The most interesting cases of stratified flow are those where the stratification plays a primary role in the mechanics of flow. It will be seen presently in section 1-2 that gravity plays an essential role in making such stratified flows much different from the flow of homogeneous fluids.

Interesting cases of stratified flow are to be found in oceanography, hydrology, and meteorology. Some common examples are the motion of cold and warm fronts, smog layers, and ocean currents. Another example is the phenomenon known as selective withdrawal. It is the main topic in this thesis and is explained in the following sections.

1-1 Selective Withdrawal

Consider a reservoir filled with water whose density ρ changes with depth (for example, because of a temperature stratification) with an outlet through the dam at the depth a below the water surface, as shown in figure 1-1, discharging at the rate, q. If the water were not stratified, the equations of motion of incompressible homogeneous fluids would show that the discharged water would originate from throughout the entire depth of the reservoir and the velocity distribution a

fair distance upstream of the outlet would be as illustrated in figure 1-1A. If the water is stratified, however, it is observed both in the laboratory and in the field that for a small enough value of q, the discharge originates only from a layer of limited depth at the level of withdrawal. The velocity distribution at some distance upstream might be as illustrated in figure 1-1B. Since certain properties of the water such as dissolved oxygen, temperature, dissolved salts, and turbidity vary with depth, it is therefore possible by choice of outlet depth to select water of the desired quality, hence the term selective withdrawal. For example, an outlet near the water surface would generally withdraw water with higher temperature, higher dissolved oxygen content, lower dissolved salts and lower turbidity than an outlet near the bottom in the same reservoir. The technique of selective withdrawal affords an easy means of controlling the quality of water.

1-2 An Important Property of Stratified Flow

Consider an incompressible stratified fluid such as water with a slight density gradient caused by temperature, salinity, or suspended material. Assume further that the density decreases with elevation and hence that the stratification is stable. (Indeed if the fluid is unstably stratified, there would be overturning which would eventually lead to a stably stratified fluid.) For such a fluid in an external force field such as the earth's gravitational field, only very limited vertical motion is expected, for reasons discussed below.

Consider a fluid parcel of volume V and density $\rho(y_0)$ at the level y_0 in the environment of a stably stratified fluid with density distribution $\rho(y)$ as illustrated in figure 1-2. For this parcel to move to a new level y_1 an amount of work

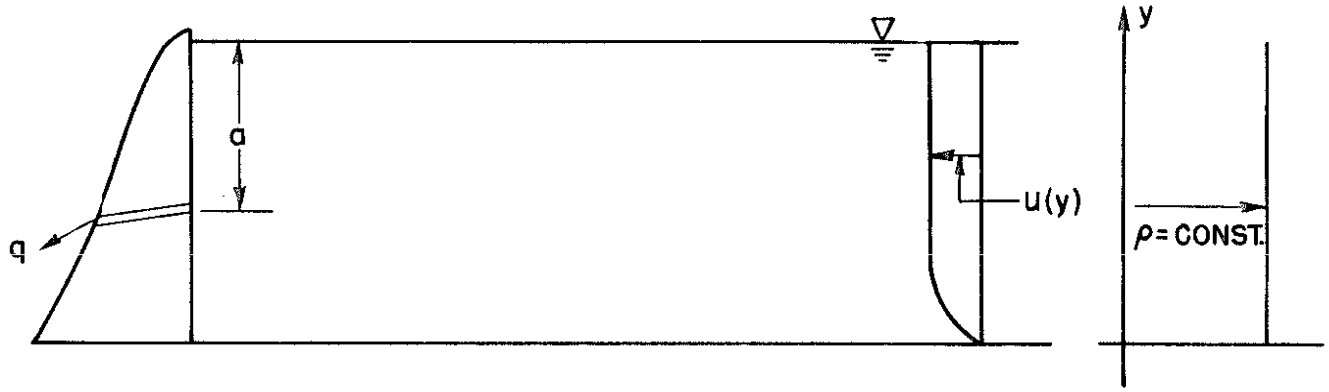

(A) Withdrawal from full depth in a homogeneous fluid.

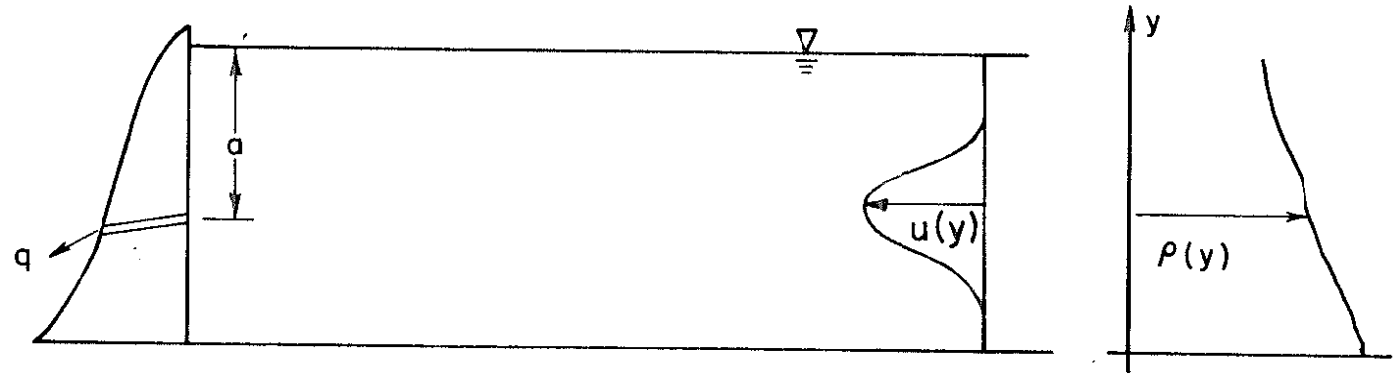

(B) Selective withdrawal in a stratified fluid.

Figure 1-1 The phenomenon of withdrawal.

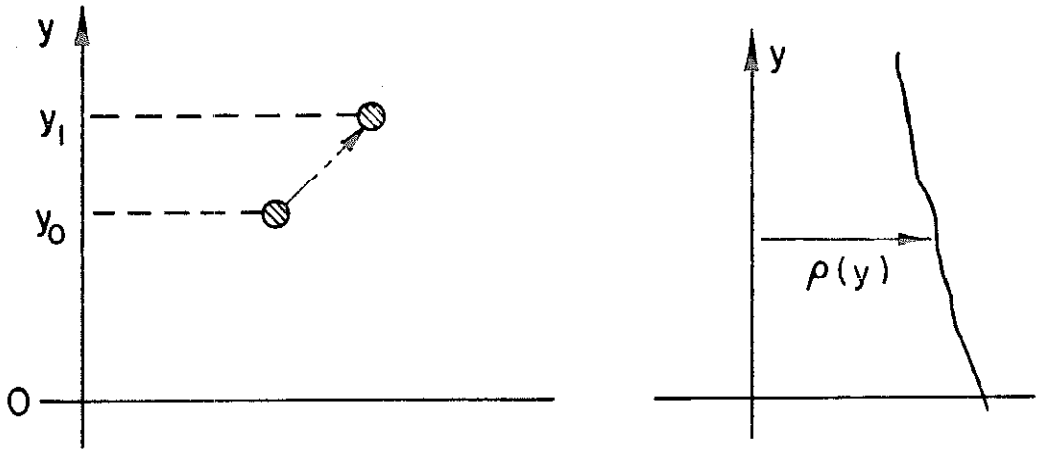

Figure 1-2

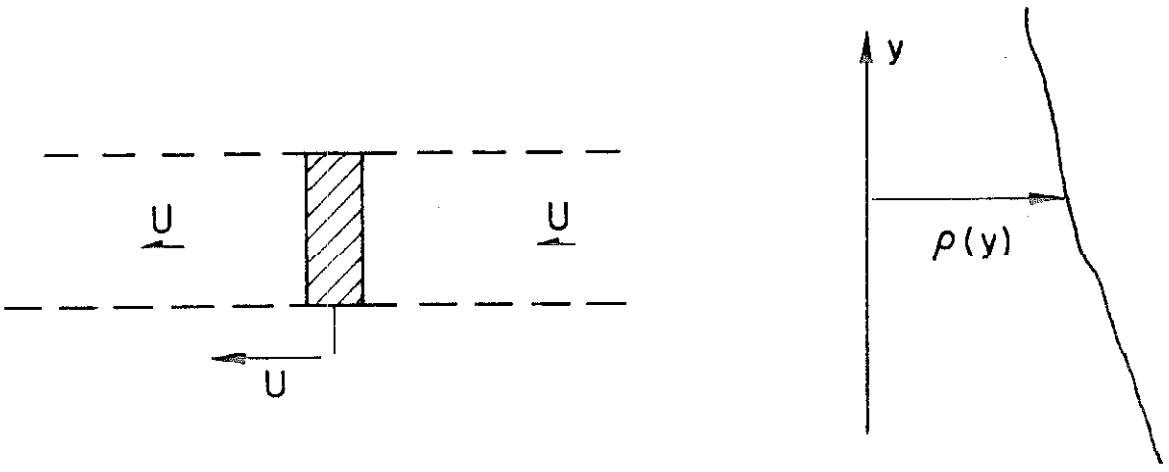

Figure 1-3 [illegible]

$$W = V \int_{y_0}^{y_1} [\rho(y_0) - \rho(y)]\, g\, dy$$

must be done on the fluid parcel. Note that this work is always positive regardless of whether $y_1 > y_0$ or $y_1 < y_0$ provided that the stratification is stable, i.e. $\rho(y)$ is monotonically non-increasing with y ($\frac{d\rho}{dy} \leq 0$) . Hence in order for two fluid parcels each of volume V at levels y_0 and y_1 to exchange positions, a total amount of work $2W$ must be performed on the system. In other words, any vertical motion requires an addition of energy no matter how slowly the motion is carried out. For a homogeneous fluid, ρ is a constant and this work would, of course, be zero and a fluid parcel may move from one position to another quasi-statically within the fluid without doing any work. Therefore, the existence of a density stratification together with a gravity field tends to inhibit vertical motion in the fluid.

Certain strange phenomena occur because of this stable stratification. For example, in two-dimensional flow, an object moving slowly in a stably stratified fluid acts somewhat as a piston. Not only is there a wake behind the object, the fluid in front of it also moves slowly forward. In the extreme case illustrated in figure 1-3, all the fluid in the horizontal layer within the two dotted lines moves forward at the same speed as the object. The explanation is that if the fluid did not move as shown, then the fluid particles immediately infront of the object must move around the object and this implies vertical motion which is inhibited by stratification. At higher speeds, when the inertia effect overcomes this gravity effect, the fluid would be able to move around the object.

Selective withdrawal is another example of such strange phenomena. The fluid at a large distance vertically from the outlet does not flow because of the resistance to vertical motion due to stable stratification.

1-3 Two-Layer Systems

The simplest example of a stably stratified fluid is the two-layer system: a layer of lighter fluid on top of a slightly heavier one. Typical examples are fresh water on top of sea water or oil above water. One of the first attempts to perform systematic though qualitative experiments to study the flow of stratified fluid was made by Bell (1) in the early 1940's . He used distinct layers of fluids of different densities. Since then various special cases of selective withdrawal and other problems in stratified flow, such as flow over obstacles, have been solved for the two-layer case. These are summarized and explained in Harleman (2) and Long (3). It should be noted that in all the selective withdrawal problems solved heretofore, inviscid flow was assumed.

1-4 Continuously Stratified Systems

Physically, it is more reasonable to have a continuously stratified body of water than one with a sharp interface separating two distinct layers since in most cases, diffusion or heat conduction would smooth out any sharp density variations.

For two-dimensional, inviscid, steady, incompressible,continuously stratified flow, Long (4) has derived a first integral to the equations of motion

$$\nabla^2\psi + \frac{1}{\rho}\frac{d\rho}{d\psi}\left[\frac{\left(\frac{\partial\psi}{\partial x}\right)^2+\left(\frac{\partial\psi}{\partial y}\right)^2}{2} + gy\right] = H(\psi) \,, \tag{1-1}$$

where ψ = stream function,

ρ = density,

g = gravitational acceleration,

x = horizontal rectangular coordinate,

y = vertical rectangular coordinate,

∇^2 = Laplacian operator,

and H = an arbitrary function of the stream function.

It is seen that the terms $\left(\frac{\partial\psi}{\partial x}\right)^2+\left(\frac{\partial\psi}{\partial y}\right)^2$ are non-linear and would render the solution to the equation difficult. By a transformation discovered by Yih (5)

$$\sqrt{\rho_o}\,\psi' = \int_o^{\psi} \sqrt{\rho}\, d\psi \,, \tag{1-2}$$

where ρ_o is a characteristic density, Long's equation may be simplified to

$$\nabla^2\psi' + gy\frac{d\rho}{d\psi'} = H_1(\psi') \,. \tag{1-3}$$

Of course, equation 1-3 may still be non-linear since $\frac{d\rho}{d\psi'}$ and $H_1(\psi')$ may be non-linear. The transformed stream function ψ' is called, by Yih, the stream function of an associated flow.

Assuming further that the density is linearly distributed far

upstream:

$$\rho = \rho_0 - \epsilon \rho_0 y \quad , \tag{1-4}$$

where ρ_0 and ϵ are constants and assuming that far upstream, the velocity U is entirely in the horizontal direction and is given by the relation

$$\rho U^2 = A^2 = \text{constant} \quad , \tag{1-5}$$

Yih (6) solved the problem of inviscid, incompressible, steady, linearly stratified, two-dimensional flow towards a line sink at the corner as illustrated in figure 1-4. Note that the assumption on the upstream velocity distribution in equation 1-5 means an essentially constant velocity distribution with respect to depth for the case when the density is nearly constant, i.e. small ϵ . A Froude number F is defined as

$$F = \frac{A}{d\sqrt{g\epsilon\rho_0}} = \frac{\sqrt{\rho}\, U}{d\sqrt{\epsilon g \rho_0}} \quad , \tag{1-6}$$

where d = depth.

The solution obtained exhibits an eddy in the corner (see figure 1-4) which grows upstream as the Froude number decreases toward $1/\pi$. For $F \leq 1/\pi$, the solution ceases to be applicable because the eddy would extend all the way to upstream infinity, and thus the assumption in equation 1-5 breaks down.

Kao (7) extended Yih's solution to be applicable to cases where

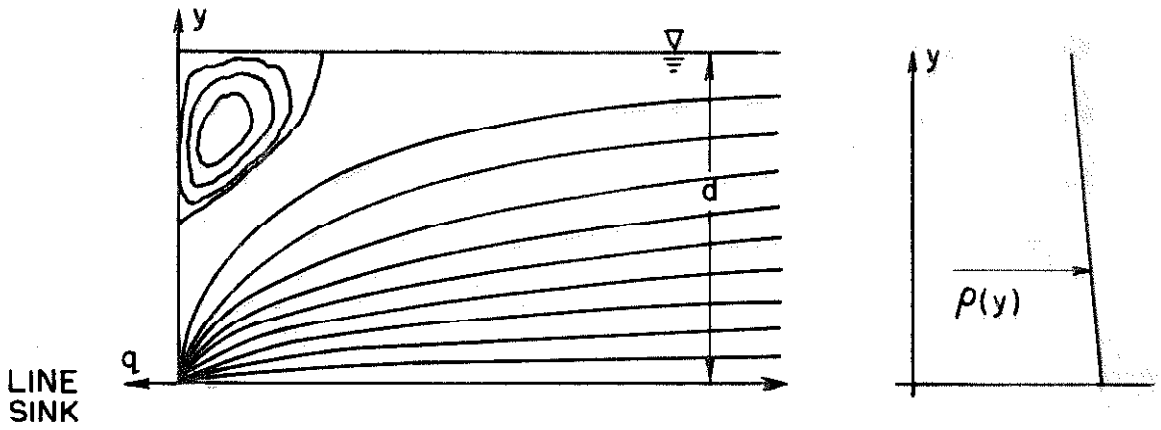

Figure 1-4 Yih's solution for F = 0.35 .
Lines shown are streamlines (from Yih (6)).

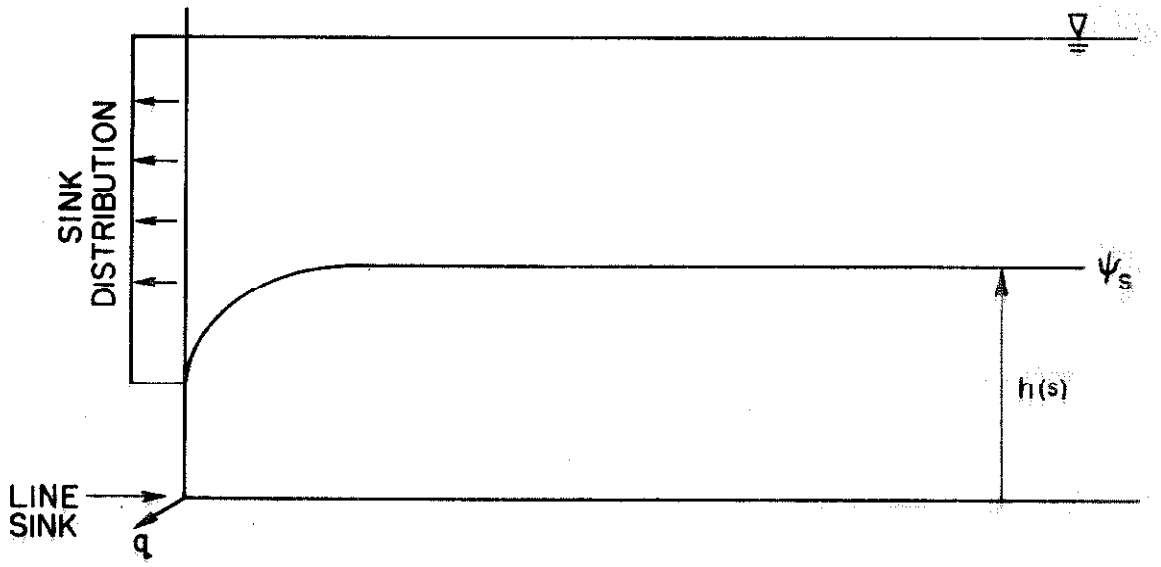

Figure 1-5 Kao's method of solution.

Froude number is less than $1/\pi$ in the following way. He assumed a sink distribution on the vertical wall in addition to the line sink at the corner and obtained the solution to the problem with both the line sink and the sink distribution. There will then be a dividing streamline ψ_s above which the flow leaves by way of the distributed sinks and below which the fluid comes out of the line sink at the corner. He required the sink distribution to be such that on the dividing streamline ψ_s, the Bernoulli equation is satisfied

$$\frac{u^2(s)}{2} + g h(s) + \frac{p(s)}{\rho} = \text{constant} \ , \tag{1-7}$$

where

s = distance along the streamline,

u = magnitude of velocity along the streamline,

h = vertical height of the streamline,

and $p(s)$, the pressure along the streamline, is prescribed to be equal to the hydrostatic pressure distribution as if the portion of the fluid above the dividing streamline is stagnant. That is,

$$p(s) = \int_{h(s)}^{d} \rho(y)\, g\, dy \cong (d-h)\rho_0 g \ . \tag{1-8}$$

All the assumptions made by Yih have also been made. The solution was obtained numerically by trial and error. After the solution is obtained, the flow in the upper portion of the dividing streamline may simply be replaced by stagnant fluid and a vortex sheet at the dividing streamline. The conclusion reached by Kao is that the Froude number is a constant equal to 0.345. That is

$$F = \frac{A}{h_o \sqrt{g \epsilon \rho_o}} = 0.345 \,, \tag{1-9}$$

where h_o is the value of h(s) infinitely far from the sink. Recalling the definition of A, in equation 1-5, and letting q = unit discharge, equation 1-9 may be rewritten for small density gradients

$$F = \frac{\sqrt{\rho}\, U}{h_o \sqrt{g \epsilon \rho_o}} \cong \frac{q}{h_o^2 \sqrt{g \epsilon}} \,. \tag{1-10}$$

Thus given the discharge q and the density gradient ϵ, the thickness of the flowing layer h_o may be calculated by the formula

$$h_o^2 = \frac{q}{(0.345)\sqrt{g \epsilon}} \,. \tag{1-11}$$

Debler (8) performed experiments in an attempt to verify Yih's results. The working portion of his tank was 8 feet long, 1/2 foot wide, and 2 feet deep. By using alternately-colored layers of water, he was able to observe the separation of the flow into a flowing layer and a stagnant layer above. A total of eighteen experiments were performed. The values of the density gradient ϵ used were approximately $\epsilon = 0.00015\ \text{cm}^{-1}$, $0.0003\ \text{cm}^{-1}$, and $0.0009\ \text{cm}^{-1}$. In three of these eighteen experiments, the flowing layer extended all the way to the water surface, and hence there was no selective withdrawal. The values of the Froude number F as defined by equation 1-10 for the remaining runs varied from 0.187 to 0.274 with an arithmetic mean of

0.236.

Gariel (9) also performed experiments in the withdrawal from a linearly stratified fluid. His tank was 6 meters long, 0.3 meter wide, and 0.6 meter deep. He prepared his linear stratification by filling his tank with two layers of water of different densities using salt water and fresh water and agitating the system suitably. After several such agitations, he claimed a linear stratification was very accurately realized. The values of the density gradient used varied from approximately $\epsilon = .0002 \text{cm}^{-1}$ to approximately $\epsilon = 0.005\ \text{cm}^{-1}$.

Withdrawal from this medium was through a slit 2 mm high and 50 mm long at the end of a withdrawal box which consisted of two vertical glass plates 50 mm apart and 1.2 m long placed in the tank. The slot was not at the corner as in Debler's experiments, but at about mid-depth.

For flow observation, small dye particles were dropped into the flowing region between the glass plates. He observed that there was a principal current flowing towards the sink bounded by two small retrograde currents. He also observed that the thickness of the currents increased gradually upstream. No detailed measurements were made in the flow field and the slight variation of current thickness with distance and the retrograde currents were considered secondary by him. The net result of his experiments is the empirically obtained formula

$$h_o \epsilon = K(\epsilon) \left[\frac{\epsilon^2 q}{\sqrt{g\epsilon}} \right]^{0.27} , \qquad (1\text{-}12)$$

where h_o is the thickness of the principal current measured 1.5 m

upstream of the slit and $K(\epsilon)$ is a function of ϵ . He concluded that because of this variation of $K(\epsilon)$ with ϵ , viscosity must play an important role though no attempt was made to investigate this variation. Note that according to equation 1-12, for a fixed density stratification ϵ , the thickness of flow h_0 is proportional to $q^{0.27}$. This, of course, is contradictory to the result by Kao that

$$\frac{q}{h_0^2\sqrt{g\epsilon}} = \text{constant} \quad , \tag{1-13}$$

which implies that h_0 is proportional to $q^{0.5}$ for fixed ϵ . The reason for this apparent discrepancy is rather clear. Kao's solution is for the inviscid case while for Gariel's experiments, as he pointed out himself, the viscous resistance played a primary role.

1-5 Purpose and Scope of the Present Investigation

All the previous analytical work on selective withdrawal has been for the inviscid case. For linearly stratified fluids, the results of Yih and Kao have been the only analytical solutions on selective withdrawal. Kao's solution predicts the value 0.345 for the densimetric Froude number based on the flowing depth as shown in equation 1-9. On the other hand, experimental work by Debler and Gariel seem both contradictory and inconclusive. Moreover, limited amounts of field measurement (10) indicate that densimetric Froude numbers are only about one-tenth of the value 0.345. It is obvious, therefore, that more work on this problem, both analytical and experimental, needs to be done.

In the present study, the problem of selective withdrawal at

very low Reynolds number will be investigated. In this case, viscous resistance, heat conduction, and molecular diffusion play primary roles. The present analysis together with the results of Yih and Kao form a bracket of the two extreme cases, between which it is hoped real cases will fall.

Long (11) was the first to study the motion of stratified fluids where viscosity and diffusivity play primary roles. He investigated the problems of the creeping boundary layer flow of a linearly stratified fluid over and behind a flat plate. Besides the Prandtl boundary layer assumptions, he also neglected all the remaining non-linear terms.

A similar theoretical approach based on the same assumptions is used here to solve the problem of the creeping flow towards a hydrodynamic sink. The deviation from the idealized case is investigated. Experiments were performed in an attempt to supplement the analysis. In these experiments, detailed measurements of the flow field were made. These are presented in detail in the next three chapters.

CHAPTER 2

ANALYTICAL CONSIDERATIONS

In this chapter, an analytical solution for the viscous stratified flow towards a line sink is presented. Based on three suitable assumptions which will be described in the next section, the basic equations are first derived. Then a boundary-layer-type assumption is made and the equations simplified accordingly. Since, as described at the end of Chapter 1, the limiting solution for very low flow rates is sought, a perturbation analysis based on a perturbation parameter proportional to the flow rate is carried out and the zeroth order solution obtained.

2-1 The Basic Equations

The following three assumptions will be made immediately:

i) The coriolis effects are negligible.

ii) The amount of stratification is small. This means that the relative change of density within the relevant flow field is much less than unity. This is almost always true in prototype examples.

iii) The parent fluid (fluid if there were no stratification) is incompressible. In other words if there were no stratification, then the motion of the parent fluid could be described as ordinary incompressible flow. This assumption is also very good in most practical cases.

With these three assumptions in mind, the basic equations will now be obtained.

i) Continuity Equation

The continuity equation for pure fluid flow is

$$\nabla \cdot (\rho \vec{u}) + \frac{\partial \rho}{\partial t} = 0 \quad , \tag{2-1}$$

where $\vec{u}$ = velocity vector,

ρ - density,

t = time,

$\nabla \cdot$ = divergence operator.

If the stratification is due to temperature variations alone, then equation 2-1 is the continuity equation for the flow. If, however, there is a foreign substance in the fluid such as dissolved salts in water, then there is the additional transfer of mass due to molecular diffusion of the salt through the water. If c is the concentration of the salt, then assuming Fick's Law of diffusion, the net efflux of mass from a closed fixed geometric surface S is

$$- \int_S (\mathcal{D} \nabla c) \cdot \vec{n} \, dS \quad ,$$

where $\mathcal{D}$ = diffusion coefficient,

$\vec{n}$ = unit outward normal to S ,

∇ = gradient operator,

and the integral is over the entire closed surface S . It is readily seen that a diffusion term must be added to the equation of continuity, yielding

$$\frac{\partial \rho}{\partial t} + \nabla \cdot (\rho \vec{u}) = \nabla \cdot [\mathcal{D} \nabla c] \quad . \tag{2-2}$$

This may be rewritten

$$\frac{d\rho}{dt} + \rho \nabla \cdot \vec{u} = \nabla \cdot [\mathcal{D} \nabla c] \,, \tag{2-3}$$

where $\frac{d}{dt} = \frac{\partial}{\partial t} + (\vec{u} \cdot \nabla)$ = material derivative.

ii) Equation of State

The equation of state for the flow of an ordinary incompressible fluid is, of course,

$$\rho = \text{constant.}$$

For a stratified fluid, one obviously no longer has the above simple relation. Instead, the continuity equation for the substance or agent causing the stratification and a relation between the concentration of this agent and the density must be considered. If salt or some other dissolved substance is the agent, and if c is its concentration, then conservation of mass gives

$$\frac{dc}{dt} = \nabla \cdot (\mathcal{D} \nabla c) \,. \tag{2-4}$$

Here, it has been assumed that the salt does not enter into any chemical reaction, that there are no sources or sinks of salt, and that the diffusion is Fickian.

If the stratification is due to a temperature variation and if T is the temperature, then it must obey the heat conduction equation

$$\frac{dT}{dt} = \nabla \cdot (K \nabla T) \,, \tag{2-5}$$

where

$$K = \frac{k}{c_p \rho} \quad , \tag{2-6}$$

k = Fourier heat conductivity,

c_p = specific heat.

Again, no sources and sinks of heat and Fourier's Law of heat conduction have been assumed.

Remembering the assumption of small density variations, it is reasonable to assume $K = \frac{k}{c_p \rho} \cong$ constant and $\mathcal{D} \cong$ constant. Equations 2-4 and 2-5 then become

$$\frac{dc}{dt} = \mathcal{D} \nabla^2 c \quad , \tag{2-7}$$

$$\frac{dT}{dt} = K \nabla^2 T \quad . \tag{2-8}$$

In order to tie these two equations in with equation 2-3, a relationship between the density ρ and the variables c and T must be obtained. Again based on the assumption of small density variations, it will be assumed that a linear relation exists between them.

$$\rho - \rho_o = \frac{\alpha}{T_o}(T - T_o) + \beta (c - c_o) \quad , \tag{2-9}$$

where ρ_o , T_o , c_o , α , and β are constants. At this point it will be assumed that the stratification is due either to the presence of salt or temperature variations, but not both. Thus for the case of the salt-induced stratified flow, equation 2-9 becomes

$$\rho - \rho_0 = \beta (C - C_0) \quad , \tag{2-10}$$

and equations 2-3 and 2-7 reduce to

$$\frac{d\rho}{dt} + \rho \nabla \cdot \vec{u} = \frac{\mathcal{D}}{\beta} \nabla^2 \rho \quad , \tag{2-11}$$

and

$$\frac{d\rho}{dt} = \mathcal{D} \nabla^2 \rho \tag{2-12}$$

respectively. These may be combined to give

$$\nabla \cdot \vec{u} = \left(\frac{1}{\beta} - 1 \right) \frac{1}{\rho} \frac{d\rho}{dt} \quad . \tag{2-13}$$

In the case of the temperature-induced stratified flow, equation 2-9 simplifies to

$$\rho - \rho_0 = \frac{\alpha}{T_0} (T - T_0) \quad , \tag{2-14}$$

and equations 2-3 and 2-8 reduce to

$$\frac{1}{\rho} \frac{d\rho}{dt} + \nabla \cdot \vec{u} = 0 \tag{2-15}$$

and

$$\frac{d\rho}{dt} = K \nabla^2 \rho \quad .$$

(2-16)

It is seen that equations 2-13 and 2-15 are both of the form

$$\nabla \cdot \vec{u} = \text{constant} \; \frac{1}{\rho} \frac{d\rho}{dt} \quad .$$

Since β defined in equation 2-9 is of order unity, so is the constant in the above equation. For steady state and in cartesian coordinates the equation may be written

$$\frac{\partial u}{\partial x} + \frac{\partial v}{\partial y} + \frac{\partial w}{\partial z} = \text{constant} \left\{ \frac{u}{\rho} \frac{\partial \rho}{\partial x} + \frac{v}{\rho} \frac{\partial \rho}{\partial y} + \frac{w}{\rho} \frac{\partial \rho}{\partial z} \right\} \quad .$$

If U is a characteristic velocity and L is a characteristic length it may be verified that the left hand side is of order

$$U/L$$

while the right hand side is of order

$$(U/L) \; \frac{\Delta\rho}{\rho} \quad ,$$

where $\frac{\Delta\rho}{\rho}$ is the total relative change in density in the relevant flow field. But this is assumed from the outset to be much less than unity. Thus

$$\frac{\left| \frac{1}{\rho} \frac{d\rho}{dt} \right|}{\left| \nabla \cdot \vec{u} \right|} \ll 1$$

for the steady state case. Hence the continuity equation may be

written in this case as

$$\nabla \cdot \vec{u} = 0 \tag{2-17}$$

This is the continuity equation which will be used in the next section.

iii) Momentum Equation

The general momentum equation may be written

$$\rho \frac{d\vec{u}}{dt} = -\nabla p + \nabla \cdot \tau + \rho \vec{G} \quad , \tag{2-18}$$

where $\vec{G}$ = external force field,

τ = stress tensor,

and p = pressure.

For a Newtonian fluid where there is a linear relationship between the stress and the rate of strain, the following relation is true:

$$\tau = \mu \left[\nabla \vec{u} + (\nabla \vec{u})^* \right] + \lambda I \, \nabla \cdot \vec{u} \quad , \tag{2-19}$$

where λ and μ are the two viscosity coefficients,

I is the identity tensor ,

and $*$ denotes the transpose.

For steady flow of a slightly stratified fluid, equation 2-17 is applicable and equation 2-19 reduces to

$$\tau = \mu \left[\nabla \vec{u} + (\nabla \vec{u})^* \right] \quad . \tag{2-20}$$

Substituting equation 2-20 into equation 2-18 gives

$$\rho \frac{d\vec{u}}{dt} = -\nabla p + \mu \nabla^2 \vec{u} + (\nabla \mu)\left[\nabla \vec{u} + (\nabla \vec{u})^*\right] + \rho \vec{G} \quad .$$

(2-21)

This is the momentum equation which will be used in the next section.

2-2 A Boundary-Layer-Type Assumption and the Reduced Equations

The basic equations for the steady flow of a slightly stratified incompressible fluid derived in the previous section, are as follows:

$$\nabla \cdot \vec{u} = 0 \quad ,$$

(2-17)

$$\rho \frac{d\vec{u}}{dt} = -\nabla p + \mu \nabla^2 \vec{u} + \rho \vec{G} + \left[\nabla \vec{u} + (\nabla \vec{u})^*\right](\nabla \mu) \quad ,$$

(2-21)

$$\frac{d\rho}{dt} = \mathcal{D} \nabla^2 \rho \quad .$$

(2-22)

The constant D in equation 2-22 is understood to be either the diffusion coefficient or the heat diffusivity depending on the agent causing the stratification. These equations will now be applied to the problem of two dimensional steady flow towards a sink, that is, to the problem of selective withdrawal. It will be assumed also that the fluid occupies all the right half plane but that even though the flow field is infinite in extent, the bulk of the motion occurs within a withdrawal layer (like a "boundary layer") whose thickness $\delta(x)$ is much smaller than the distance x from the sink. The flow field and the velocity distributions

might be as illustrated in figure 2-1. This is the same type of assumption that Prandtl used in obtaining his famous boundary layer equations. In the present case, equations 2-17, 2-21 and 2-22 reduce to

$$\frac{\partial u}{\partial x} + \frac{\partial v}{\partial y} = 0 \quad , \tag{2-23}$$

$$\rho\left(u\frac{\partial u}{\partial x} + v\frac{\partial u}{\partial y}\right) + \frac{\partial p}{\partial x} = \frac{\partial}{\partial y}\left(\mu\frac{\partial u}{\partial y}\right) \quad , \tag{2-24}$$

$$\frac{\partial p}{\partial y} = -\rho g \quad , \tag{2-25}$$

$$u\frac{\partial \rho}{\partial x} + v\frac{\partial \rho}{\partial y} = \mathcal{D}\frac{\partial^2 \rho}{\partial y^2} \quad , \tag{2-26}$$

where x, y are the rectangular coordinates

and u, v are the velocity components in the x and y directions respectively. Terms of the order $\frac{\delta(x)}{x}$ and higher have been neglected. For a more detailed account of the process of this simplification, see Schlichting (12).

Equation 2-23 implies the existence of a stream function ψ such that

$$u = \frac{\partial \psi}{\partial y} \quad , \qquad v = -\frac{\partial \psi}{\partial x} \quad . \tag{2-27}$$

Let perturbations of the density and viscosity be defined as

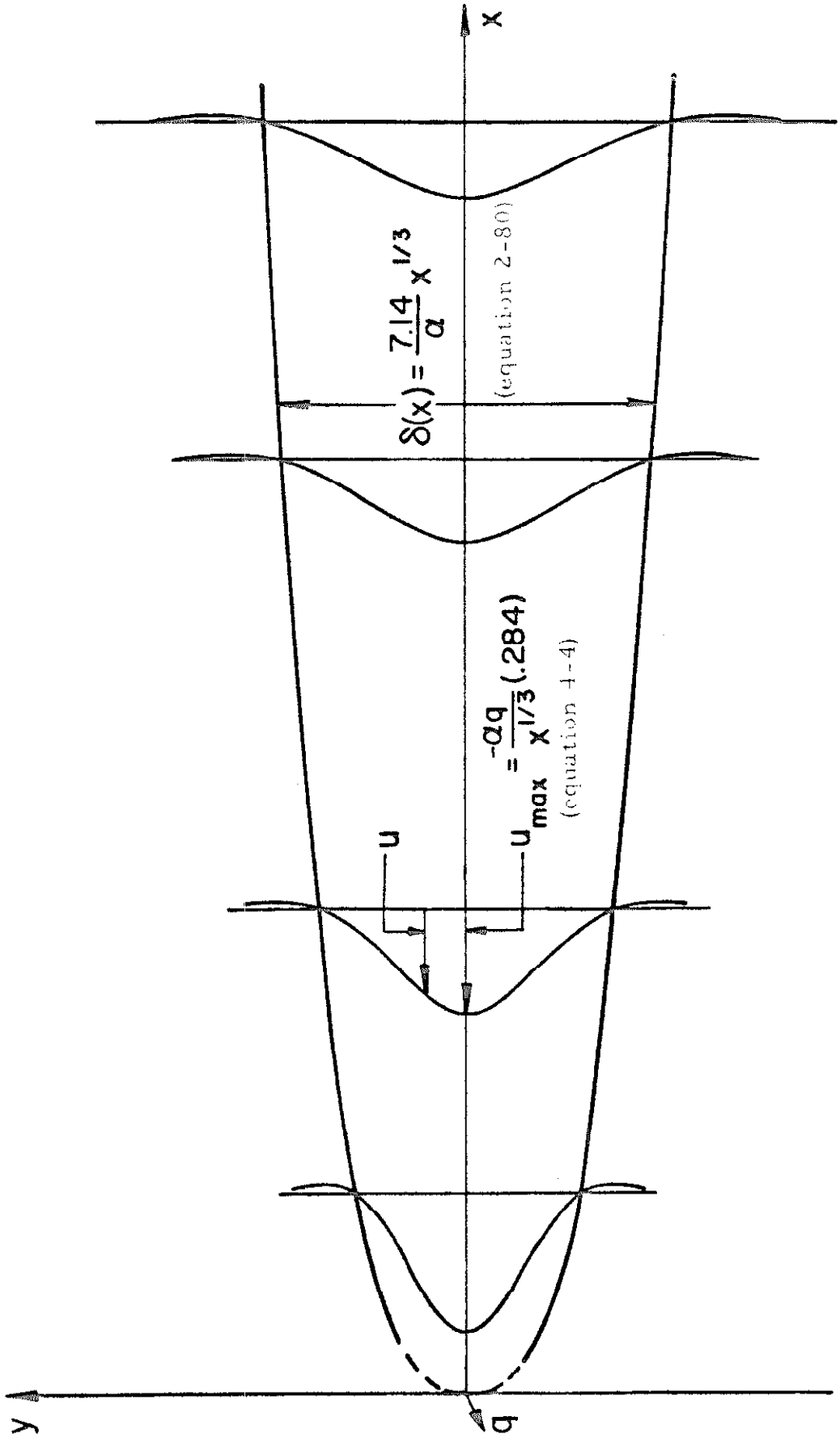

Figure 2-1 Viscous stratified flow towards a line sink: the withdrawal layer.

$$\rho(x,y) = \rho_0 + S_0(y) + S(x,y) \quad , \tag{2-28}$$

$$\mu(x,y) = \mu_0 + \theta_0(y) + \theta(x,y) \quad , \tag{2-29}$$

where ρ_0 = density of the undisturbed fluid at the sink level,

μ_0 = viscosity of the undisturbed fluid at the sink level,

$\rho_0 + S_0(y)$ = density distribution if there were no motion,

and $\mu_0 + \theta_0(y)$ = viscosity distribution if there were no motion.

Substituting equations 2-27, 2-28, and 2-29 into equations 2-24, 2-25, and 2-26 gives

$$(\rho_0 + S_0 + S)\left[\frac{\partial\psi}{\partial y}\frac{\partial^2\psi}{\partial x\partial y} - \frac{\partial\psi}{\partial x}\frac{\partial^2\psi}{\partial y^2}\right] = -\frac{\partial p}{\partial x} + \frac{\partial}{\partial y}\left[(\mu_0 + \theta_0 + \theta)\frac{\partial^2\psi}{\partial y^2}\right] , \tag{2-30}$$

$$\frac{\partial p}{\partial y} = -(\rho_0 + S_0 + S)g \quad , \tag{2-31}$$

$$\frac{\partial\psi}{\partial y}\frac{\partial S}{\partial x} - \frac{\partial\psi}{\partial x}\left[\frac{dS_0}{dy} + \frac{\partial S}{\partial y}\right] = D\left[\frac{d^2S_0}{dy^2} + \frac{\partial^2 S}{\partial y^2}\right] . \tag{2-32}$$

The pressure terms may be eliminated between equations 2-30 and 2-31 by cross differentiation. This gives

$$g\frac{\partial S}{\partial x} = \frac{\partial}{\partial y}\left\{(\rho_0+S_0+S)\left[\frac{\partial\psi}{\partial y}\frac{\partial^2\psi}{\partial x\partial y} - \frac{\partial\psi}{\partial x}\frac{\partial^2\psi}{\partial y^2}\right]\right\} - \frac{\partial^2}{\partial y^2}\left[(\mu_0+\theta_0+\theta)\frac{\partial^2\psi}{\partial y^2}\right] \quad . \tag{2-33}$$

But it has been assumed from the outset that the stratification is small. That is

$$\left|\frac{S_0+S}{\rho_0}\right| << 1 \quad , \tag{2-34}$$

and

$$\left|\frac{\theta_0+\theta}{\mu_0}\right| << 1 \tag{2-35}$$

in the region of flow. Hence equation 2-33 may be simplified to

$$g\frac{\partial S}{\partial x} = \rho_0\frac{\partial}{\partial y}\left[\frac{\partial\psi}{\partial y}\frac{\partial^2\psi}{\partial x\partial y} - \frac{\partial\psi}{\partial x}\frac{\partial^2\psi}{\partial y^2}\right] - \mu_0\frac{\partial^4\psi}{\partial y^4} \quad . \tag{2-36}$$

Thus equations 2-32 and 2-36 are two equations for the two unknown functions $\psi(x,y)$ and $S(x,y)$. They have been obtained based on the three assumptions listed at the beginning of this chapter and the following two further assumptions:

(i) Steady, two-dimensional flow in an infinite field.

(ii) A boundary-layer-type assumption; i.e. the relevant flow field is a zone or a withdrawal layer whose thickness $\delta(x)$ is much smaller than the distance x from the sink.

These assumptions, of course, pose certain limitations on the applicability of any solution to these equations. First of all, in any physical situation, the fluid is not truly infinite in extent. In particular, in a reservoir, there is always a water surface. However, as long as

the relevant flow field given by the withdrawal zone of thickness $\delta(x)$ is well within the reservoir (i.e. $\delta(x) \ll$ depth), the assumptions are valid. The greatest objection is perhaps the third assumption (i.e. the boundary-layer-type assumption), which is based on physical observation and intuition and must, therefore, be verified a postiori. It will be seen later that firstly, a solution may be obtained which satisfies this, and secondly that this assumption is also valid for the experiments, provided one excludes the neighborhood of the sink. In the neighborhood of the sink, x is small and the boundary-layer-type assumption would certainly break down.

2-3 Normalized Equations

Before normalizing the equations, it is convenient at this point to specify the parent density distribution, i.e. the density distribution existing if there were no motion. Assume that the hydrostatic density distribution is linear:

$$S_o(y) = -\epsilon \rho_o y \quad , \tag{2-37}$$

where

$$\epsilon = \text{constant} = -\frac{1}{\rho_o}\frac{ds_o}{dy} \quad . \tag{2-38}$$

Note that since the fluid is assumed to be infinite in extent, this density distribution implies negative density for large enough y. However, the "withdrawal layer" of thickness $\delta(x)$ is assumed to be small in the sense that $\frac{\delta(x)}{x} \ll 1$. Thus the density at large y is not important to the main flow when $\frac{\delta(x)}{y} \ll 1$.

To non-dimensionalize the equations, define new variables as follows:

$$\sigma_o = \left[\frac{Dg}{\epsilon^3 q_f^2 \nu}\right]^{2/3} \frac{S_o}{\rho_o} \quad ,$$

$$\sigma = \left[\frac{Dg}{\epsilon^3 q_f^2 \nu}\right]^{2/3} \frac{S}{\rho_o} \quad ,$$

$$\varphi = \psi / q_f \quad ,$$

$$\xi = \frac{q_f \nu \epsilon^4}{g} x \quad ,$$

$$\eta = \left[\frac{q_f^2 \nu \epsilon^3}{Dg}\right]^{1/6} \epsilon y \quad ,$$

$$F^2 = \frac{q_f^2 \epsilon^3}{g} \quad ,$$

$$\beta = \left[\frac{q_f^2 \nu \epsilon^3}{Dg}\right]^{5/6} \quad ,$$

(2-39)

where q_f = unit discharge

and $\nu = \frac{\mu_o}{\rho_o}$ = kinematic viscosity.

The significance of this normalization will be clear later. Substitution of the above into equations 2-32 and 2-36 gives

$$\frac{\partial \sigma}{\partial \xi} + \frac{\partial^4 \varphi}{\partial \eta^4} = \frac{F^2}{\beta^{1/5}} \left[\frac{\partial \varphi}{\partial \eta} \frac{\partial^3 \varphi}{\partial \xi \partial \eta^2} - \frac{\partial \varphi}{\partial \xi} \frac{\partial^3 \varphi}{\partial \eta^3}\right]$$

(2-40)

and

$$\frac{\partial^2 \sigma}{\partial \eta^2} - \frac{\partial \varphi}{\partial \xi} = \beta \left[\frac{\partial \varphi}{\partial \eta} \frac{\partial \sigma}{\partial \xi} - \frac{\partial \varphi}{\partial \xi} \frac{\partial \sigma}{\partial \eta} \right] .$$

(2-41)

2-4 The Boundary Conditions

The physical problem to be solved is the problem of the flow towards a sink as depicted schematically in figure 2-1. A hydrodynamic line sink is situated at x=0, y = 0. The fluid which is linearly stratified occupies the entire right half plane. Hence the boundary conditions which must be satisfied are

$$\int_{-\infty}^{\infty} u(x,y)\, dy = -q = \text{constant} ,$$

(2-42)

$$s, v, u, \frac{\partial u}{\partial y} \to 0 \quad \text{as} \quad y \to \pm\infty , \; x > 0 ,$$

$$s \to 0 \quad \text{as} \quad x \to \infty . \qquad (2-43)$$

Expressed in terms of the non-dimensional variables, they may be written

$$\int_{-\infty}^{\infty} \frac{\partial \varphi}{\partial \eta}\, d\eta = -1 ,$$

(2-44)

$$\sigma, \frac{\partial \varphi}{\partial \xi}, \frac{\partial \varphi}{\partial \eta}, \frac{\partial^2 \varphi}{\partial \eta^2} \to 0 \quad \text{as} \quad \eta \to \pm\infty , \; \xi > 0 ,$$

$$\sigma \to 0 \quad \text{as} \quad \xi \to \infty . \qquad (2-45)$$

Thus the equations 2-40 and 2-41 are to be solved subject to the boundary conditions, equations 2-44 and 2-45.

2-5 A Perturbation Scheme

The equations 2-40 and 2-41 are non-linear and of high order. Even though the boundary conditions are fairly simple, the complete solution to the problem as posed so far is beyond the present status of applied mathematics. The non-linear terms in the right side of the equation 2-40 and 2-41 are multiplied by the constants $F^2/\beta^{1/5}$ and β respectively. Both of these contain the unit discharge q. Inasmuch as this thesis is mainly concerned with the case of very low velocities and hence low unit discharge, these terms might conceivably be neglected as a first approximation. Rather than straightforwardly neglecting them, however, a perturbation scheme will be set up based on a perturbation parameter proportional to q and the zeroth order solution obtained.

Since the flow field is infinite in extent there is no geometric characteristic length. The boundary conditions are also of such a nature as to suggest a similarity type solution. Let $\zeta = \eta/\xi^{1/3}$ and

$$\varphi(\xi,\eta) = f_0(\zeta) + \frac{\beta}{\xi^{2/3}} f_1(\zeta) + \left(\frac{\beta}{\xi^{2/3}}\right)^2 f_2(\zeta) + \cdots, \tag{2-46}$$

$$\sigma(\xi,\eta) = \frac{1}{\xi^{1/3}}\left\{ h_0(\zeta) + \frac{\beta}{\xi^{2/3}} h_1(\zeta) + \left(\frac{\beta}{\xi^{2/3}}\right)^2 h_2(\zeta) + \cdots \right\}, \tag{2-47}$$

and substitute them into the equations 2-40 and 2-41. Assuming $\beta/\xi^{2/3} \ll 1$, the terms may be grouped according to their order. The net results are:

i) Zeroth Order

$$h_o'' + \frac{\zeta}{3} f_o' = 0 \quad , \tag{2-48}$$

$$f_o'''' - \frac{1}{3}\left[\zeta h_o' + h_o\right] = 0 \quad , \tag{2-49}$$

where primes denote differentiation with respect to ζ. h_o may be eliminated by combining equations 2-48 and 2-49 giving

$$\frac{d^6 f_o}{d\zeta^6} + \frac{1}{9}\left\{\zeta^2 \frac{d^2 f_o}{d\zeta^2} + 4\zeta \frac{df_o}{d\zeta}\right\} = 0 \quad . \tag{2-50}$$

The boundary conditions, equations 2-44 and 2-45 become

$$\int_{-\infty}^{\infty} \frac{df_o}{d\zeta}\, d\zeta = -1 \tag{2-51}$$

$$h_0, \quad \frac{df_0}{d\zeta}, \quad \frac{d^2f_0}{d\zeta^2} \to 0$$

$$\text{as} \quad \zeta \to \pm\infty .$$

(2-52)

ii) First Order

$$h_1'' + \frac{1}{3}\left[\zeta f_1' + 2 f_1\right] = -\frac{1}{3} f_0' h_0 \quad ,$$

(2-53)

$$f_1'''' - \frac{1}{3}\left[\zeta h_1' + 3 h_1\right] = -\frac{2}{5}\lambda f_0' f_0'' \quad ,$$

(2-54)

where $\lambda = F^2/\beta^{6/5} = \frac{D}{\nu}$. h_1 may be eliminated from these equations by combining them, giving

$$\frac{d^6 f_1}{d\zeta^6} + \frac{1}{9}\left\{\zeta^2 \frac{d^2 f_1}{d\zeta^2} + 6\zeta \frac{df_1}{d\zeta} + 10 f_1\right\}$$

$$= -\frac{5}{3}\frac{df_0}{d\zeta}\frac{d^4 f_0}{d\zeta^4} - \frac{1}{3}\zeta \frac{d^2 f_0}{d\zeta^2}\frac{d^4 f_0}{d\zeta^4} - \frac{3}{2}\frac{d^5 f_0}{d\zeta^5}\frac{d^6 f_0}{d\zeta^6} - \frac{1}{6}\zeta^2 \frac{df_0}{d\zeta}\frac{d^6 f_0}{d\zeta^6}$$

$$- \frac{2}{3}\lambda\left\{3\frac{d^2 f_0}{d\zeta^2}\frac{d^3 f_0}{d\zeta^3} + \frac{df_0}{d\zeta}\frac{d^4 f_0}{d\zeta^4}\right\} .$$

(2-55)

The boundary conditions are

$$\int_{-\infty}^{\infty} \frac{df_1}{d\zeta}\, d\zeta = 0 \quad , \tag{2-56}$$

$$h_1 \, , \; \frac{df_1}{d\zeta} \, , \; \frac{d^2 f_1}{d\zeta^2} \to 0 \qquad \text{as} \quad \zeta \to \pm\infty \, . \tag{2-57}$$

Similarly one may obtain the equations for f_2, f_3, . . . , although these will not be carried out here. In fact, only the zeroth order equations will be solved. The purpose of this perturbation analysis is primarily to show the effect of the neglected quantities. Note that the perturbation parameter is $\beta/\xi^{2/3}$ which is inversely proportional to the 2/3 power of the distance from the sink. Thus, the greater the distance from the sink, the better the approximation.

2-6 Solution to the Zeroth Order Equations

We begin by rewriting the differential equation 2-50 and the boundary conditions equations 2-51 and 2-52.

$$\frac{d^6 f_0}{d\zeta^6} + \frac{1}{9}\left\{ \zeta^2 \frac{d^2 f_0}{d\zeta^2} + 4\zeta \frac{df_0}{d\zeta} \right\} = 0 \quad , \tag{2-50}$$

$$\int_{-\infty}^{\infty} \frac{df_0}{d\zeta}\, d\zeta = -1 \quad , \tag{2-51}$$

$$\frac{df_0}{d\zeta} \to 0 \, , \; \frac{d^2 f_0}{d\zeta^2} \to 0 \qquad \text{as} \quad \zeta \to \pm\infty \, . \tag{2-52}$$

Note that the differential equation does not contain f_o explicitly and it is linear and homogeneous. Hence a solution is determined up to an arbitrary additive constant. Without loss of generality one may, therefore, put

$$f_o(0) = 0 \quad . \tag{2-58}$$

Next observe that by putting

$$\hat{\zeta} = -\zeta \quad , \tag{2-59}$$

the differential equation and the boundary condition in equation 2-52 remain unchanged while the boundary condition in equation 2-51 becomes

$$\int_{-\infty}^{\infty} \frac{df_o}{d\zeta}\, d\zeta = 1 \quad . \tag{2-60}$$

Therefore,

$$f_o(\zeta) = -f_o(-\zeta) \quad . \tag{2-61}$$

In other words, f_o is an odd function of ζ. Thus

$$f_o''(0) = 0 \quad , \tag{2-62}$$

$$f_o'''(0) = 0 \quad . \tag{2-63}$$

The differential equation 2-50 is a sixth-order linear one and hence it has six linearly independent solutions. One of those is, of course, f_o = constant. These six solutions will be denoted by $K_i(\zeta)$, i = 0, 1, ..., 5, with, as mentioned before, $K_o(\zeta)$ = constant. The

solutions $K_i(\zeta)$ will now be obtained in the form of power series.

The origin $\zeta = 0$ is an ordinary point of the differential equation 2-50. Hence let

$$f_0(\zeta) = \sum_{n=0}^{\infty} a_n \zeta^n \quad . \tag{2-64}$$

Substituting into the equation 2-50 gives the recursion relation

$$\frac{a_{n+6}}{a_n} = -\frac{1}{9} \frac{n(n+3)}{(n+6)(n+5)(n+4)(n+3)(n+2)(n+1)} \tag{2-65}$$

from which it may be demonstrated that

$$K_1(\zeta) = \zeta \sum_{n=0}^{\infty} (-1)^n \frac{(6n-2)!!!}{(6n+1)!} \left(\frac{\zeta^6}{9}\right)^n , \tag{2-66}$$

$$K_2(\zeta) = \zeta^2 \sum_{n=0}^{\infty} (-1)^n \frac{(6n-1)!!!}{(6n+2)!} \left(\frac{\zeta^6}{9}\right)^n , \tag{2-67}$$

$$K_3(\zeta) = \zeta^3 \sum_{n=0}^{\infty} (-1)^n \frac{(6n)!!!}{(6n+3)!} \left(\frac{\zeta^6}{9}\right)^n , \tag{2-68}$$

$$K_4(\zeta) = \zeta^4 \sum_{n=0}^{\infty} (-1)^n \frac{(6n+1)!!!}{(6n+4)!} \left(\frac{\zeta^6}{9}\right)^n , \tag{2-69}$$

$$K_5(\zeta) = \zeta^5 \sum_{n=0}^{\infty} (-1)^n \frac{(6n+2)!!!}{(6n+5)!} \left(\frac{\zeta^6}{9}\right)^n , \tag{2-70}$$

where the triple factorial is defined by the formulae

$$0!!! = 1!!! = 2!!! = 1 \quad ,$$

$$n!!! = (n)\left[(n-3)!!!\right] \quad ,$$

$$(-n)!!! = 1 \quad ,$$

(2-71)

where n is a positive integer.

The normalization of the series for $K_i(\zeta)$ is by the condition

$$\frac{d^i K_i(0)}{d\zeta^i} = 1 \quad , \qquad i = 1, 2, \cdots, 5 \, .$$

(2-72)

These series are found to be absolutely convergent for all finite ζ . It is seen from equations 2-67 and 2-69 that $K_2(\zeta)$ and $K_4(\zeta)$ are even functions of ζ . Hence they cannot appear in the solution. Moreover, in view of the normalization expressed in equation 2-72, the solution to our problem is

$$f_0(\zeta) = f_0'(0)\, K_1(\zeta) + f_0'''(0)\, K_3(\zeta) + f_0''''(0)\, K_5(\zeta) \, ,$$

(2-73)

where the constants $f_0'(0)$, $f_0'''(0)$, and $f_0''''(0)$ are to be determined by requiring that the solution satisfy the boundary conditions. The most obvious way of obtaining the numerical values of the $K_i(\zeta)$ is, of course, to sum the series. However, since the convergence of the series becomes poorer for larger ζ , one needs progressively more terms as ζ increases. Also the terms of the series become very large and the value of the functions are differences between these large terms. Without resorting to double or triple precision, even computers cannot handle these large terms. The series being alternating

and the size of each term becoming very large as ζ becomes large, it is expected that the solutions $K_i(\zeta)$ are oscillatory functions with rapidly growing amplitude. The most logical way then, to compute the functions $K_i(\zeta)$ is as solutions to the differential equation by using a numerical integration subroutine.

The functions $K_i(\zeta)$ were obtained by numerical integration of the differential equation 2-50 with the initial conditions

$$f_o^{(n)}(o) = 0 \quad , \quad n \neq i ,$$

$$f_o^{(i)}(o) = 1 \quad .$$

(2-74)

They were found to be oscillatory functions of rapidly growing amplitude. The numerical integration was performed on an IBM 7090 digital computer using a fourth order Runge-Kutta method with partial double precision in the form of a subroutine called SCOOT originally programmed by Fred Lesh and adapted to FORTRAN by Wilson Sileby. This is a modification of D222 RW F. P. SHARE Distribution No. 450 (International Business Machines). The step size used was 0.002.

In order to determine the constants $f_o'(o)$, $f_o'''(o)$, and $f_o^{'''''}(o)$ in equation 2-73, an asymptotic solution of the equation 2-50 will be obtained. For large ζ , one may neglect, as a first approximation, the first term in equation 2-50. Thus the differential equation reads

$$\frac{d^2 f_o}{d\zeta^2} + \frac{4}{\zeta}\frac{df_o}{d\zeta} = 0 \quad ,$$

(2-75)

which has the simple solution

$$\frac{df_o}{d\zeta} = \frac{A}{\zeta^4} \quad , \tag{2-76}$$

where A = constant. The neglected term is then

$$\frac{d^6 f_o}{d\zeta^6} \sim O\left(\frac{1}{\zeta^9}\right) \quad ,$$

which for large ζ is truly a higher order term. Successive approximations may be obtained by iteration. We shall, however, make use of only the one term asymptotic representation, equation 2-76.

In order to determine the values of the constants $f_o'(o)$, $f_o'''(o)$, and $f_o'''''(o)$ in equation 2-73 so that $f_o(\zeta)$ would satisfy the boundary conditions, one matches the solution as given by equation 2-73 with the asymptotic representation, equation 2-76, at an appropriate value of ζ, say ζ_o. Thus one has the set of algebraic equations

$$f_o'(o)\, K_1'(\zeta_o) + f_o'''(o)\, K_3'(\zeta_o) + f_o'''''(o)\, K_5'(\zeta_o) = \frac{A}{\zeta_o^4} \quad ,$$

$$f_o'(o)\, K_1''(\zeta_o) + f_o'''(o)\, K_3''(\zeta_o) + f_o'''''(o)\, K_5''(\zeta_o) = -\frac{4A}{\zeta_o^5} \quad ,$$

$$f_o'(o)\, K_1'''(\zeta_o) + f_o'''(o)\, K_3'''(\zeta_o) + f_o'''''(o)\, K_5'''(\zeta_o) = \frac{20A}{\zeta_o^6} \quad , \tag{2-77}$$

to be solved for the two constants $\alpha = \frac{f_o'''(0)}{f_o'(0)}$ and $\gamma = \frac{f_o''''(0)}{f_o'(0)}$. These were done for the three values of ζ_o of 10.0, 15.0, and 20.0. They are found to be as follows:

ζ_o	$\alpha = \frac{f_o'''(0)}{f_o'(0)}$	$\gamma = \frac{f_o''''(0)}{f_o'(0)}$
10.0	-0.373282	0.336978
15.0	-0.373282	0.336978
20.0	-0.373282	0.336978

The solution of the equation 2-50 subject to the set of boundary conditions

$$f_o(0) = 0 \quad ,$$

$$f_o'(0) = -1 \quad ,$$

$$f_o''(0) = 0 \quad ,$$

$$f_o'''(0) = 0.373282 \quad ,$$

$$f_o''''(o) = o \quad ,$$

$$f_o'''''(o) = -0.336978 \quad ,$$

(2-78)

was obtained from an IBM 7090 computer using the same program as before. From this solution, it was found that $-f_o \to 1.762$ as $\zeta \to \infty$. Thus the solution should be normalized by multiplying by the number -1/2(1.762) in order to satisfy the boundary condition in equation 2-51. The normalized solution is listed in table 2-1 and plotted in figure 2-2.

2-7 The Density Field

In the previous section, the zeroth order solution for the stream function was obtained. The velocity as a function of space is also presented in the form of $f_o'(\zeta)$. Another interesting function is, of course, the density function S or $h_o(\zeta)$. Equation 2-48 for h_o and the boundary conditions $h_o \to o$ as $\zeta \to \pm\infty$ may be used to obtain the solution. It may be shown from equation 2-48 and the boundary conditions that

$$h_o(\zeta) = \int_o^{\zeta} \int_{\infty}^{\zeta_1} -\frac{\zeta_2 f_o'(\zeta_2)}{3} \, d\zeta_2 \, d\zeta_1 \quad . \tag{2-79}$$

The functions $h_o(\zeta)$ and $h_o'(\zeta)$ were computed numerically

Table 2-1 The Non-dimensional Stream Function $f_o(\zeta)$ and its Derivatives. $f_o(\zeta) = \psi(x,y)/_{\nu}$.

$\zeta = \frac{\alpha_o y}{x^{1/3}}$, $\alpha_o = \left(\frac{\epsilon g}{\mathcal{D}\nu}\right)^{1/6}$.

ζ	$-f_o(\zeta)$	$-f_o'(\zeta)$	$-f_o''(\zeta)$
0.0	0.0000	0.2838	0.0000
0.1	0.0284	0.2832	-0.0106
0.2	0.0566	0.2817	-0.0211
0.3	0.0847	0.2790	-0.0313
0.4	0.1124	0.2754	-0.0414
0.5	0.1397	0.2708	-0.0510
0.6	0.1665	0.2652	-0.0602
0.7	0.1927	0.2588	-0.0689
0.8	0.2182	0.2515	-0.0769
0.9	0.2430	0.2434	-0.0843
1.0	0.2669	0.2346	-0.0910
1.1	0.2899	0.2252	-0.0969
1.2	0.3119	0.2153	-0.1020
1.3	0.3329	0.2048	-0.1063
1.4	0.3529	0.1940	-0.1098
1.5	0.3717	0.1829	-0.1124
1.6	0.3894	0.1716	-0.1142
1.7	0.4060	0.1601	-0.1151
1.8	0.4214	0.1486	-0.1152
1.9	0.4357	0.1371	-0.1146
2.0	0.4489	0.1257	-0.1132
2.1	0.4609	0.1145	-0.1111
2.2	0.4718	0.1035	-0.1083
2.3	0.4816	0.0928	-0.1049
2.4	0.4904	0.0825	-0.1011
2.5	0.4981	0.0726	-0.0967
2.6	0.5049	0.0632	-0.0920
2.7	0.5108	0.0543	-0.0869
2.8	0.5158	0.0458	-0.0815
2.9	0.5200	0.0380	-0.0759

ζ	$-f_o(\zeta)$	$-f_o'(\zeta)$	$-f_o''(\zeta)$
3.0	0.5234	0.0307	-0.0702
3.1	0.5261	0.0239	-0.0644
3.2	0.5282	0.0178	-0.0586
3.3	0.5297	0.0122	-0.0529
3.4	0.5306	0.0072	-0.0472
3.5	0.5311	0.0028	-0.0417
3.6	0.5312	-0.0011	-0.0364
3.7	0.5309	-0.0045	-0.0312
3.8	0.5303	-0.0074	-0.0264
3.9	0.5295	-0.0098	-0.0218
4.0	0.5284	-0.0118	-0.0176
4.1	0.5271	-0.0133	-0.0136
4.2	0.5257	-0.0145	-0.0100
4.3	0.5242	-0.0153	-0.0067
4.4	0.5227	-0.0158	-0.0038
4.5	0.5211	-0.0161	-0.0012
4.6	0.5194	-0.0161	0.0011
4.7	0.5178	-0.0159	0.0030
4.8	0.5163	-0.0155	0.0047
4.9	0.5147	-0.0150	0.0060
5.0	0.5133	-0.0143	0.0071
5.2	0.5106	-0.0128	0.0085
5.4	0.5082	-0.0110	0.0091
5.6	0.5062	-0.0092	0.0090
5.8	0.5045	-0.0074	0.0085
6.0	0.5030	-0.0058	0.0076
6.5	0.5020	-0.0027	0.0048
7.0	0.5016	-0.0014	0.0023
7.5	0.5013	-0.0007	0.0007
8.0	0.5010	-0.0004	0.0002
9.0	0.5007	-0.0002	0.0001
10.0	0.5005	-0.0002	0.0001
12.0	0.5003	-0.0001	0.0000
14.0	0.5002	0.0000	0.0000

ζ	$-f_o(\zeta)$	$-f_o'(\zeta)$	$-f_o''(\zeta)$
20.0	0.5001	0.0000	0.0000
25.0	0.5000	0.0000	0.0000

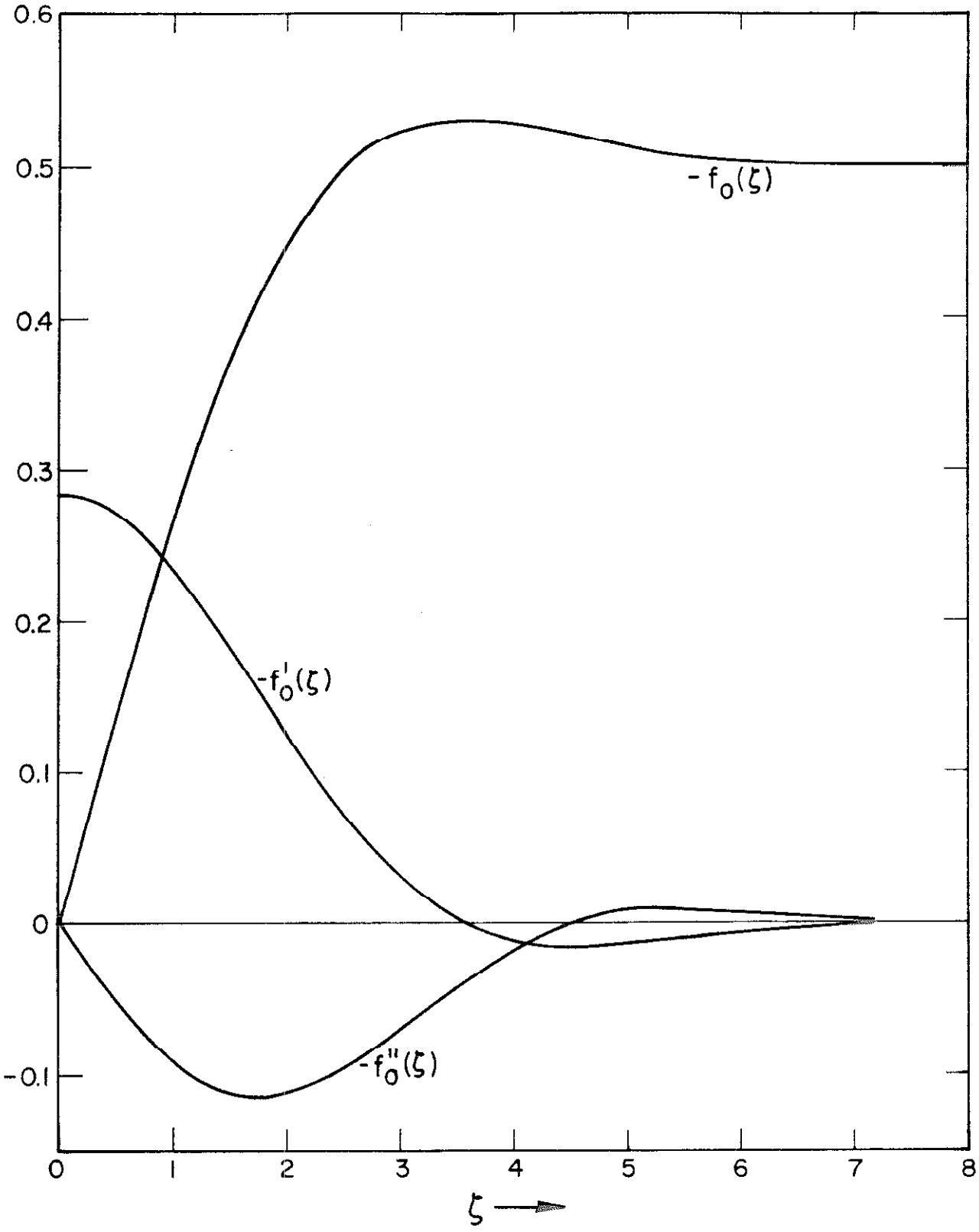

Figure 2-2 The non-dimensional stream function and its derivatives.

on an IBM 7090 computer in much the same way as the function $f_o(\zeta)$. They are tabulated in table 2-2 and shown graphically in figure 2-3.

2-8 The Withdrawal Layer

From figure 2-2, the velocity distribution may easily be visualized. The flow field indeed looks like the one shown in figure 2-1 with the withdrawal layer growing in thickness like $x^{1/3}$. If one defines the δ as the thickness of the forward flow, then from figure 2-2 or table 2-1,

$$\delta(x) = \frac{7.14\, x^{1/3}}{\alpha_o} \quad , \tag{2-80}$$

where $\alpha_o = \left(\frac{\epsilon g}{\mathcal{D}\nu}\right)^{1/6}$.

The significance of the boundary layer assumption may now be readily seen. From equation 2-80

$$\frac{\delta}{x} = \frac{7.14}{\alpha_o\, x^{2/3}} \quad . \tag{2-81}$$

For large enough x, $\frac{\delta}{x}$ may be made as small as one please provided α_o is not zero. The region of validity of the boundary layer assumption is thus strongly dependent on both x and α_o.

The other parameters assumed small for the validity of the solution are: $g/\mathcal{D}\alpha_o x^{2/3}$, which is the perturbation parameter; $g/\nu\alpha_o x^{2/3}$, which occurs disguised as $\lambda = \frac{\mathcal{D}}{\nu}$ in the first order equations (equations 2-54 and 2-55); and $\epsilon\delta$, which is the total relative change in density in the relevant flow field.

Table 2-2 The Non-dimensional Density Function $f_o(\zeta)$ and its Derivative. $f_o(\zeta) = \xi^{1/3}\sigma(\xi,\eta) = \frac{s}{\rho_0 \epsilon}\frac{\mathcal{D}}{q}\alpha_o^2 x^{1/3}$.

$\zeta = \frac{\alpha_o y}{x^{1/3}}$, $\alpha_o = \left(\frac{\epsilon q}{\mathcal{D}\nu}\right)^{1/6}$.

ζ	$f_o(\zeta)$	$f_o'(\zeta)$
0.0	0.0	-.1426
0.1	-.0142	-.1421
0.2	-.0284	-.1407
0.3	-.0424	-.1384
0.4	-.0560	-.1351
0.5	-.0694	-.1310
0.6	-.0822	-.1261
0.7	-.0946	-.1205
0.8	-.1063	-.1141
0.9	-.1174	-.1071
1.0	-.1277	-.0995
1.1	-.1372	-.0915
1.2	-.1460	-.0830
1.3	-.1538	-.0743
1.4	-.1608	-.0653
1.5	-.1669	-.0562
1.6	-.1720	-.0470
1.7	-.1763	-.0379
1.8	-.1796	-.0289
1.9	-.1821	-.0201
2.0	-.1837	-.0116
2.1	-.1844	-.0034
2.2	-.1844	.0044
2.3	-.1835	.0118
2.4	-.1820	.0187
2.5	-.1798	.0250
2.6	-.1770	.0308
2.7	-.1737	.0359
2.8	-.1699	.0405
2.9	-.1656	.0445
3.0	-.1610	.0479

ζ	$h_0(\zeta)$	$h_0'(\zeta)$
3.1	-.1561	.0506
3.2	-.1509	.0528
3.3	-.1455	.0544
3.4	-.1400	.0555
3.5	-.1344	.0561
3.6	-.1288	.0562
3.7	-.1232	.0558
3.8	-.1177	.0550
3.9	-.1122	.0539
4.0	-.1069	.0525
4.1	-.1017	.0508
4.2	-.0967	.0489
4.3	-.0920	.0468
4.4	-.0874	.0445
4.5	-.0831	.0421
4.6	-.0790	.0397
4.7	-.0751	.0372
4.8	-.0715	.0347
4.9	-.0682	.0322
5.0	-.0651	.0298
5.2	-.0596	.0252
5.4	-.0550	.0210
5.6	-.0512	.0173
5.8	-.0480	.0142
6.0	-.0455	.0116
6.5	-.0409	.0073
7.0	-.0379	.0055
7.5	-.0353	.0047
8.0	-.0331	.0041
9.0	-.0294	.0033
10.0	-.0265	.0027
12.0	-.0221	.0018
15.0	-.0177	.0012

ζ	$h_0(\zeta)$	$h_0'(\zeta)$
20.0	-.0133	.0007
30.0	-.0088	.0003
50.0	-.0053	.0001
100.0	-.0027	.0000
1000.0	-.0003	.0000
10,000.0	-.0000	.0000

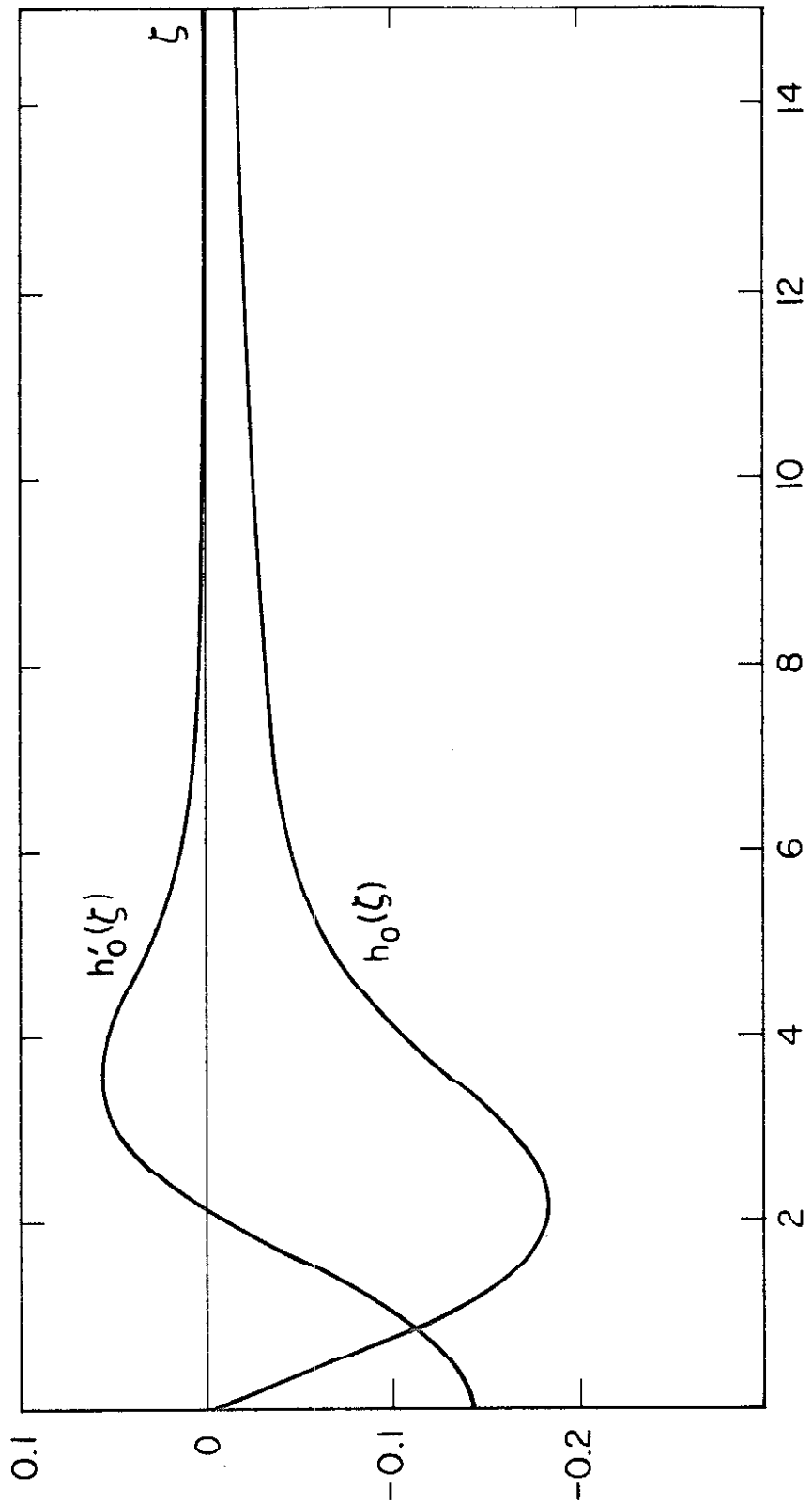

Figure 2-3 The non-dimensional density function and its first derivative.

2-9 Summary

The solution to the problem of selective withdrawal from a stratified reservoir for very low flows has thus been obtained. The neglected terms in the equations may be shown to be of order $q/D\alpha_0 x^{2/3}$, $q/\nu\alpha_0 x^{2/3}$, δ/x, and $\epsilon\delta$ or higher by simply using the zeroth order solution and calculating the neglected terms.

The theoretical solution by Kao indicates that as the discharge decreases to zero, the thickness of the withdrawal layer also decreases to zero which is, of course, not very realistic. This is because Kao's solution, being for the inviscid case, is not applicable as the discharge decreases to zero since viscosity and diffusivity become increasingly more important. It is reasonable to expect that as the discharge tends to zero, the flow field would tend to a limiting flow field. The solution presented herein is exactly this limiting solution of the stratified flow toward a line sink as the flow rate tends to zero. Kao's solution, on the other hand, may be thought of as the limiting solution for the other extreme of infinite Reynolds number.

To supplement this analysis, a series of experiments were performed. These will be discussed in the next two chapters.

CHAPTER 3

APPARATUS AND PROCEDURE

To supplement the analytical solution, a series of experiments were performed in the laboratory which consists of withdrawal from a slit on the side of a tank filled with a stratified liquid. The zeroth order solution developed in the previous chapter is strictly applicable only when the parameters $\epsilon\delta$, $q/D\alpha_0 x^{2/3}$, $q/\nu\alpha_0 x^{2/3}$, and δ/x are much less than unity. Experiments were performed in an attempt to see how much less than unity they must be for the validity of the zeroth order solution and to investigate the departures from the solution when they are no longer small. The experimental results will be discussed in the next chapter.

In this chapter the procedure and apparatus used for the experiments will be discussed. In these experiments, density gradients were achieved in two different ways: i) by means of a temperature gradient (these runs are designated as T-series runs), ii) by means of dissolved salt (designated as N-series runs).

The experimental procedure will first be described in a general brief way to give an overall picture. The apparatus will then be described in greater detail. Finally, the individual steps in the experimental procedure will be explained in detail.

3-1 General Description of the Procedure

For the N-series runs, the experimental reservoir was first filled with layers of water containing appropriate quantities of salt (NaCl) to give a linear gradient of density from top to bottom. This water was then allowed to stand for one evening or about 15 hours so that the density

distribution would become smoothly linear by molecular diffusion. The next morning the density profile was measured indirectly by measuring the electrical conductivity of the solution at various levels in the reservoir. The discharge valve was then opened and the flow rate regulated. After about five to ten minutes for the system to reach a quasi-steady state, dye particles were dropped into the reservoir at different stations upstream of the slit. As the dye particles fell, they left distinct vertical traces. Photographs were taken at time intervals so that the horizontal motions of the vertical dye lines were recorded intermittently. Typical photographs are shown in figure 3-1. Approximately ten minutes after the time the first set of dye particles were introduced, a second set was introduced in the same way and photographs taken as before. The discharge valve was then shut off and the remaining liquid in the reservoir saved. After the dye had disappeared by diffusion (about 24 hrs.) a density profile was taken again and another experiment could be performed with the remaining liquid at a different flow rate. For each filling of the reservoir, three experiments were performed. After that, the color of the water became so blue from the dye that no further dye streaks could be readily distinguished.

For the T-series runs, the reservoir was filled with layers of water at appropriately varying temperatures. A temperature profile was then measured with a thermometer and the experiment was performed immediately in the same way as for the N-series runs. Only one experiment was performed for each filling of the reservoir.

The discharge was measured volumetrically for both series. Velocity profiles were measured from displacements of the vertical dye lines on photographs taken at different times, (figure 3-1).

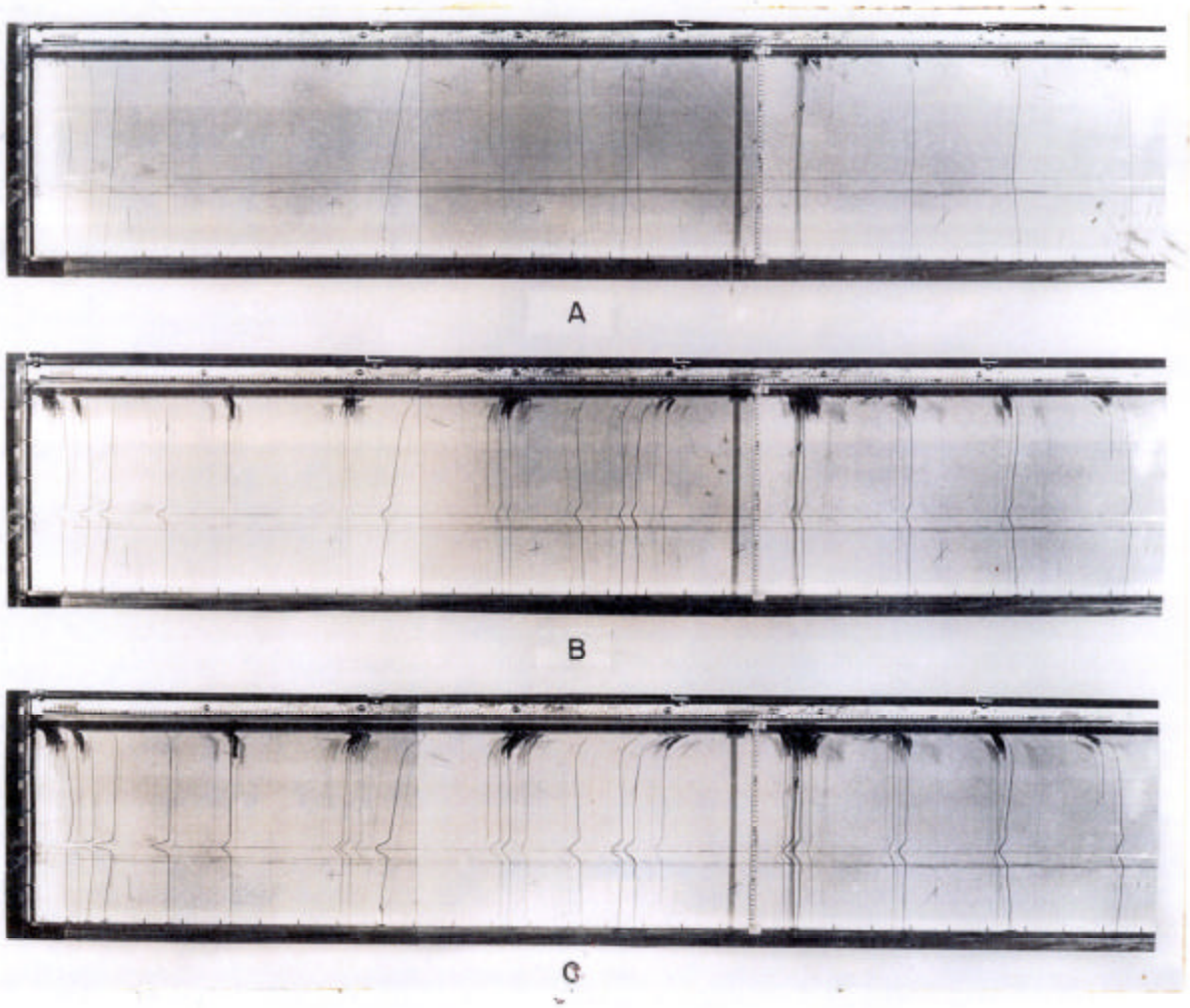

Figure 3-1 Typical time lapse photographs of dye lines (Run N-50-0.5)

(A) at time $t = t_o$

(B) at time $t \cong t_o + 55$ sec

(C) at time $t \cong t_o + 110$ sec

3-2 The Experimental Reservoir

The reservoir for the selective withdrawal experiments was a long tank constructed of clear lucite, 3/8" thick. A schematic drawing and a photograph of the reservoir are shown in figure 3-2 A and B respectively. A detailed drawing of the discharge end of the reservoir is also shown in figure 3-2 A. It is 45 cm deep, 250 cm long, and 26 cm wide with a milk-white lucite partition in the middle along the length of the tank extending from one end to a point 13 cm from the opposite end. This partition essentially doubles the length of the reservoir. On the discharge end was a slit 0.15 cm wide located 16 cm from the bottom and extending the width of the tank as divided (12.6 cm). Two valves in series were connected to the slit through a diffuser.

3-3 The Conductivity Probes and the Sanborn Recorder

Two conductivity probes were used in the N-series runs to measure the electrical conductivity of the salt solution as a measure of its density. These probes were developed by the Hydrodynamics Laboratory at the Massachusetts Institute of Technology. The probes are shown schematically and photographically in figure 3-3. The electrodes were 1/8" x 1/8" x 30 mil platinum plates 1/8" apart. They were platinized so that polarization and capacitance effects were minimized. The longer one was used for the measurement of the conductivity profile of the stratified liquid in the reservoir. The shorter one was installed at the discharge end of the tank for the continuous measurement of the conductivity of the discharging water as a function of time.

The longer one was calibrated, although the shorter probe was not. The calibration was by means of a set of standard solutions made

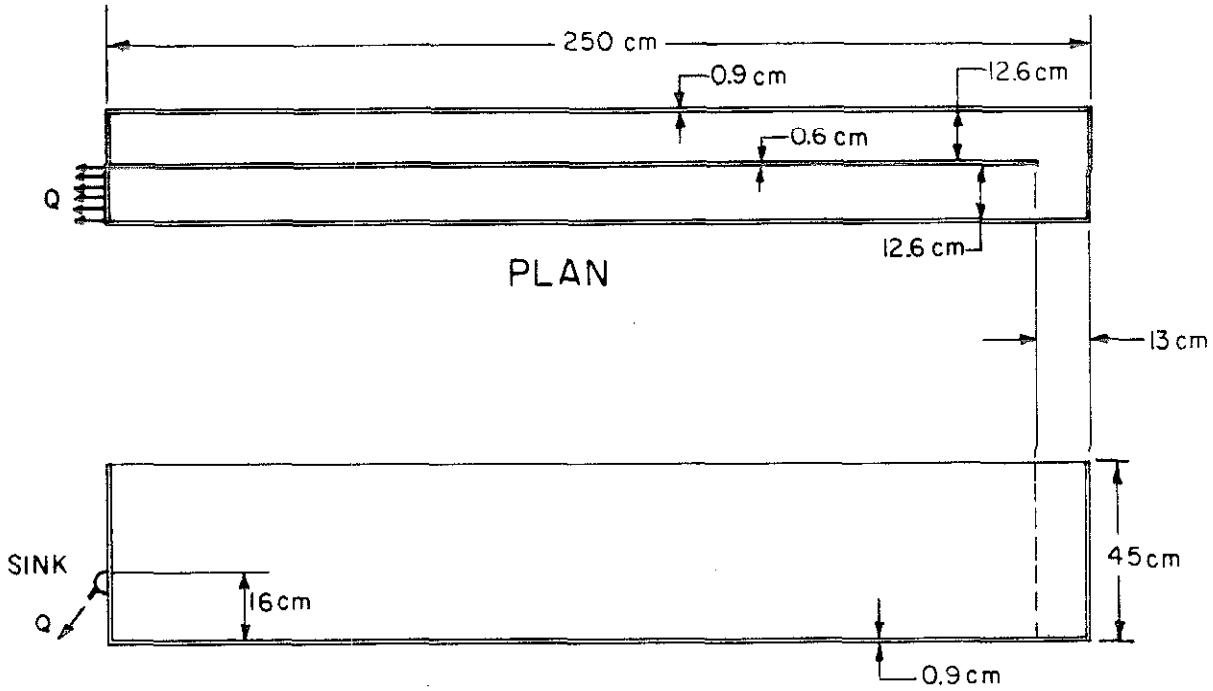

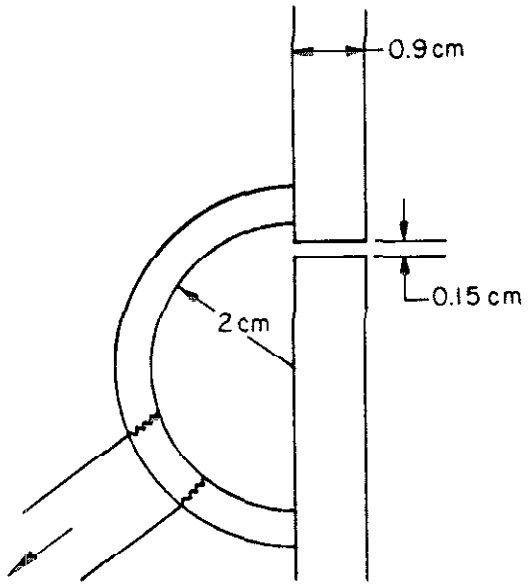

Figure 3-2 A Schematic drawing of the experimental reservoir.

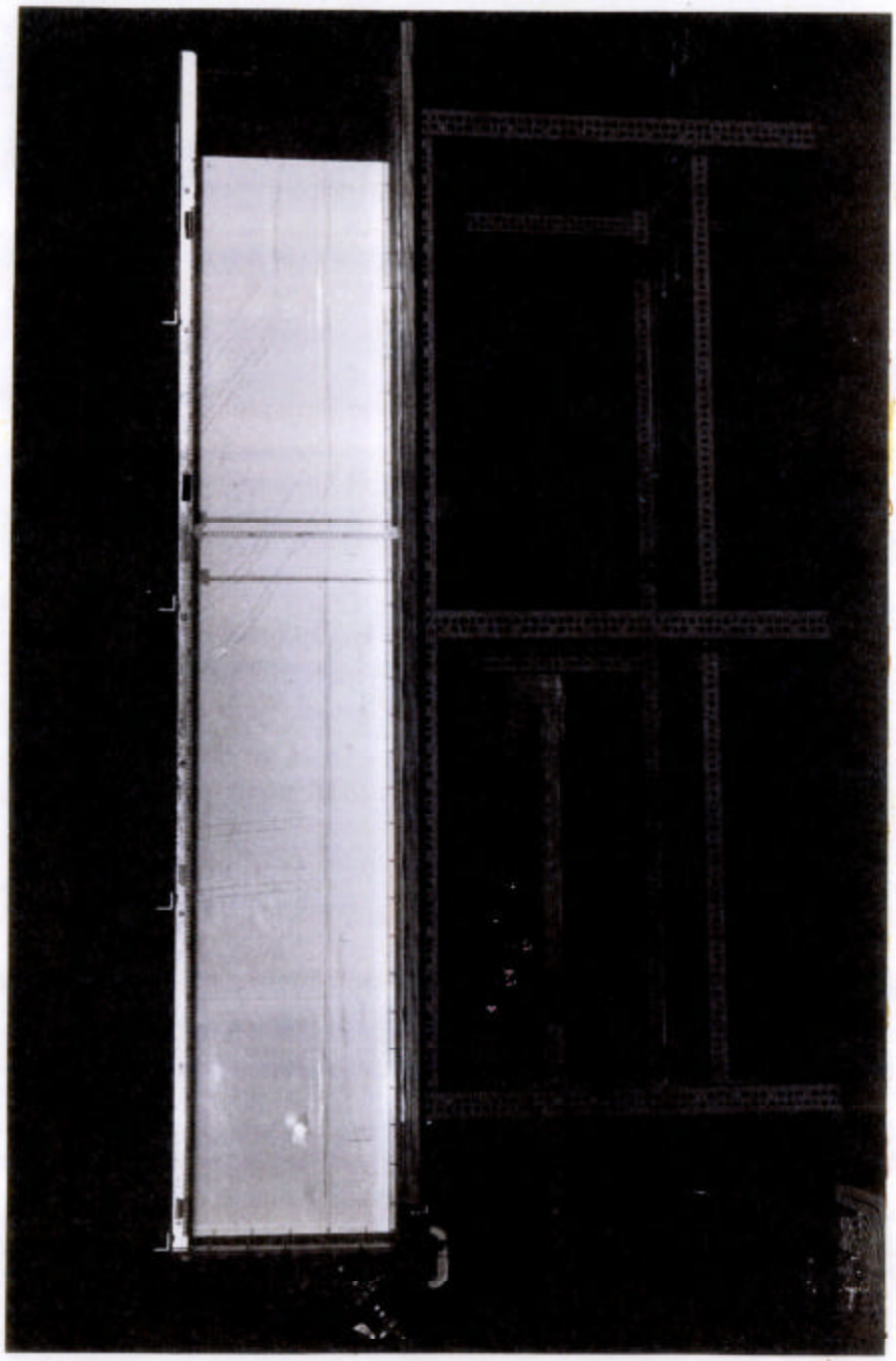

Figure 3-2B Photograph of the reservoir used in the experiments.

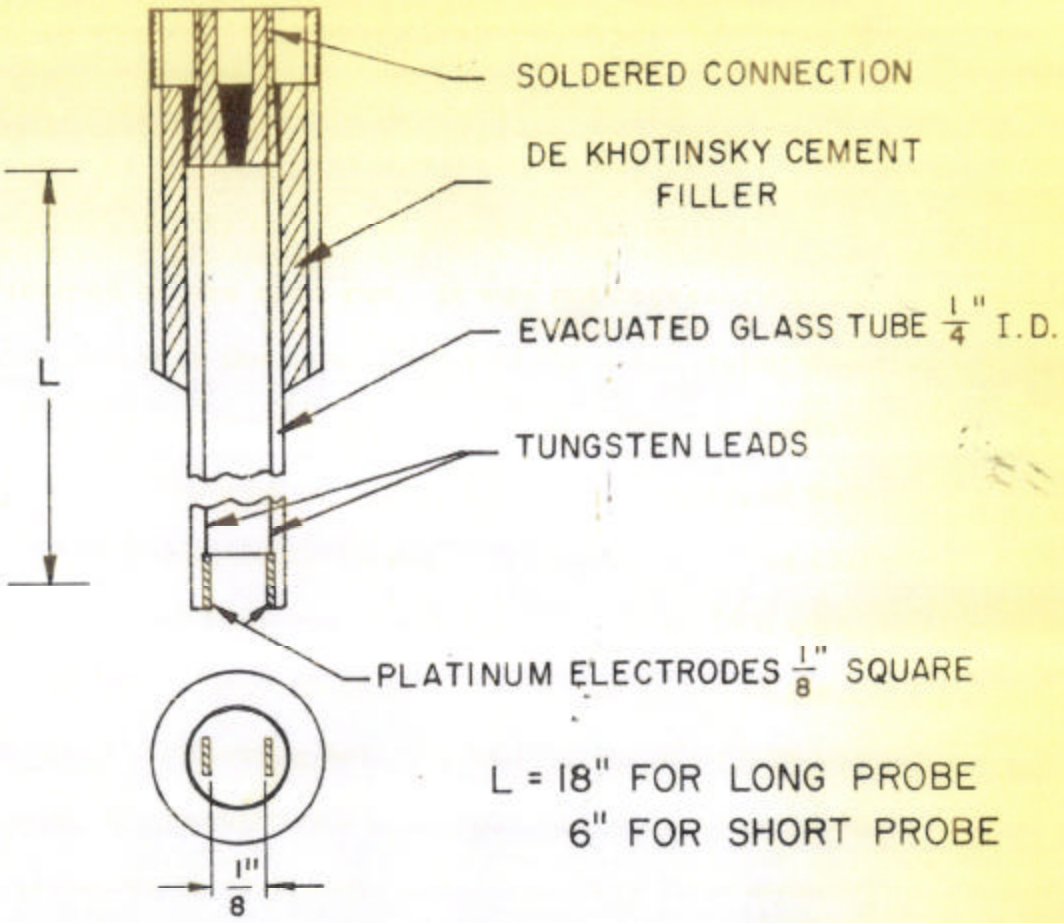

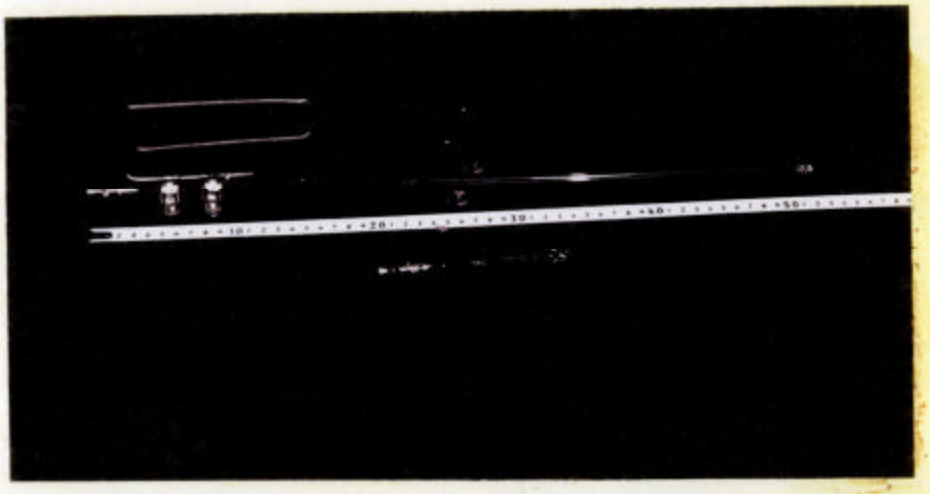

Figure 3-3 The conductivity probes.

up by carefully weighing out the amounts of salt to make solutions of specific gravity 1.00, 1.0005, 1.001, 1.002, 1.005, 1.010, 1.015, 1.020, and 1.025 respectively at a temperature of 22 1/2° C. The solutions were stored in tightly stoppered ground glass bottles. This calibration was performed before each run. It was not necessary to calibrate the short probe because the conductivity of the discharging water was found to be constant throughout each experiment. The conductivity of the discharge was measured by collecting some discharged water and measuring its conductivity by the long probe which was calibrated.

A Sanborn Two-channel Recorder (Model 150) with 1100 AS Carrier Amplifiers were used for the measurement of the conductivity. A circuit diagram showing both the half bridge elements used in conjunction with the conductivity probe and the connections to the internal Sanborn elements is shown in figure 3-4. The measurements are quite accurate for the range of conductivity encountered in the experiments. The error in the parameter ϵ, the density gradient, is estimated to be less than three percent, making only 0.5% error in the parameter α_o attributable to ϵ.

3-4 Dye Particles

To trace the motion of the fluid, a blue dye (Blue A-5-G-3 obtained form Krieger Color and Chemical Co.) was used. Dye particles were dropped at various stations along the reservoir simultaneously with the aid of a special long triangular wooden trough on the top of the tank. Dye particles of about 0.5 mm to 1 mm diameter were selected and placed about 10 to 25 cm apart along the trough, and then turning it over by hand, all the particles could be made to drop into the water in

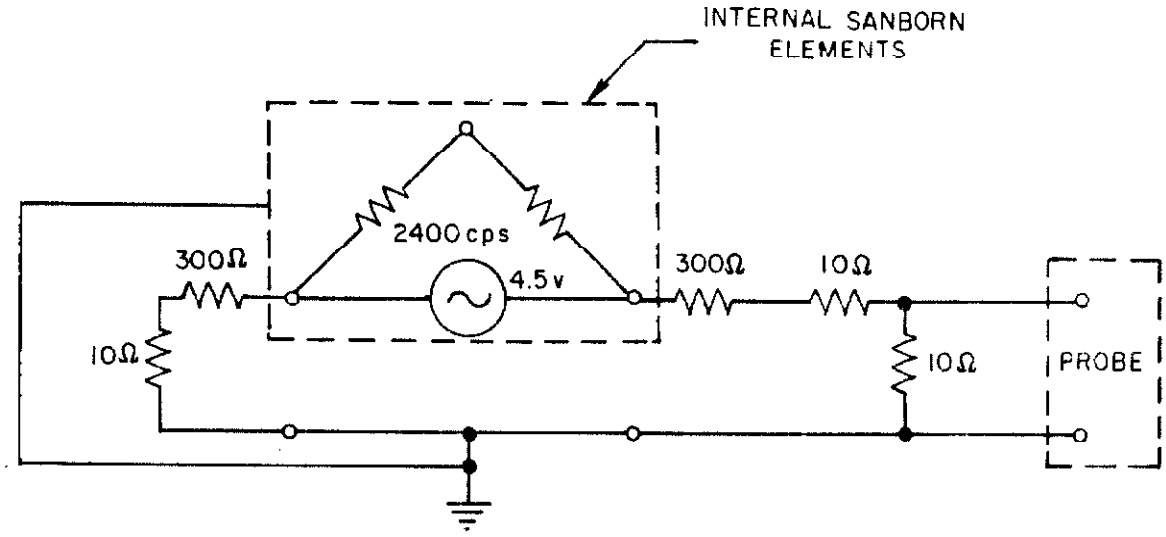

Figure 3-4 The bridge circuit used in conjunction with the Sanborn recorder for the measurement of the conductivity.

the reservoir at the same time.

3-5 Photography

A Nikon F single lens reflex 35 mm camera was used to photograph the dye streaks in these experiments. It was equipped with a 135 mm f/3.5 Auto-Nikkor lens. Kodak Plus X film was used at ASA160 and developed in D-76 diluted 1:1. The reason for the telephoto lens is to minimize parallax error which was calculated to be less than 2% for the setup used.

Since the tank is 250 cm long and only 45 cm deep with a length to depth ratio of about 5 to 1, and since the length-width ratio of a 35 mm frame is 1 1/2 to 1, three photographs were taken for the complete coverage of the tank so that the film frame was fully utilized. This is so that the degree of enlargement was kept at a minimum without resorting to a larger format camera. Thus the first photograph would cover from $x = 0$ to about $x = 80$ cm, the next $x = 80$ cm to $x = 160$ cm, and the last one from 160 cm to 250 cm. An ordinary tripod was thus not suitable to position the camera. For correct superposition, the camera must be brought back to the same position for the photographs of the same location in the reservoir. A special camera stand was made of wood and was clamped onto a table which was never moved; on the wood are three blocks against which the camera may be rested for its correct positioning. Thus the camera could be quickly and easily moved among the three positions. A schematic drawing is shown in figure 3-5 and a photograph of the stand and camera in use is shown in figure 3-6.

3-6 Filling the Reservoir

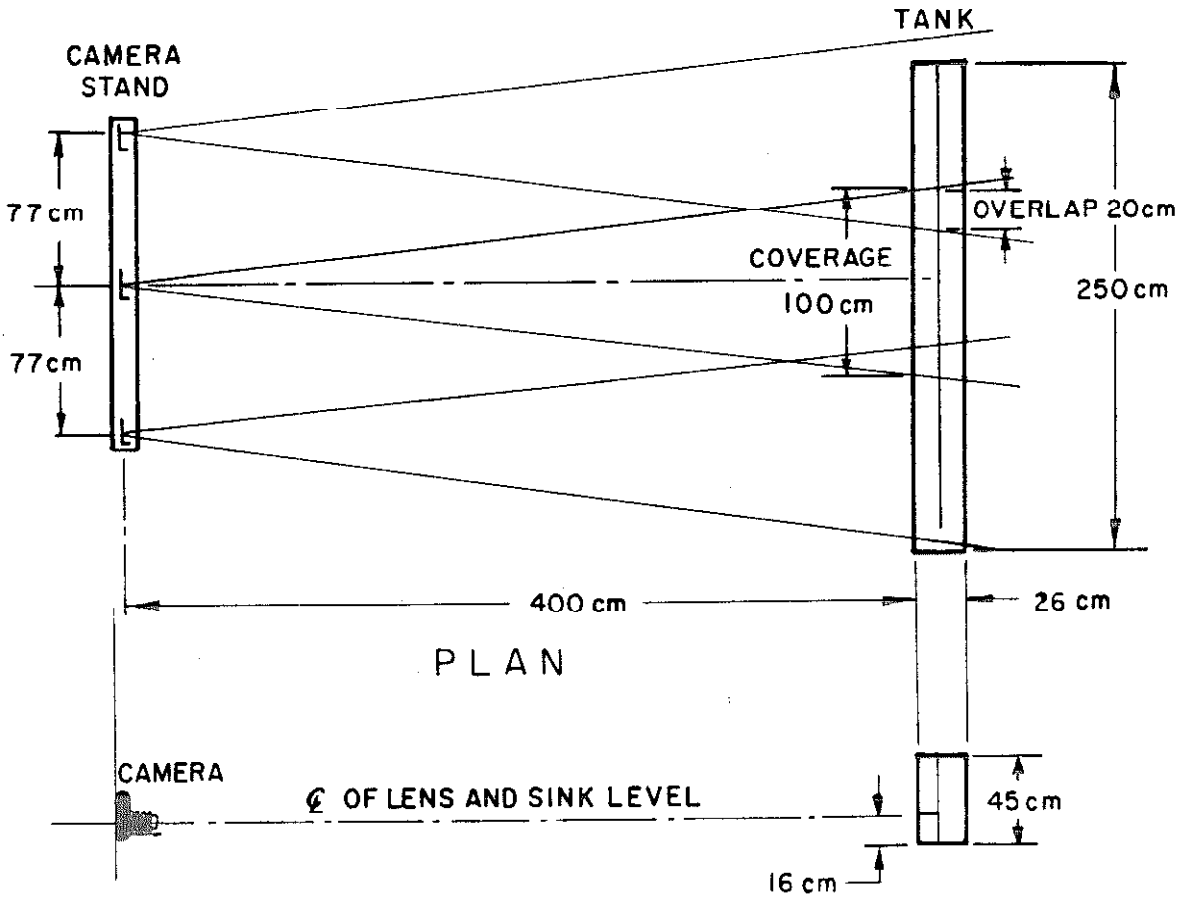

SCALE - 1:40

ALL DIMENSIONS NOMINAL

Figure 3-5 The photographic setup

Figure 3-6 The camera and camera stand in use.

A schematic diagram of the operations followed to produce a density-stratified reservoir is shown in figure 3-7. Before the beginning of the filling operation, a stock solution of NaCl was made by dissolving six pounds of Na Cl in distilled water to make eighteen liters of stock solution. The amounts of salt necessary to produce 20 liters of solution of the desired densities were computed and the corresponding volumes of the stock solution calculated. This volume for the lowest layer was then measured out from the stock solution and poured into a 20 liter plastic bottle with a bottom drain used for filling the reservoir. Distilled water was then added to make up 20 liters in the filler bottle; the liquid in this bottle was then thoroughly mixed by blowing air into it through a glass tube so that the air bubbles rose from the bottom of the bottle. The thoroughness of this mixing was checked by inserting the conductivity probe into the solution and checking the conductivity at various positions. The bottom drain of the filling bottle was then opened and the liquid was allowed to drain slowly onto the floating filling device and into the reservoir. This filling device is shown in figure 3-8. The water first entered through a hose, then went through the many holes in the lucite tube and the screens. Finally it floated onto the water already in the reservoir. It took about half an hour to drain one bottleful in this way. When all the liquid in the filler bottle was drained the process was repeated for the next layer. Since a total of twelve or thirteen layers were used, it usually took one working day to fill the tank.

For the T-series runs where the density stratification was due to temperature variations, a direct connection between the laboratory water taps and the filling device was established. The faucets were

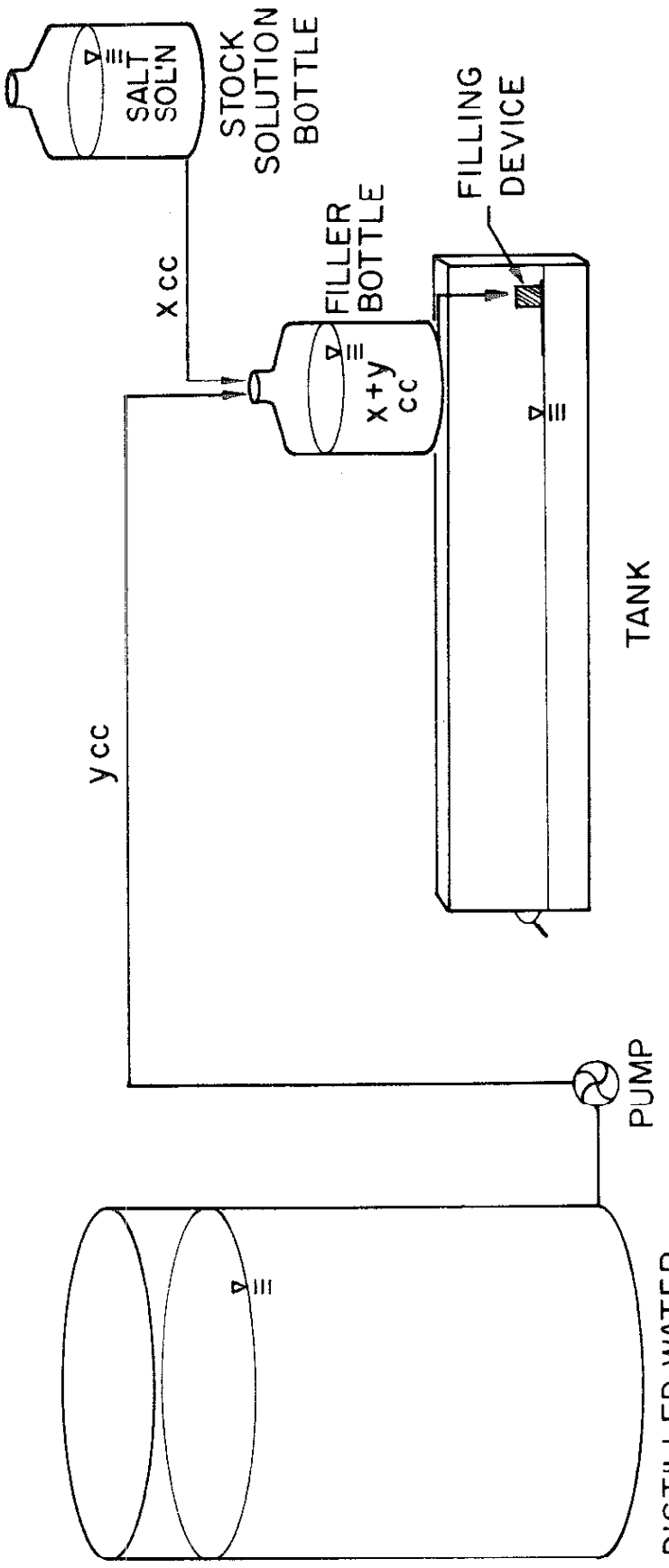

Figure 3-7 Filling the reservoir in layers to produce continuous density stratifications.

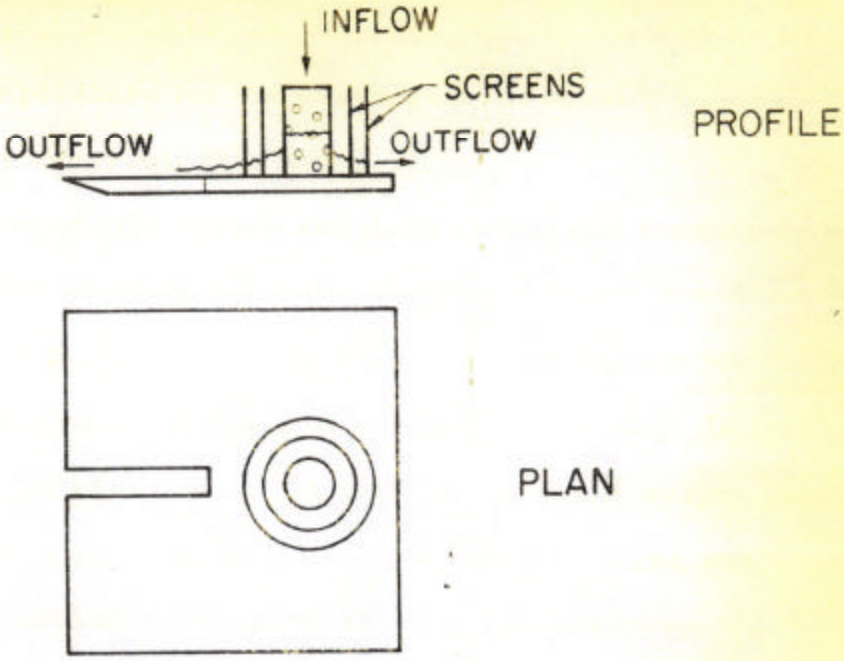

Figure 3-8 The filling device.

adjusted so that the water filling the reservoir was of the predetermined temperatures. Two sets of faucets were used in such a way that when one set was filling the tank, the other one was on standby or adjusted to the correct temperature for the next layer. It usually required five hours to fill the reservoir this way.

Because of heat losses and daily changes in temperatures in the laboratory, it was found in both the T-series and the N-series experiments that there was a layer on the surface which was homogeneous. This layer was the extent of vertical convection. In the T-series runs this might be as much as 10 cm thick. In the N-series runs, this was rarely over 5 cm. As long as the withdrawal layer was well within the properly stratified zone, however, this homogeneous top layer would have no effect. This layer may be seen in figure 3-1 by the dye diffusion through overturning.

3-7 Measurements of Conductivity Profiles and Temperature Profiles

When the reservoir was filled with a salt-stratified fluid in the N-series runs, it was allowed to stand for approximately fifteen hours or overnight so that diffusion would render the density distribution smoothly linear. The density profile was measured indirectly by measuring, in this case, the conductivity profile. After the calibration, which was done before each run, the longer probe was mounted on a point gage and the conductivity profile taken by measurements at 0.05 ft intervals, first with the probe going down from the free surface to the bottom and then a second traverse in the other direction. A very slight difference was observed between the two measurements and the average was taken as the correct value. From the calibration, the specific gravity

may be obtained directly. The density profile may then be plotted and the gradient of density, ϵ , obtained. A typical density profile is shown in figure 3-9. A photograph of the process of measuring the conductivity profile is shown in figure 3-10.

For the T-series runs, the temperature profile was taken at the beginning and end of each experiment. These were almost identical and the mean was taken as the correct value. The specific gravity of the water corresponding to the observed temperatures were obtained from the table in the Handbook of Chemistry and Physics, 38th Edition, p. 1990. The value of the specific gravity so obtained is, of course, slightly incorrect since the table is for distilled water and tap water was used. However, the important parameter ϵ , the density gradient, is essentially correct.

3-8 Measurement of Discharge

After the conductivity profile (in N-series runs) or the temperature profile (in T-series runs) had been measured, the valve at the discharge end of the tank was opened and the flow rate adjusted. The flow was by gravity. The discharge went through the slit, the diffuser, the valves and through a three-foot length of plastic tubing. The end of the tubing was inserted in a beaker and the discharge overflowed over the rim of the beaker, thus maintaining a relatively constant head during each experiment. The discharge was measured volumetrically by allowing the flow to go into another beaker for an interval of time and measuring the volume. This was done three times during each experiment, once at the beginning, once just before the introduction of the second set of dye particles and once at the end of the experiment. In

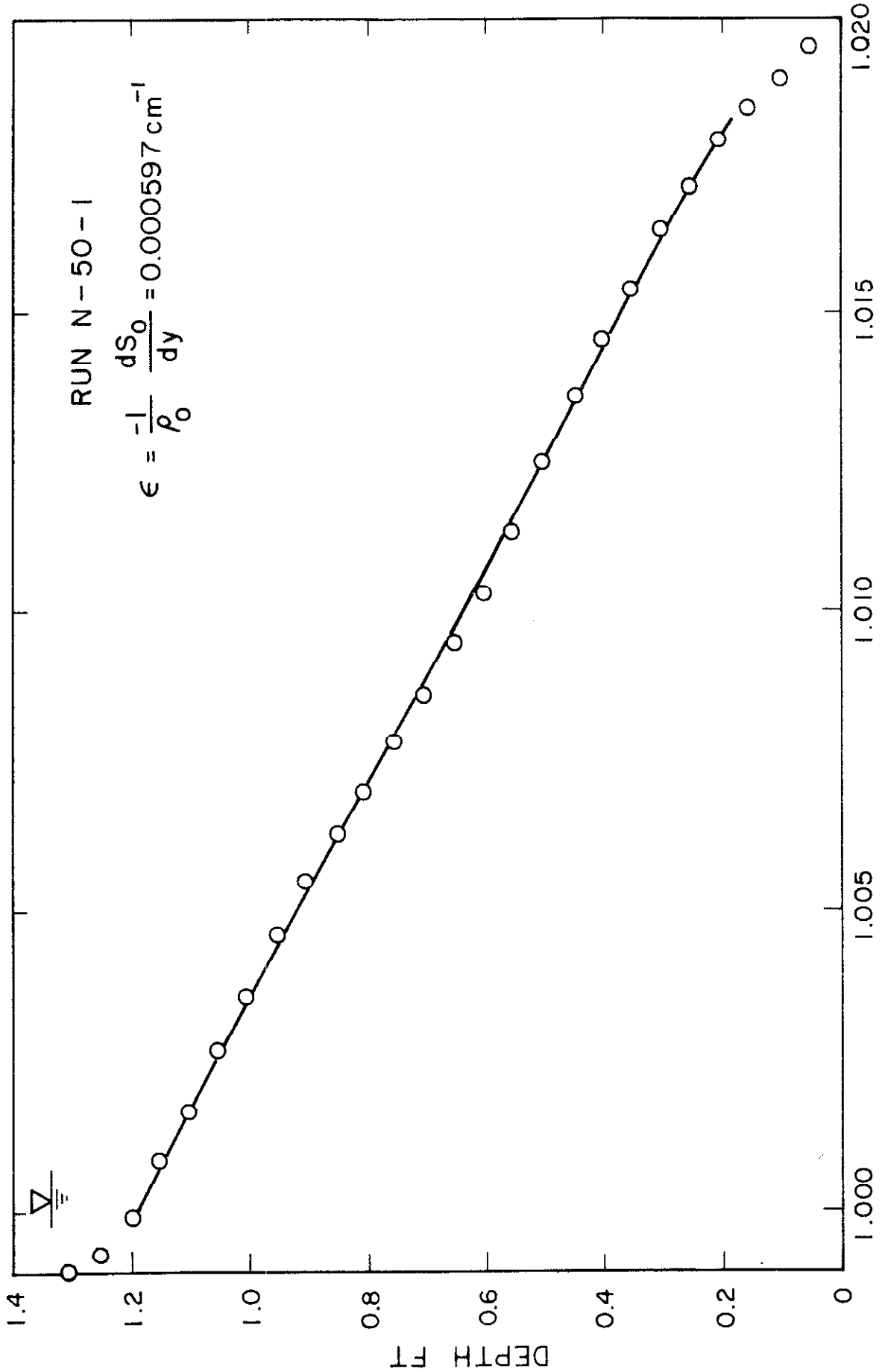

Figure 3-9 Typical measured density profile.

Figure 3-10 Measuring the conductivity profile with the conductivity probe and the Sanborn recorder.

all the N-series runs and two of the T-series runs, these three measurements agreed to within 0.5% of one another. In the other two T-series runs, T-16-0.6 and T-18-2.0, because of a slight leak in the plastic tubing connection, these measurements varied about 5%.

The discharge measurements were not used directly in the calculation of any results which will be presented in the next chapter. They were made merely to establish the fact that the discharge was constant during each experiment. The reasons for not using the discharge measurements as measured volumetrically are: (i) the sidewall effect and (ii) the effect of the finite length of the tank. These will be discussed fully in Chapter 5.

3-9 Measurement of Velocity Profile

After waiting a period of 10 minutes for the flow to reach a quasi-steady state, the dye particles were dropped from the trough and vertical streaks were formed at various distances upstream from the sink. This process may be readily visualized with the help of figure 3-1. Photographs were taken with the camera successively in the three camera stations. After roughly fifteen pictures over a 15-minute period, another set of dye particles was dropped and another series of photographs taken.

When the film was developed, the negative of the first picture was then placed in the enlarger in the darkroom and the magnification adjusted so that the projected image was either full or half of true size. A dye streak was then traced on a sheet of paper. Reference marks in the shape of crosses on the front side of the tank at various distances upstream were also traced onto the paper. A horizontal line at the

level of the sink had also been drawn on the side of the tank and was also traced. The negative for the next photograph taken at the same position was then projected on the same paper, which was lined up with the help of the various cross marks and the horizontal line at the level of the sink. The new image of the same dye streak may then be traced onto the same piece of paper. This tracing was repeated for other suitable profiles. Approximately ten profiles were selected with locations between about 15 cm to about 175 cm from the sink. The velocity profiles may then easily be calculated from these traces by measuring the distance travelled by the dye lines in known time. The station or distance from the sink, x, may be determined from the scale fixed to the side of the tank.

3-10 Measurement of Time between Pictures

To measure the velocity by using the dye traces, it was necessary to know the time interval between pictures. This was accomplished by using the flash contact on the camera and the remote time marker on the Sanborn Recorder. The camera flash contacts were connected through a relay (since the internal contacts in the camera should not be subjected to too much current or voltage) to the remote time marker contacts on the Sanborn Recorder. When the picture was taken, a mark was produced on the recording paper. This measurement was checked against a stop clock and found to be very accurate. Typical time intervals measured were 20 seconds and the accuracy was within 0.2 second.

CHAPTER 4

EXPERIMENTAL RESULTS

The analysis presented in Chapter 2 for withdrawal from a stratified reservoir is valid provided that $\epsilon\delta$, $q/D\alpha_0 x^{2/3}$, $q/\nu\alpha_0 x^{2/3}$, and δ/x are all much smaller than unity. These conditions are satisfied when the flow rate is small and when x is large as discussed at the end of Chapter 2. In the experiments performed, $\epsilon\delta$ was less than 0.01, $q/D\alpha_0 x^{2/3}$ varied from 10^{-1} to 10^{3}, $q/\nu\alpha_0 x^{2/3}$ varied from 10^{-2} to 10, and δ/x from 0.03 to 0.3. Notice again that three of these parameters are necessarily large for small x, that is, near the sink. Therefore, in the experiments no data were collected from the region close to the sink.

In this chapter, the experiments will first be outlined in general with regard to the ranges of the parameters covered. Then the significant experimental results will be presented one by one and finally the conclusions derived from these experiments will be summarized.

4-1 Basic Data for the Experiments

A total of twenty five experiments were performed with water as the fluid. The density variations were achieved by either a temperature variation or a variation in the concentration of salt (NaCl). The values of the pertinent physical parameters involved are listed in table 4-1. This table will now be explained column by column.

Column 1. Run number. The letter N beginning the run number implies salt-induced density change and the letter T implies temperature-induced density change. The number in the middle is a nominal rough estimate of the density gradient in 10^{-5} cm^{-1}. The last number is a rough estimate of the total discharge in cc/sec (total discharge Q = qx width of the tank).

Table 4-1 Summary of Basic Experimental Parameters for Each Run

	$\epsilon = \frac{-1}{\rho_0}\frac{d\rho}{dy}$	q	D	ν	T	d	α_0
Run No.	Density gradient	Unit discharge measured at outlet	Diffusivity	Kinematic viscosity	Temp.	Depth	
	10^{-5} cm^{-1}	cm^2/sec	10^{-5} cm^2/sec		°C	cm	cm$^{-2/3}$
N-8-1.7	7.35	0.127	1.25	900	25.0	43.8	9.13
N-8-3.5	6.76	.271	1.25	900	25.1	43.4	9.0
N-8-11.7	6.76	.904	1.25	900	25.1	43.0	9.0
N-12-0.15	12.8	.0108	1.25	950	22.5	41.3	10.0
N-12-0.3	12.8	.0232	1.25	950	22.5	41.8	10.0
N-12-0.9	12.8	.0723	1.25	970	21.5	41.0	10.0
N-12-2.3	14.4	.179	1.25	950	22.5	41.2	10.2
N-12-4.4	14.4	.335	1.25	960	22.0	40.6	10.2
N-12-10	14.4	.760	1.25	960	22.0	40.5	10.2
N-25-0.04	29.5	.0032	1.25	960	22.0	41.4	11.5
N-25-0.2	26.0	.0153	1.25	960	22.0	41.5	11.3
N-25-0.5	28.9	.0392	1.25	960	22.0	41.6	11.5

	$\epsilon = \frac{-1}{\rho_0}\frac{d\rho_0}{dy}$	$\frac{q}{\beta}$	D	ν	T	d	α_0
	10^{-5} cm^{-1}	cm^2/sec	10^{-5} cm^2/sec		°C	cm	cm$^{-2/3}$
N-25-1.5	26.2	.121	1.25	960	21.8	42.6	11.3
N-25-5	25.6	.412	1.25	960	22.0	43.7	11.2
N-25-9	25.9	.710	1.25	960	22.0	42.0	11.4
N-50-0.13	59.7	.0100	1.25	950	23.0	41.3	13.0
N-50-0.5	59.7	.0376	1.25	950	23.0	41.5	13.0
N-50-1	59.7	.0727	1.25	950	22.5	40.8	13.0
N-50-3	57.0	.245	1.25	960	22.0	41.6	12.9
N-50-6	67.4	.474	1.25	960	22.0	39.7	13.2
N-50-11.7	63.0	.896	1.25	960	22.0	40.0	13.1
T-16-0.6	16.4	.0485	144-149	700-880	26.0-37.0	39.7	4.91
T-18-2.0	18.2	.154	144-149	690-890	25.5-38.0	39.7	5.00
T-21-2.4	20.9	.188	144-150	660-890	25.5-40.0	39.7	5.15
T-10-5	9.5	.388	144-147	760-930	23.6-32.8	41.0	4.45

Thus "Run no. N-8-1.7" means that the density gradient is induced by salt, that the hydrostatic density gradient $\epsilon = \frac{-1}{\rho_0}\frac{ds_0}{dy}$ is roughly 0.00008 cm^{-1}, and that the total discharge is roughly 1.7 cc/sec.

Column 2. $\epsilon = \frac{-1}{\rho_0}\frac{ds_0}{dy}$ is the density gradient, which is measured at the beginning of each experiment. The method of measurement has already been described in section 3-7.

Column 3. q , the unit discharge, is obtained by dividing the total discharge, measured volumetrically at the outlet, by the width of the tank. The local unit discharge may be different from this due to the sidewall effect and the effect of the finite length of the tank. These will be discussed in sections 5-1 and 5-2.

Column 4. D , the diffusivity, is either the molecular diffusivity of salt in water or the thermal diffusivity of water. These values have been obtained from the International Critical Tables, Vol. V, p. 67, and the Handbook of Chemistry and Physics, 38th Edition, p. 2257 respectively.

Column 5. T , the temperature, was measured by a thermometer at the end of each experiment in the N-series experiments. For the T-series experiments, in which the temperature of course changed with depth, the ranges of temperatures are given.

Column 6. ν , is the kinematic viscosity. These values are for pure water taken from the Handbook of Chemistry and Physics, 38th Edition, p. 2030.

Column 7. d , is the total depth of the water measured at the beginning of each experiment.

Column 8. $\alpha_0 = \left(\frac{\epsilon g}{D\nu}\right)^{1/6}$ is a parameter computed from the previous columns. In all the N-series runs $\nu = 10^{-2} cm^2/sec$ was used in this

calculation. In the T-series runs, the means of the range of the ν values were used.

4-2 Measurement and Calculation of Data from Velocity Profiles

Besides the basic measured quantities listed in table 4-1 and the velocity profiles discussed below in section 4-3, the following parameters were measured from selected dye traces (refer to figure 4-1):

i) x, cm, the distance of the dye traces from the sink.

ii) $u_{max}(x)$, cm/sec, the maximum horizontal velocity on a vertical profile at distance x. This is found to be always along the level of the sink.

iii) $y_o(x)$, cm, half the thickness of the withdrawal layer as measured by the intersection of the dye images. This measurement is not very accurate since it is strongly influenced by any misalignment in the process of superposition of the dye images.

iv) $q_f(x)$, cm^2/sec, the forward flowing unit discharge as measured by the area enclosed by the dye images. Throughout the calculations leading to the experimental results, q_f, the measured local unit forward discharge, has been used instead of the average unit discharge q, measured at the outlet. More detailed explanations of the reasons for using q_f rather than q will be discussed in Chapter 5. Suffice it to mention that the finiteness of the tank in length and width is the primary reason for this choice. Thus q was never used in the calculation of any experimental result.

To facilitate comparison between the experimental result and the analytical solution, the same change of q to q_f may be

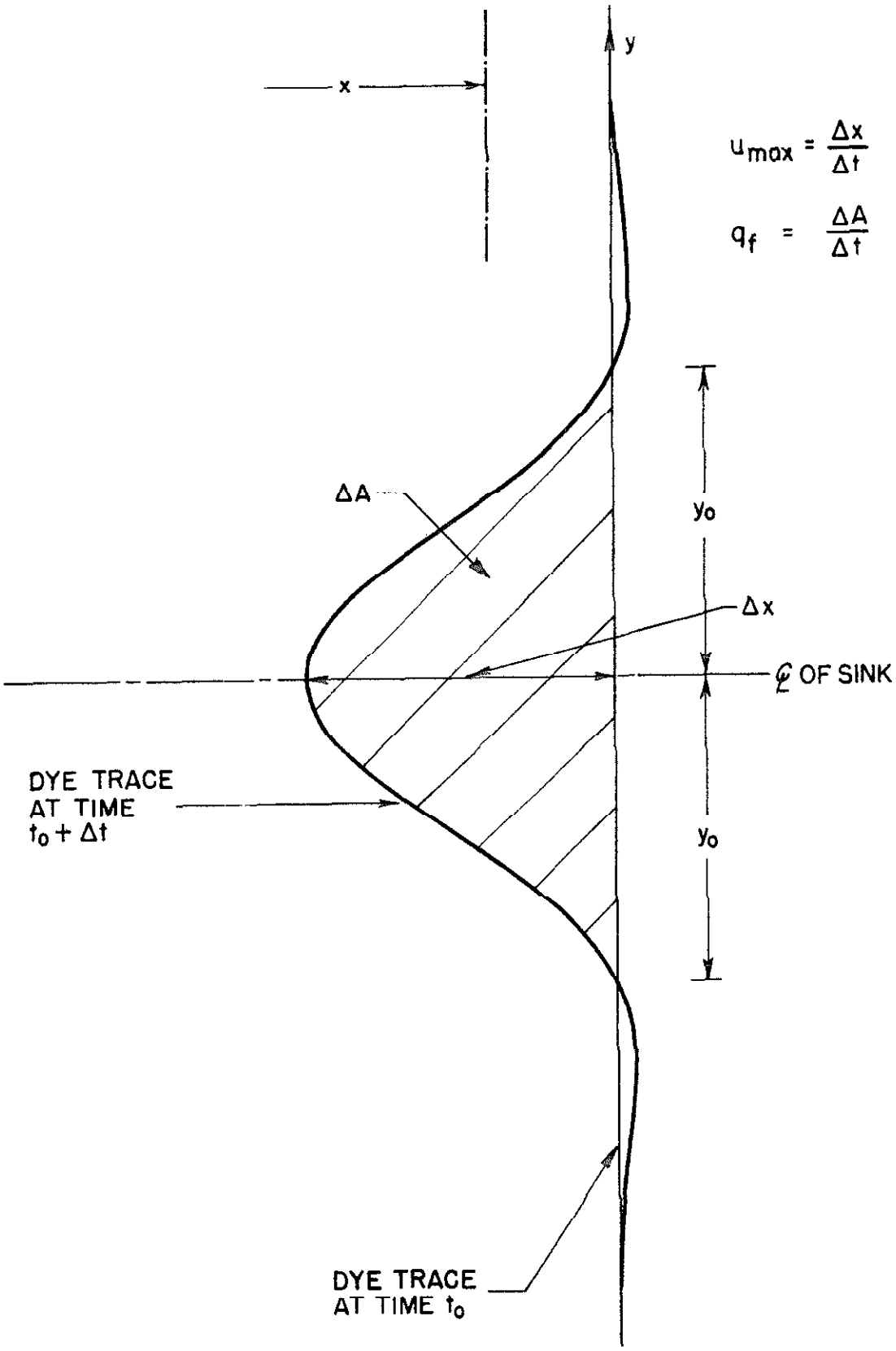
y
x
$u_{max} = \frac{\Delta x}{\Delta t}$
$q_f = \frac{\Delta A}{\Delta t}$
ΔA
y_o
Δx
℄ OF SINK
DYE TRACE
AT TIME
$t_o + \Delta t$
y_o
DYE TRACE
AT TIME t_o

Figure 4-1

accomplished in the analytical solution. Referring to table 2-1 and figure 2-2, it may be verified that

$$\left[\frac{q_{bf}}{q_b}\right]_{theory} = \frac{f_o(3.57)}{f_o(\infty)} = \frac{0.531}{0.500} = 1.06 \quad . \tag{4-1}$$

From these measured quantities, the experimental parameters such as

$$\chi = \frac{\alpha}{\alpha_o} = \frac{|u_{max}|\, x^{1/3}}{q_{bf}\, \alpha_o\, (0.267)} \quad , \quad \frac{q_{bf}}{D\, \alpha_o\, x^{2/3}}$$

may easily be calculated.

4-3 Similarity in the Velocity Profiles.

As has been discussed in sections 3-1 and 3-9, a number of velocity profiles were measured for each experiment. These velocity profiles were for various distances upstream, i.e. various values of x. From the experimental observations, it was noted that there was similarity among these velocity profiles; in other words, when the velocity profiles were plotted in the form u/u_{max} vs. $y/\bar{y}_o$, the curves were the same for all the runs and all the values of x except those very near the sink. Here u_{max} is the maximum velocity which was found to be always at the level of the sink and $\bar{y}_o$ is defined to be

$$\bar{y}_{do} = \frac{q_{bf}}{|u_{max}|}(0.955) \quad , \tag{4-2}$$

where q_f is the forward flowing unit discharge; and the factor 0.955 is used to facilitate comparison with theory, as described below (see

figure 4-1). In plotting the data this way, all the velocity profiles pass through the point $\frac{u}{u_{max}} = 1$ at $\frac{y}{\bar{y}_o} = 0$. Also, in defining $\bar{y}_o$ by equation 4-2, the area under the curve from $y = 0$ to the point where $\frac{u}{u_{max}}$ crosses the $\frac{y}{\bar{y}_o}$ axis is forced to be a constant, since

$$\int_0^{y=y_o} \frac{u}{u_{max}} d\left(\frac{y}{\bar{y}_o}\right) = \int_0^{y_o} \frac{u\,dy}{0.955\, q_f} = \frac{1}{(0.955)2} .$$

The purpose of the dimensionless velocity graphs, figures 4-2 to 4-30, is to demonstrate the similarity in the shape of the velocity profiles for the various experiments. Approximately three to five profiles were selected at random from each experiment and plotted in this way. This similarity in the velocity profiles is one of the most significant results of the experiments.

Although strictly speaking the analytical solution for the velocity distribution should not be applied to the majority of the experiments, it may also be represented in the form $\frac{u}{u_{max}}$ vs. $\frac{y}{\bar{y}_o}$. In fact the number 0.955 in the definition of $\bar{y}_o$ in equation 4-2 was so chosen that the analytical solution represented in that same way, would pass through the point $\frac{u}{u_{max}} = 0$ at $\frac{y}{\bar{y}_o} = 1$. As a comparison, the analytical solution has been drawn in each of the figures 4-2 through 4-30, as the solid line. It is readily seen that as far as the shape of the velocity profiles is concerned, the experimental results fit the analytical solution extremely well even though the analysis was carried out for values of $\epsilon\delta$, δ/x, $q_f/D\alpha_o x^{2/3}$, and $q_f/\nu\alpha_o x^{2/3}$ all small compared to 1.

From figures 4-2 through 4-5, where complete velocity profiles were shown, it may be seen that the profiles were symmetrical about the line $y = 0$. Thus, in figures 4-6 through 4-30, only the mean of the measured profiles above and below the level of the sink $y = 0$ was

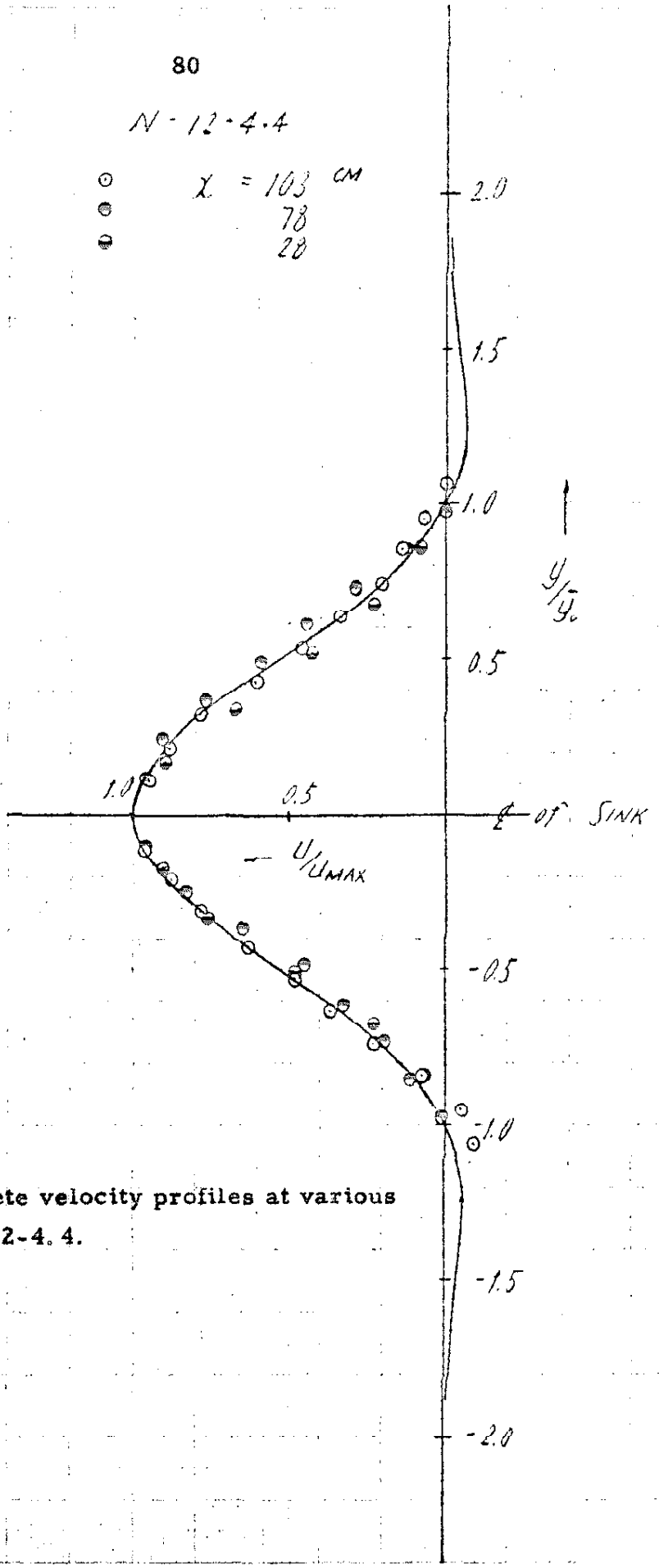

Figure 4-2 Complete velocity profiles at various stations for run N-12-4.4.

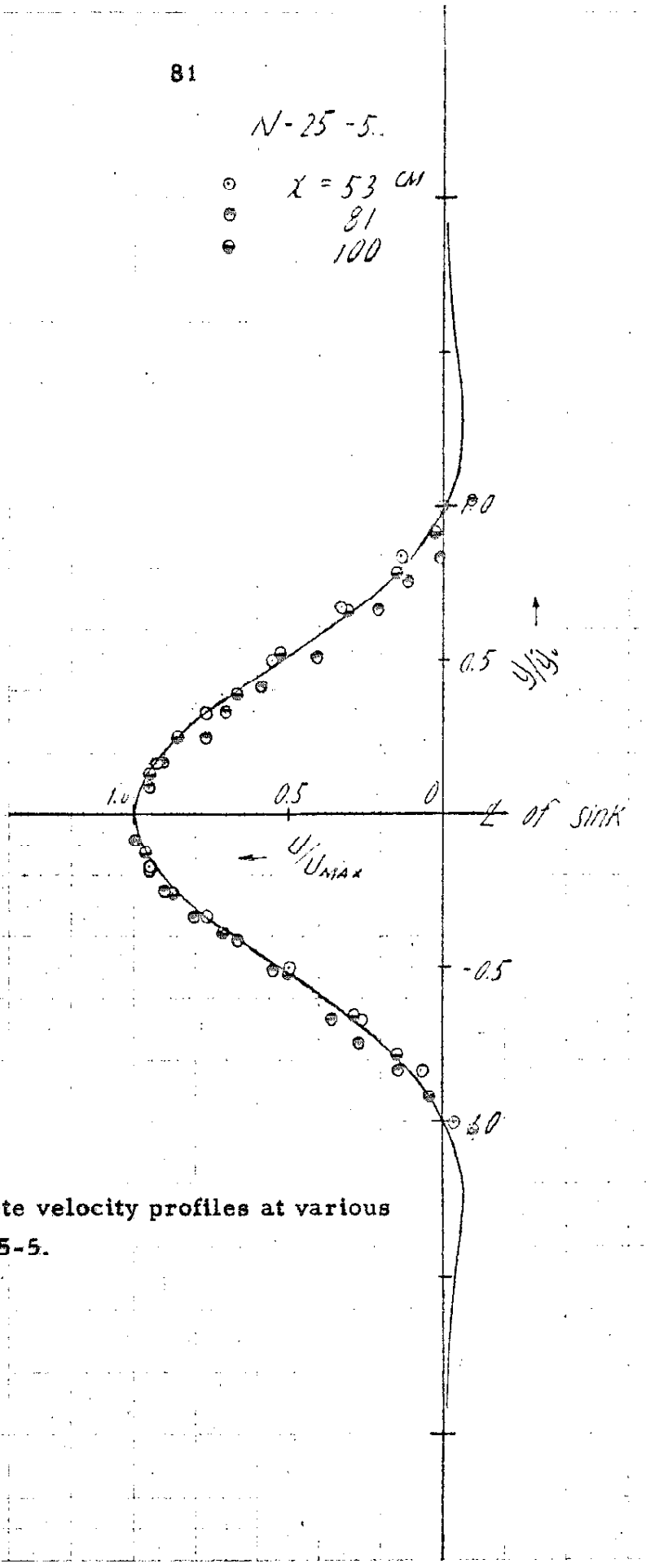

Figure 4-3 Complete velocity profiles at various stations for run N-25-5.

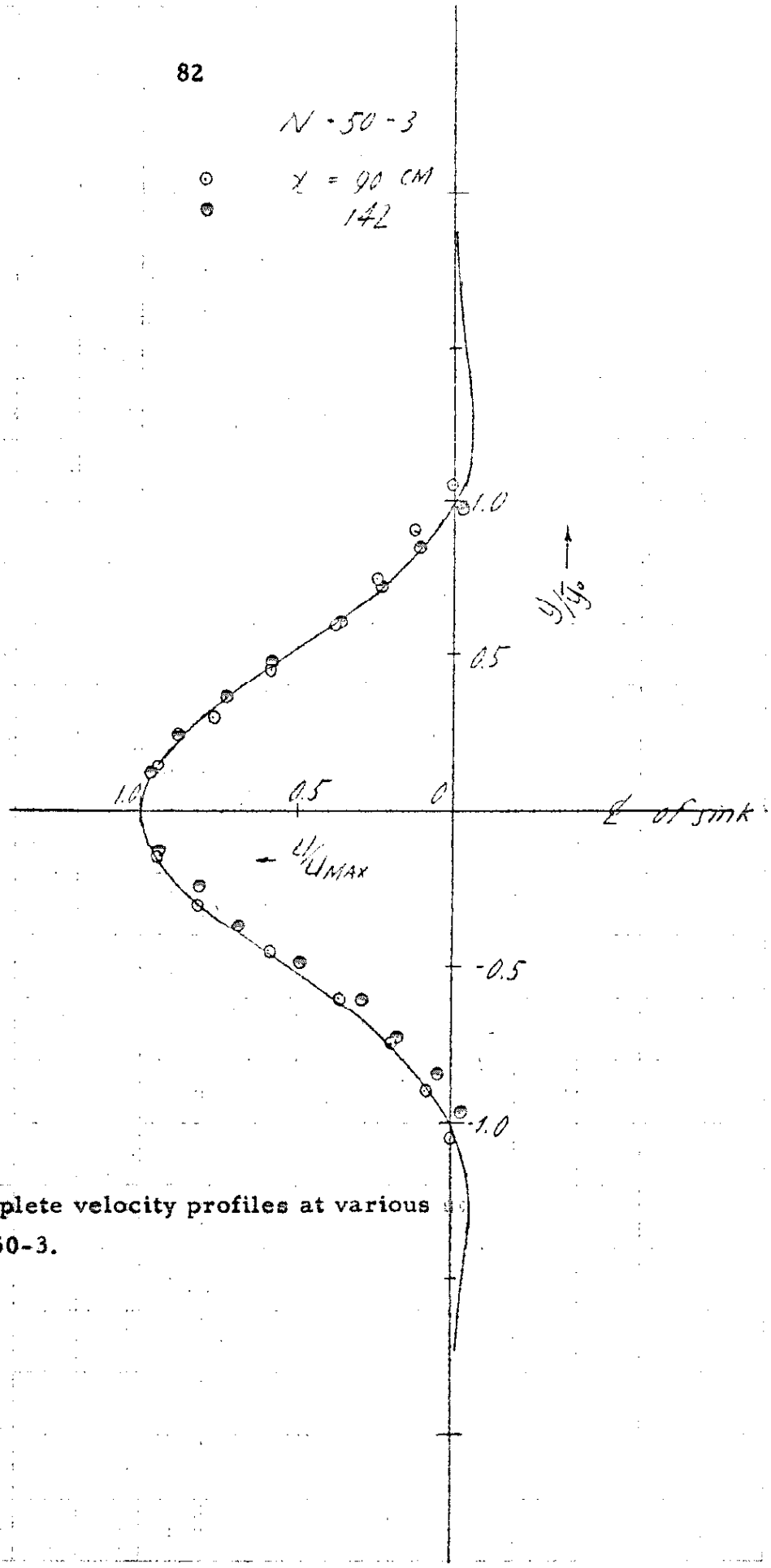

Figure 4-4 Complete velocity profiles at various stations for run N-50-3.

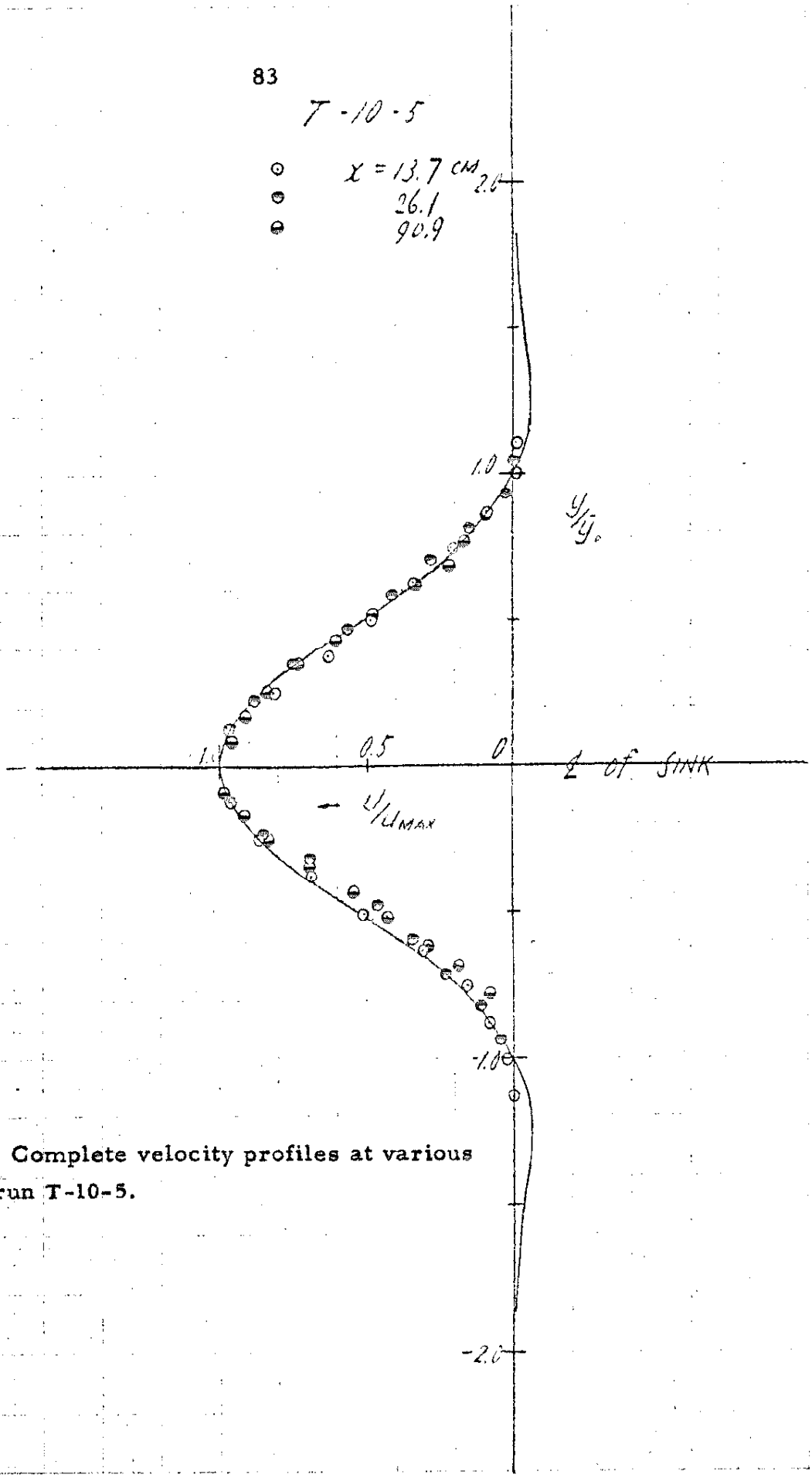

Figure 4-5 Complete velocity profiles at various stations for run T-10-5.

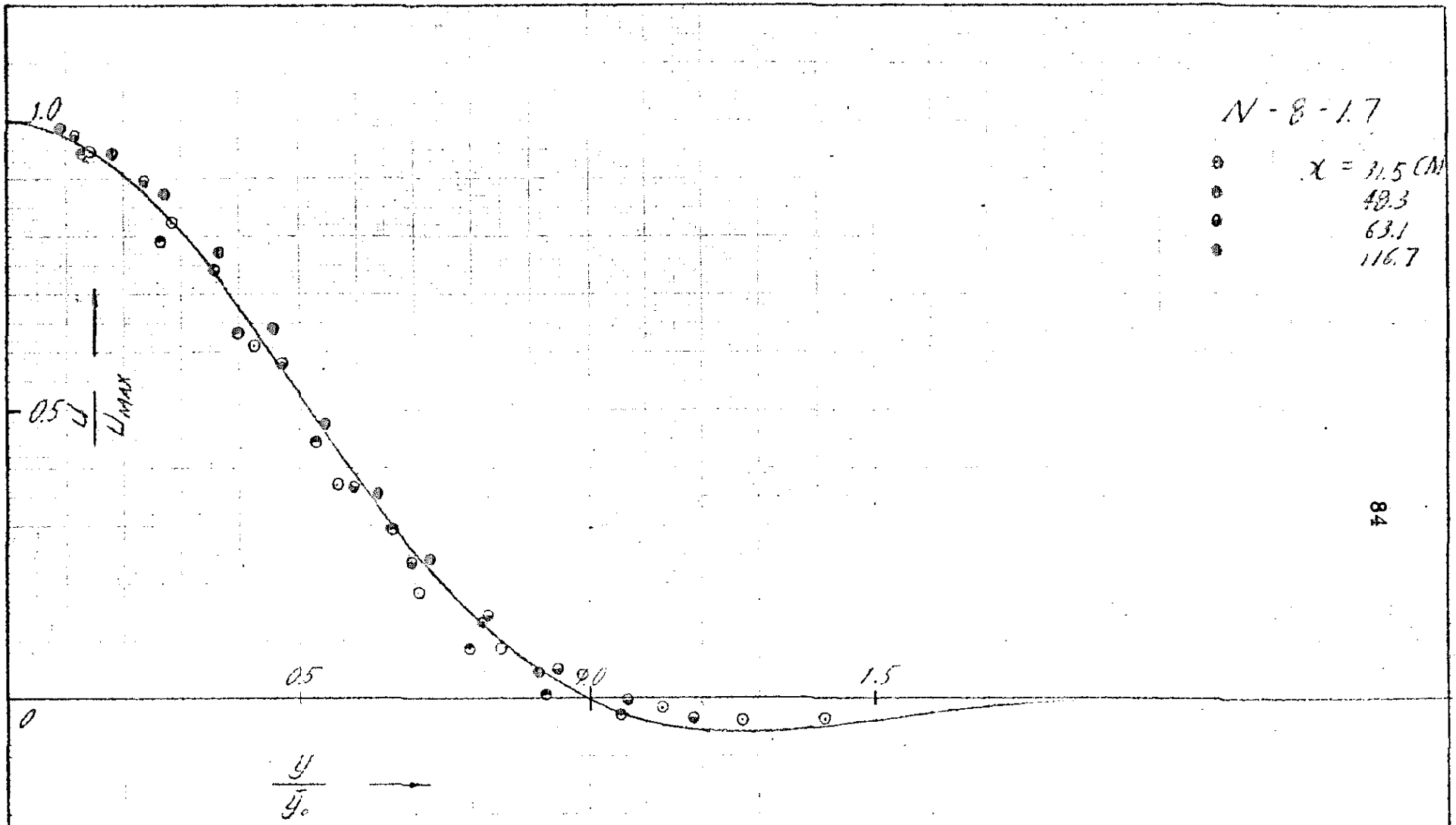

Figure 4-6 Velocity profiles at various stations for run N-8-1.7.

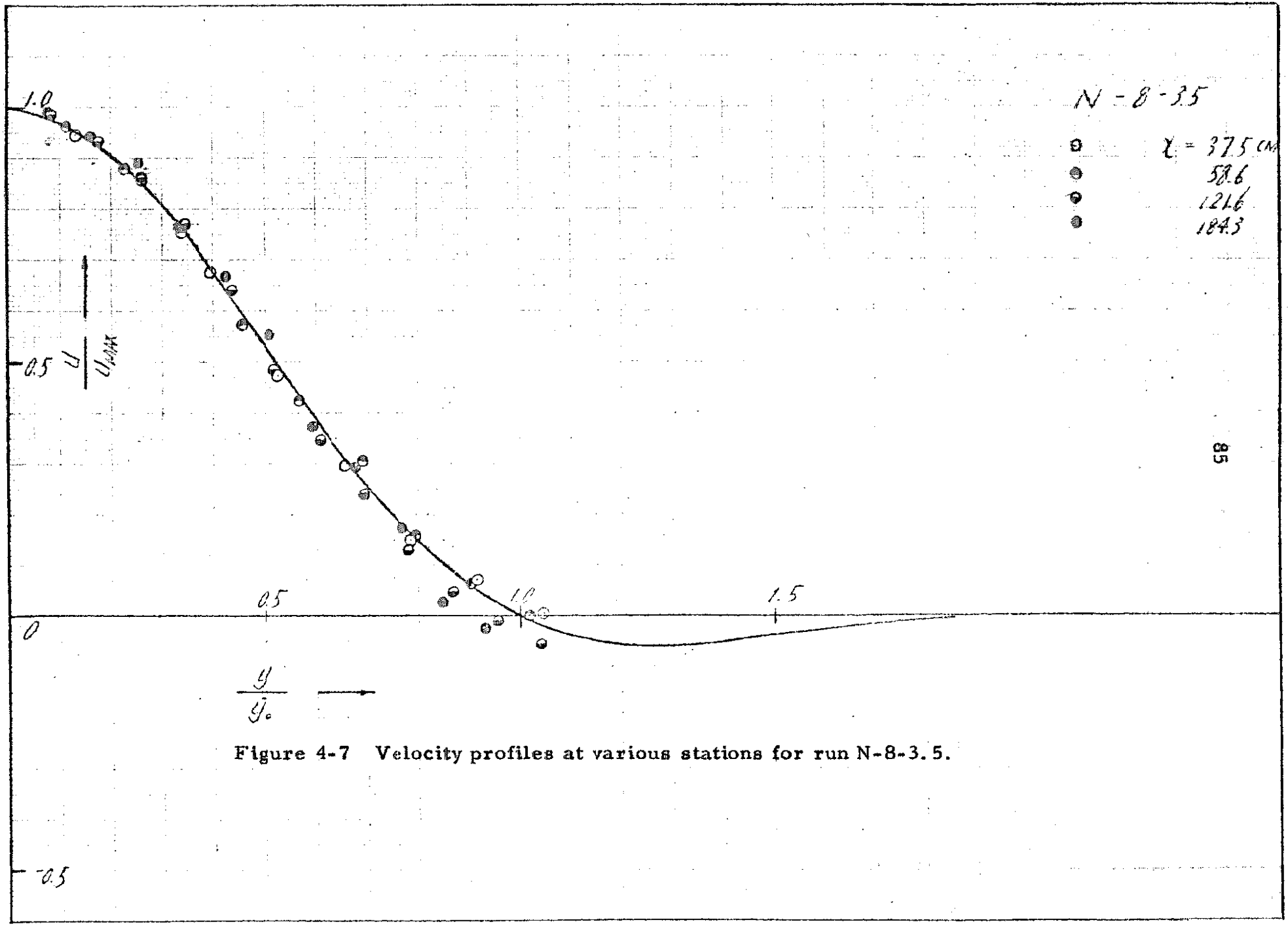

Figure 4-7 Velocity profiles at various stations for run N-8-3.5.

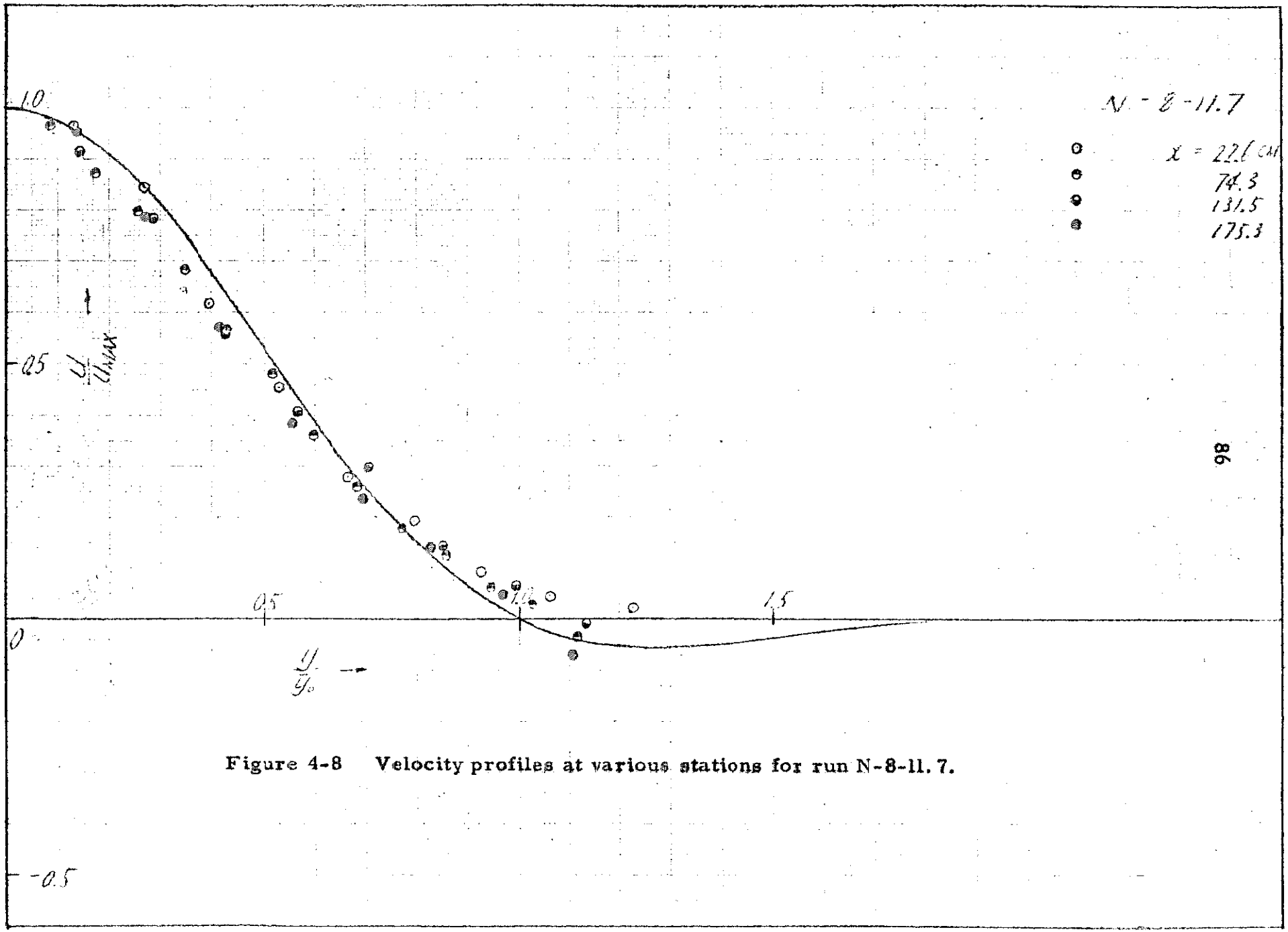

Figure 4-8 Velocity profiles at various stations for run N-8-11.7.

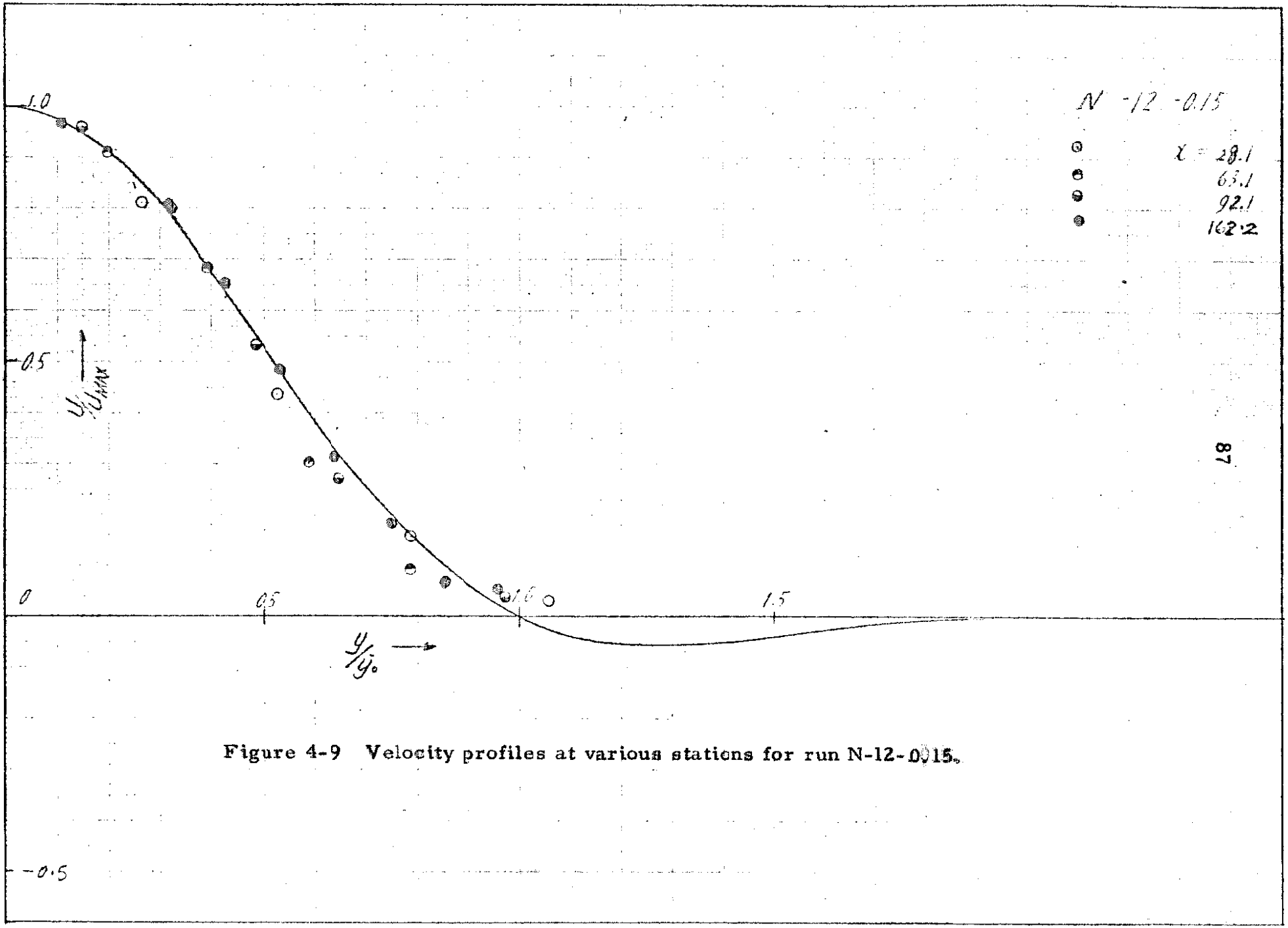

Figure 4-9 Velocity profiles at various stations for run N-12-0.15.

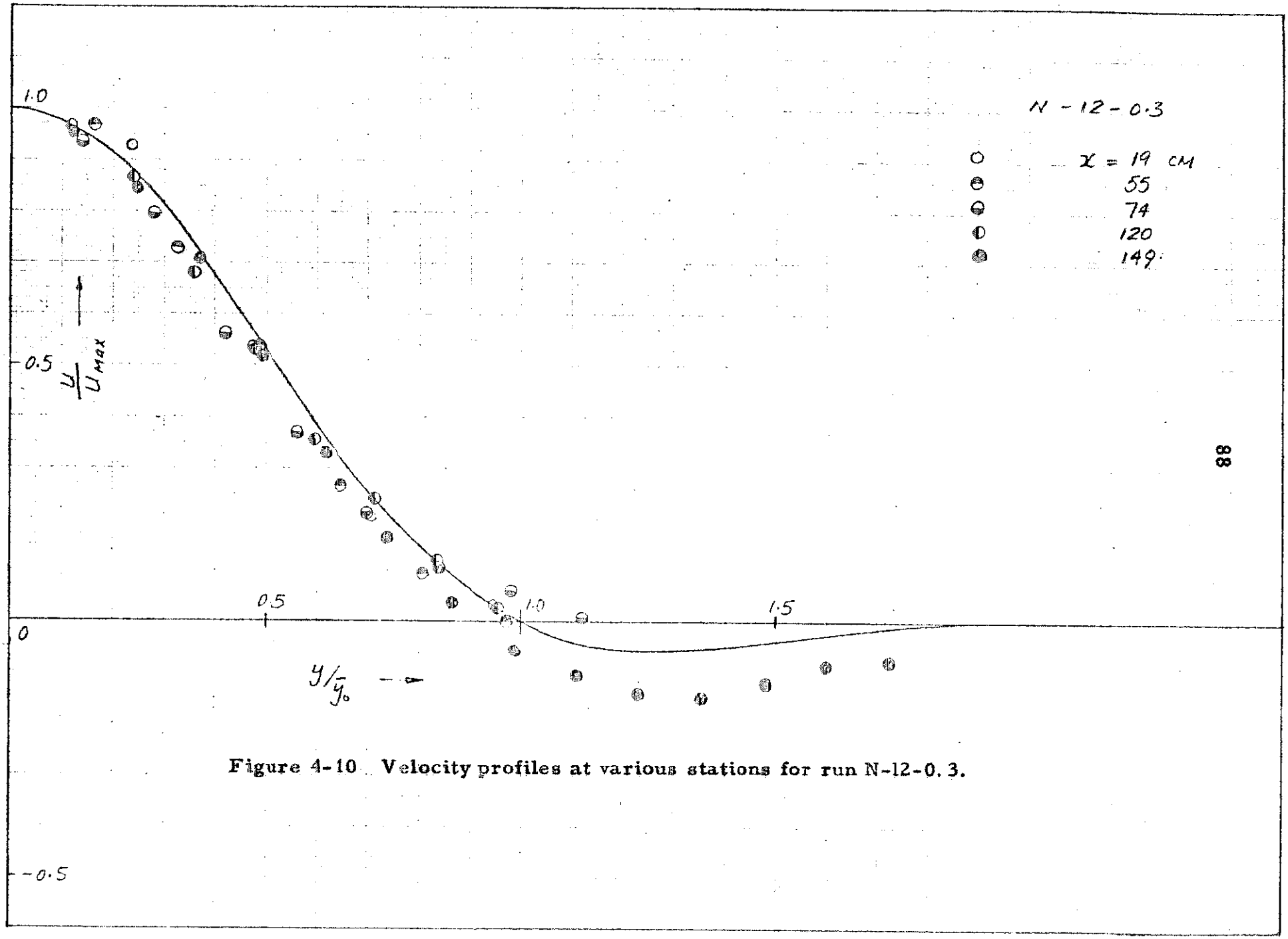

Figure 4-10 Velocity profiles at various stations for run N-12-0.3.

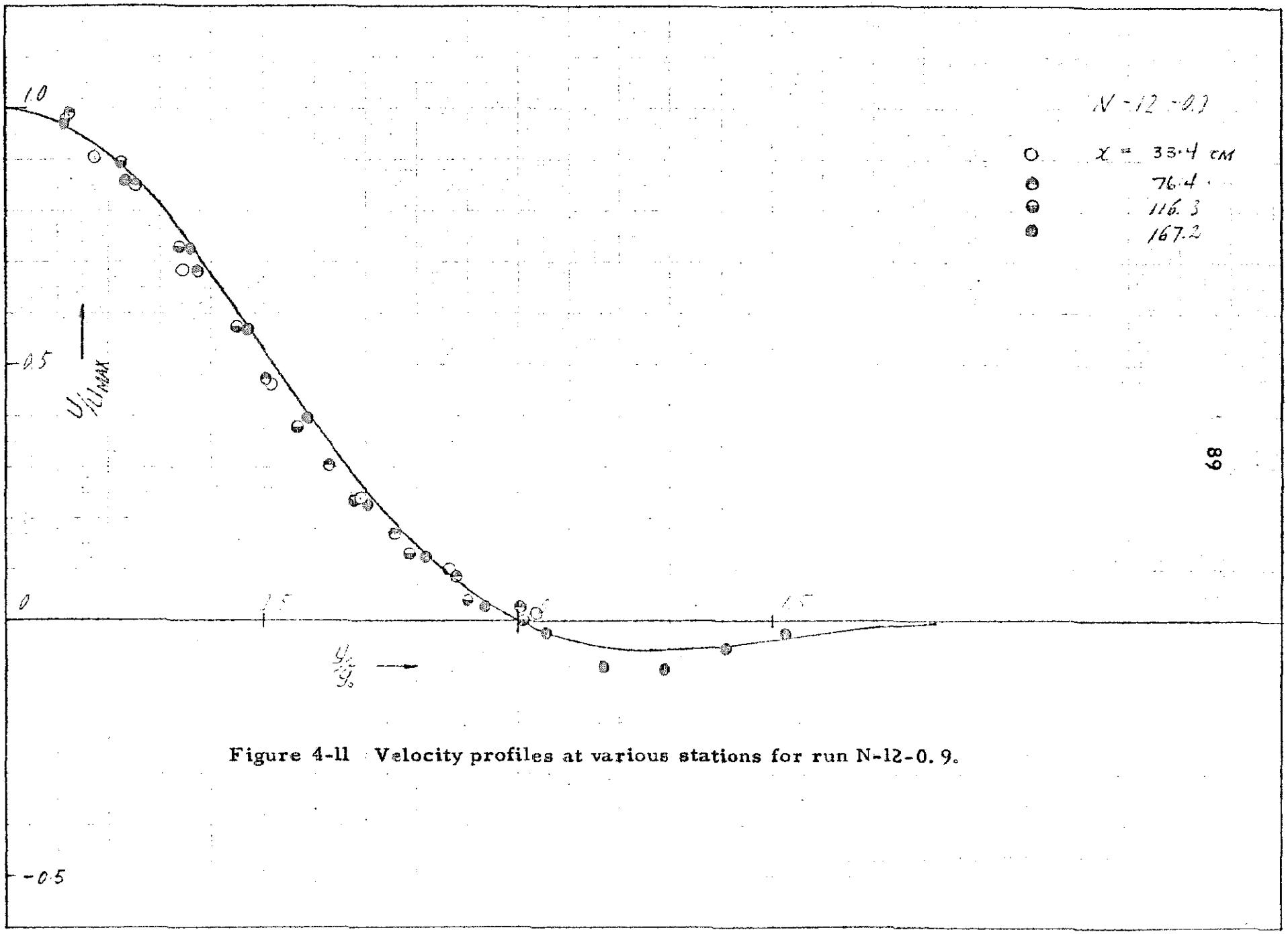

Figure 4-11 Velocity profiles at various stations for run N-12-0.9.

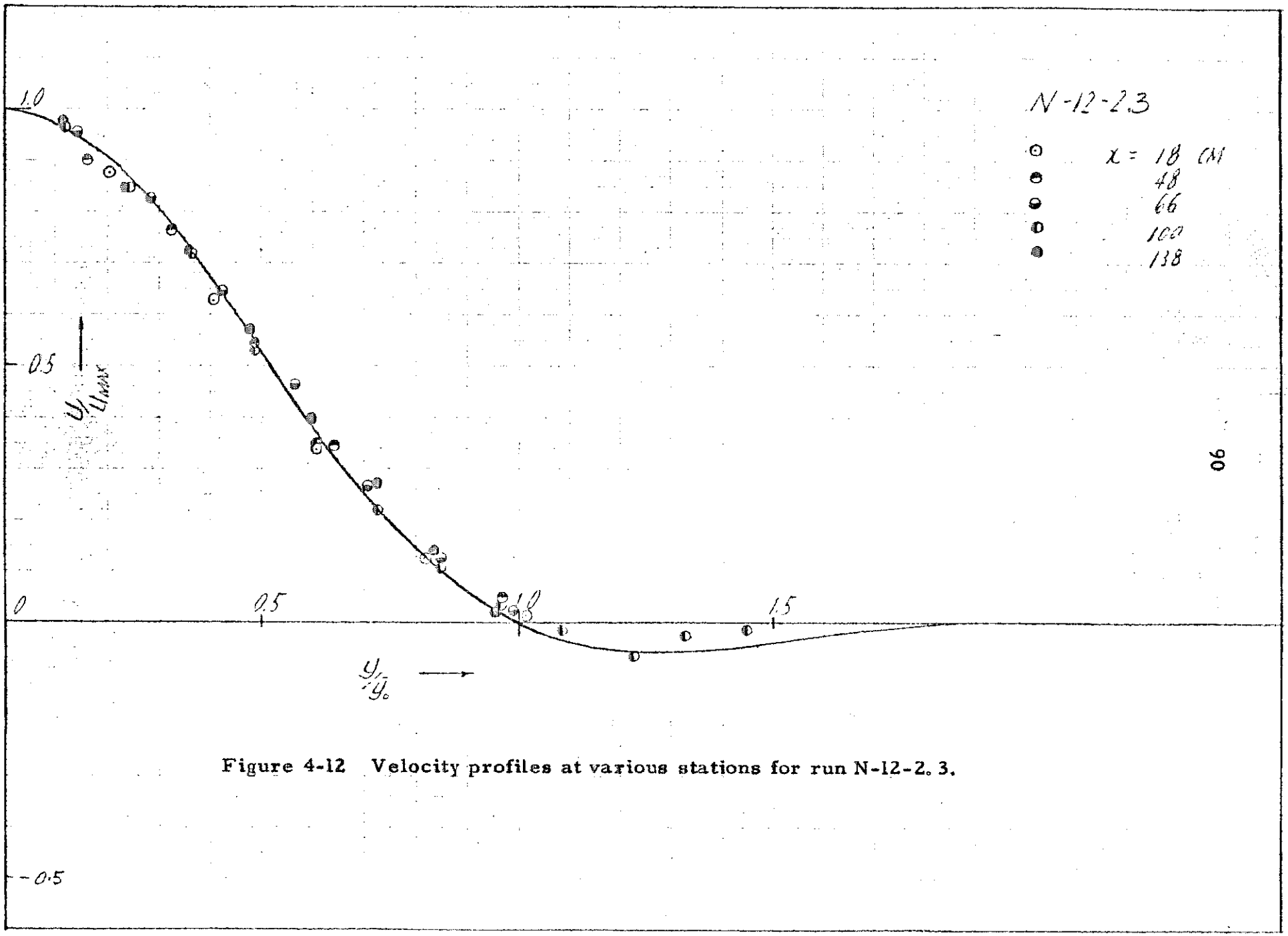

Figure 4-12 Velocity profiles at various stations for run N-12-2.3.

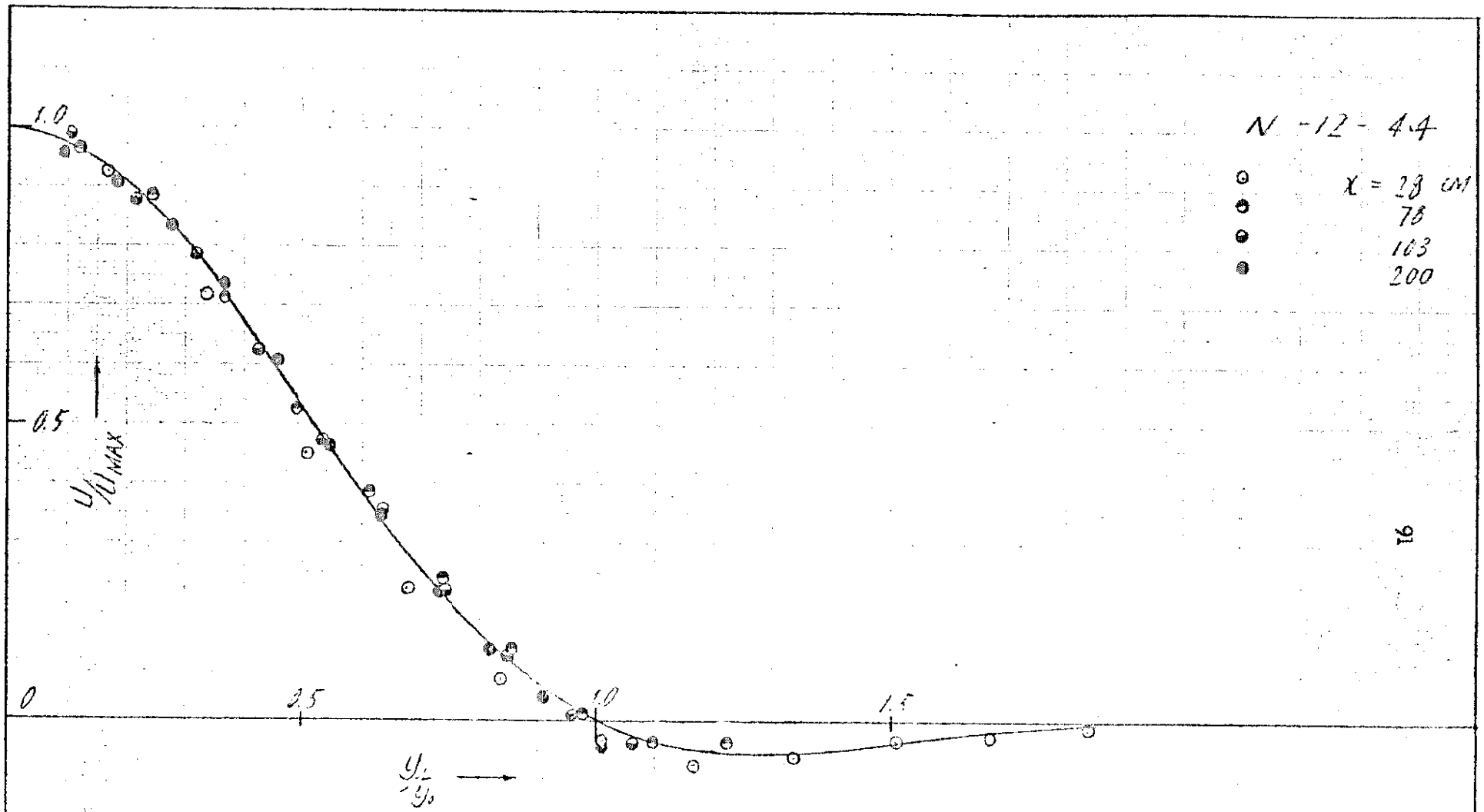

Figure 4-13 Velocity profiles at various stations for run N-12-4.4.

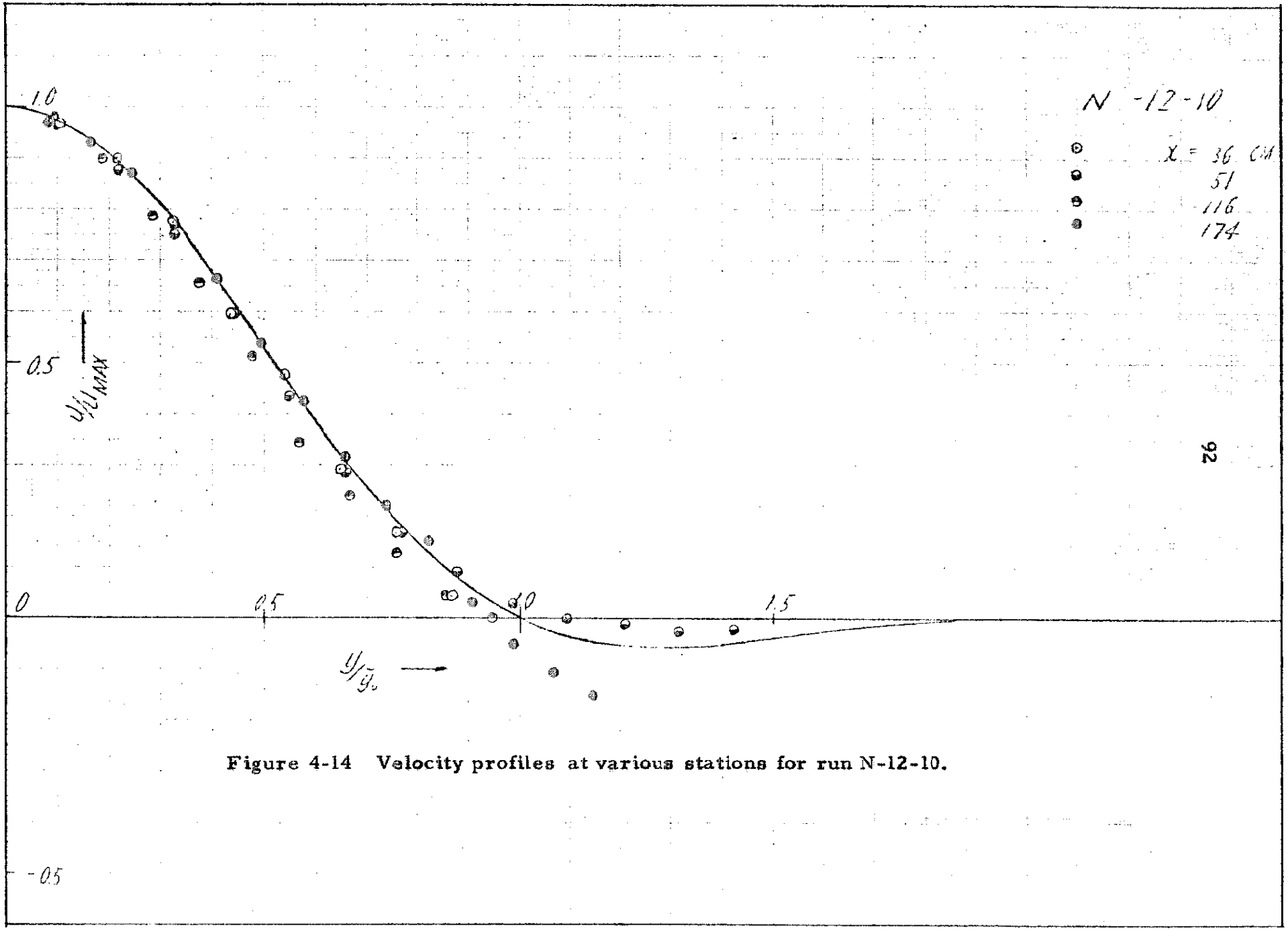

Figure 4-14 Velocity profiles at various stations for run N-12-10.

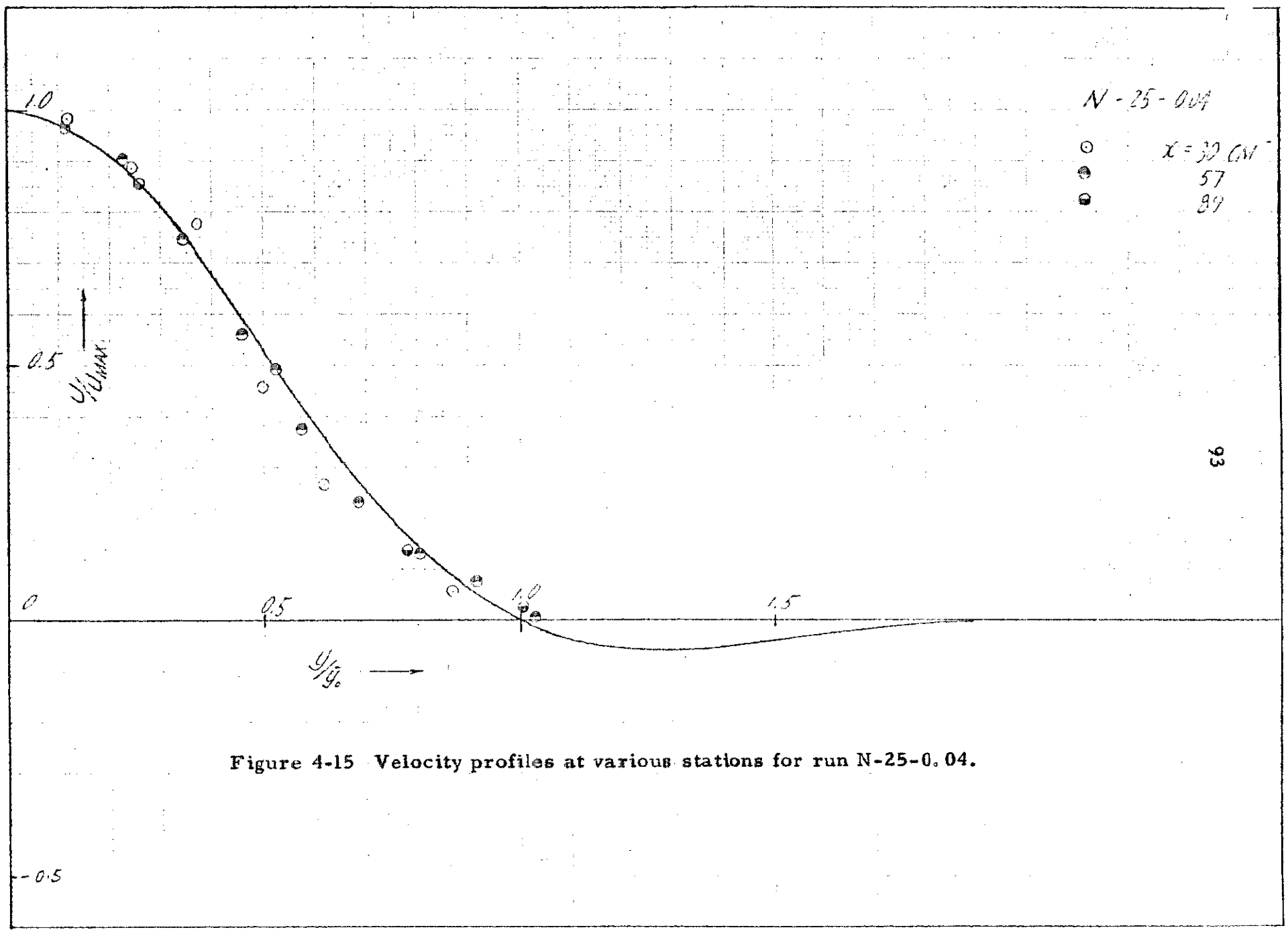

Figure 4-15 Velocity profiles at various stations for run N-25-0.04.

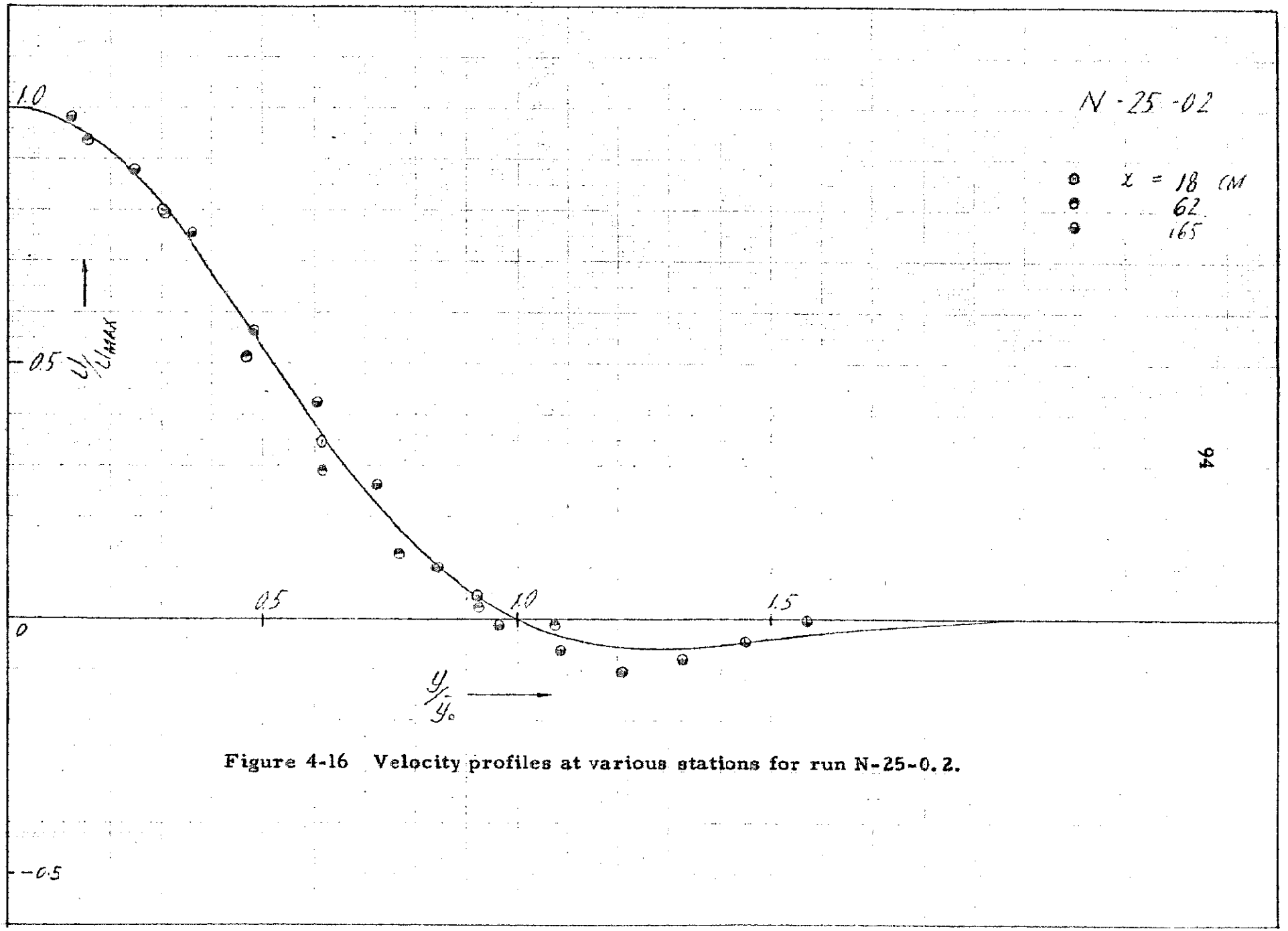

Figure 4-16 Velocity profiles at various stations for run N-25-0.2.

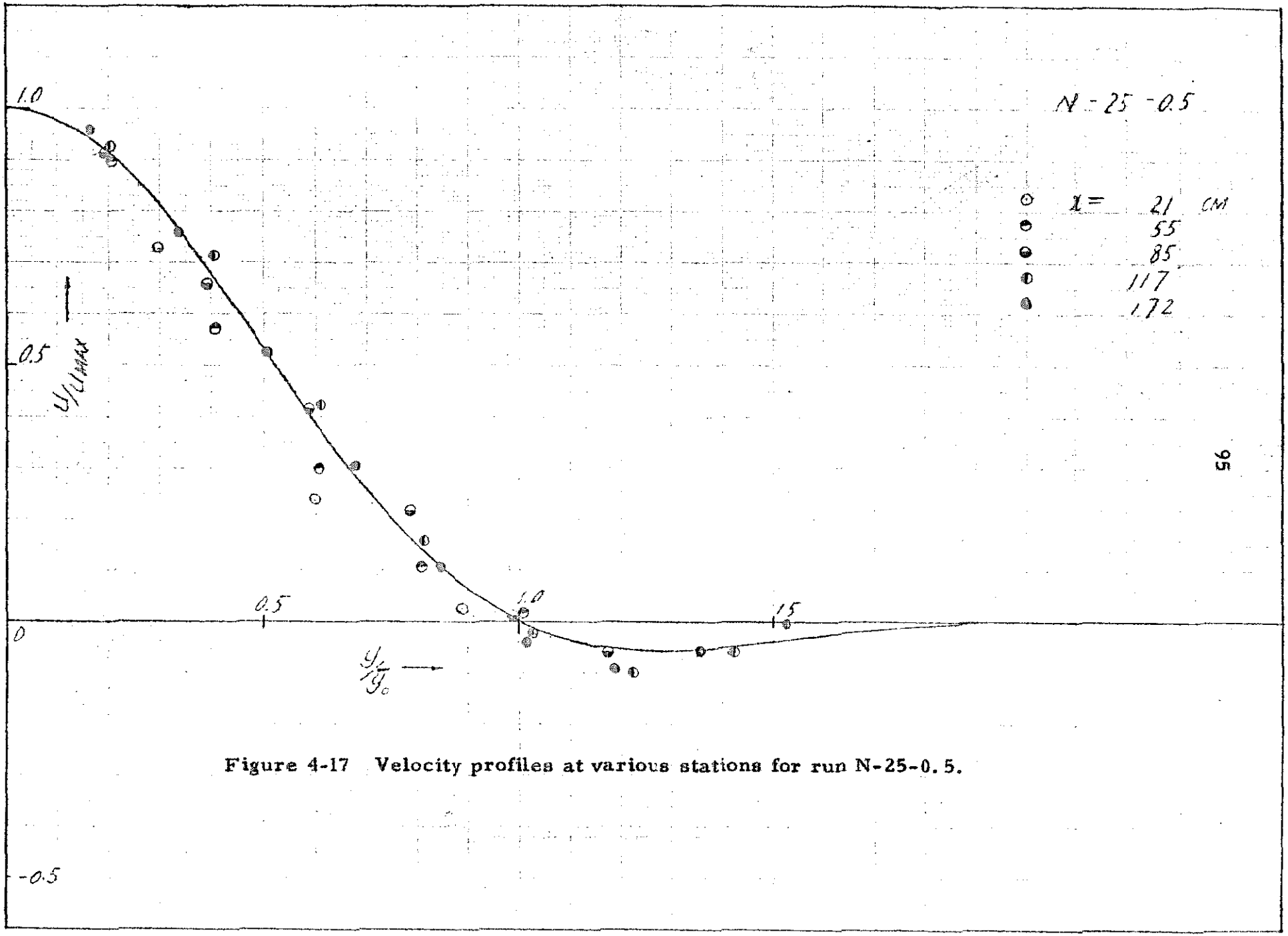

Figure 4-17 Velocity profiles at various stations for run N-25-0.5.

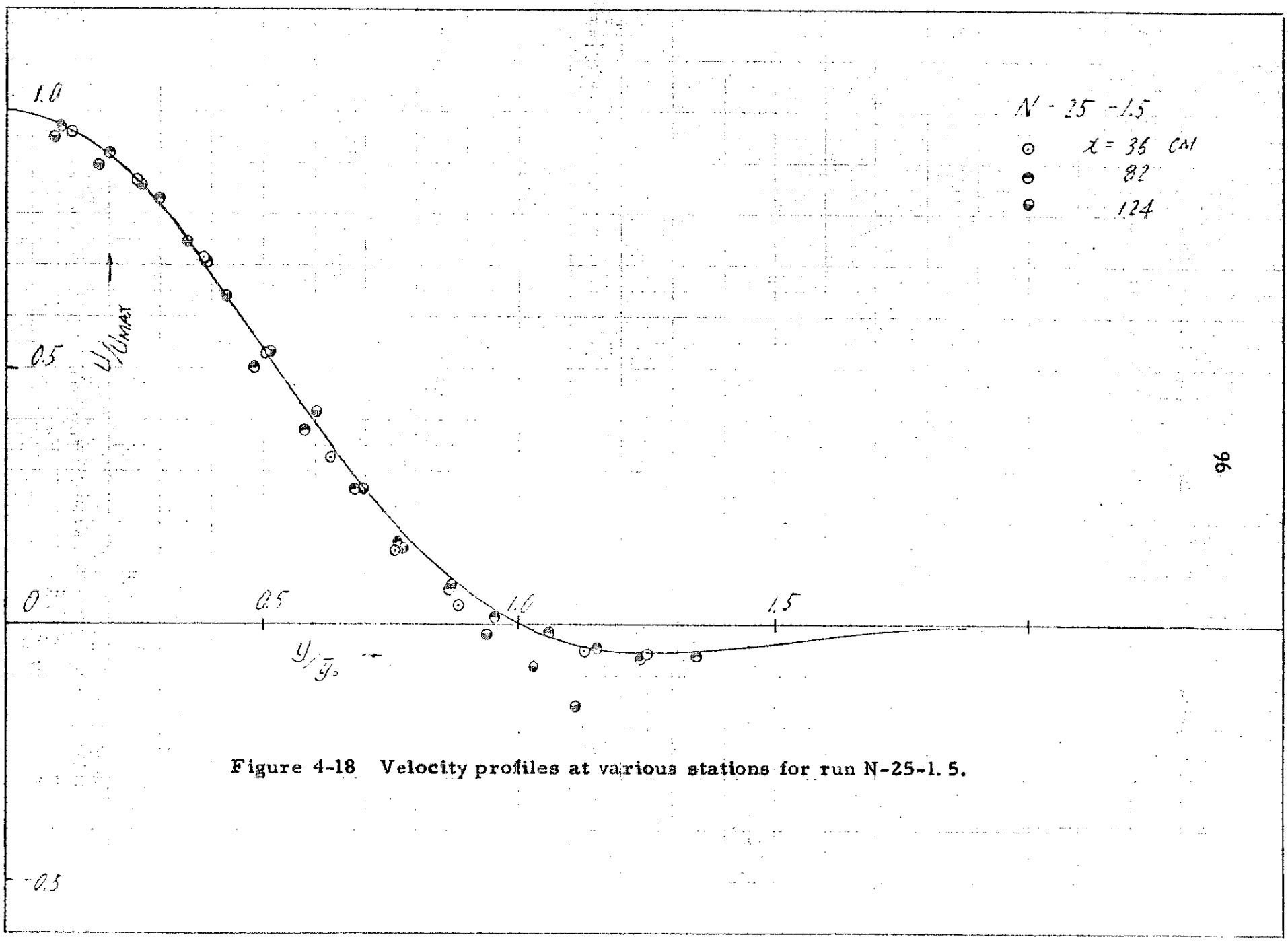

Figure 4-18 Velocity profiles at various stations for run N-25-1.5.

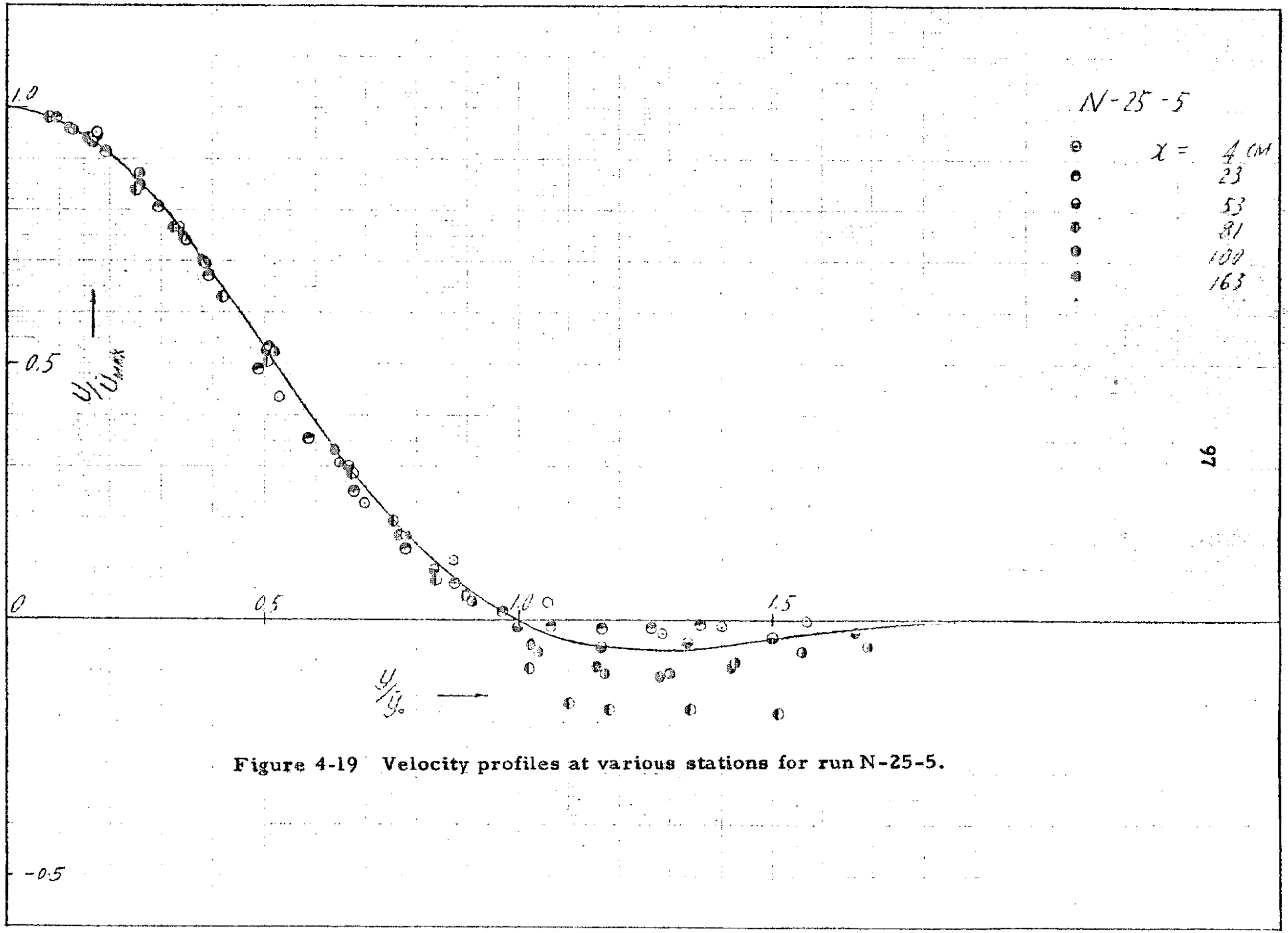

Figure 4-19 Velocity profiles at various stations for run N-25-5.

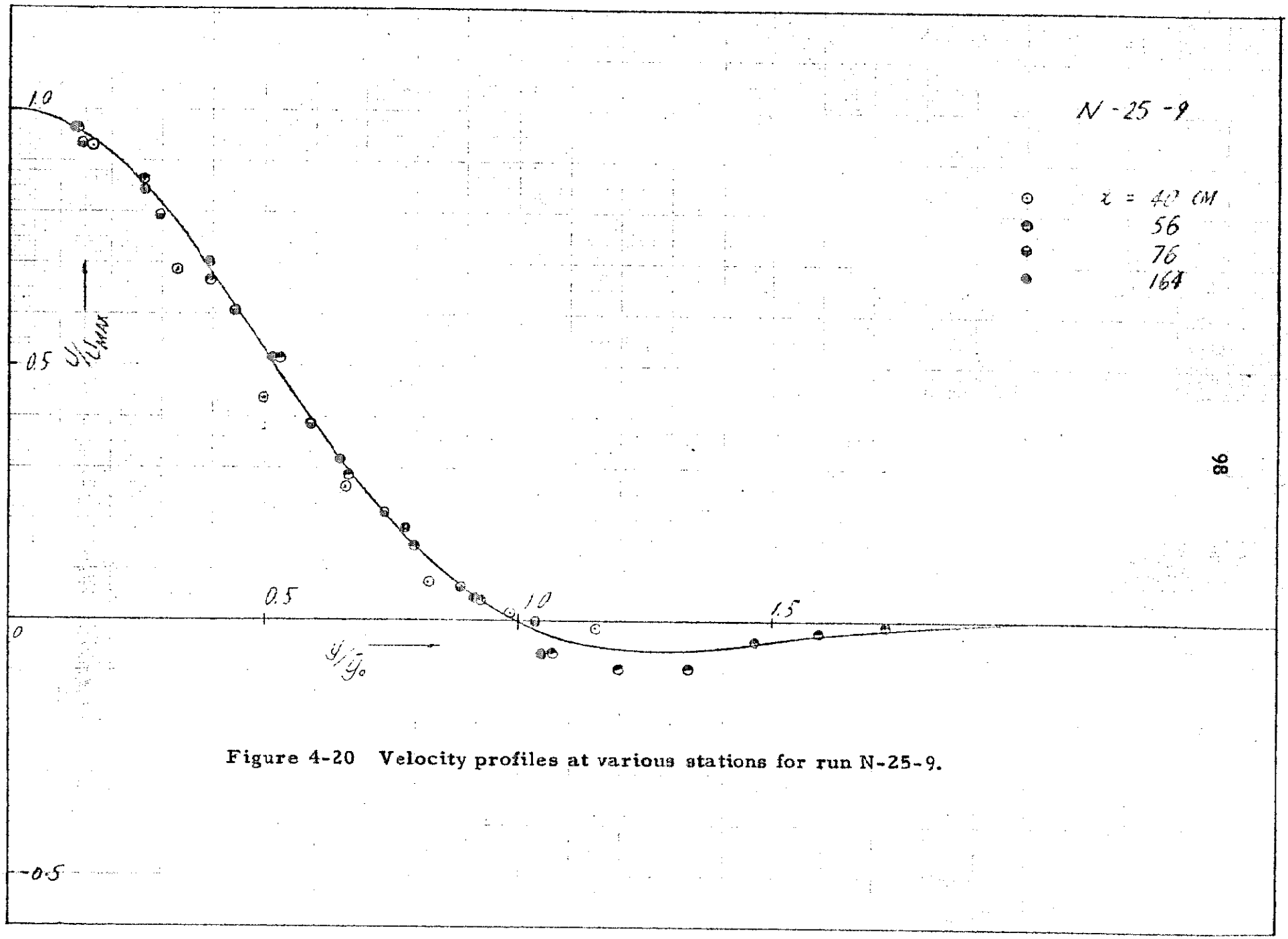

Figure 4-20 Velocity profiles at various stations for run N-25-9.

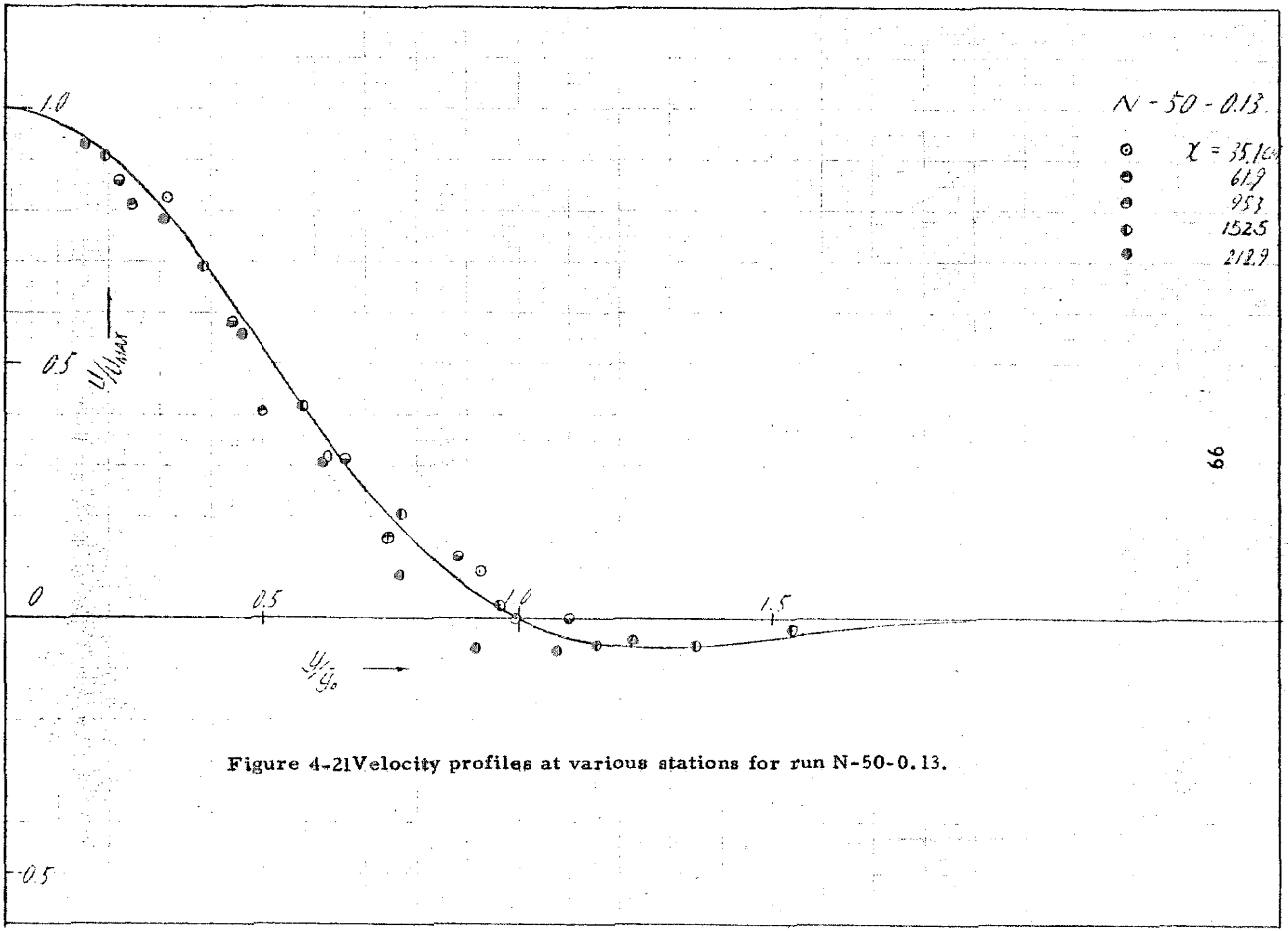

Figure 4-21 Velocity profiles at various stations for run N-50-0.13.

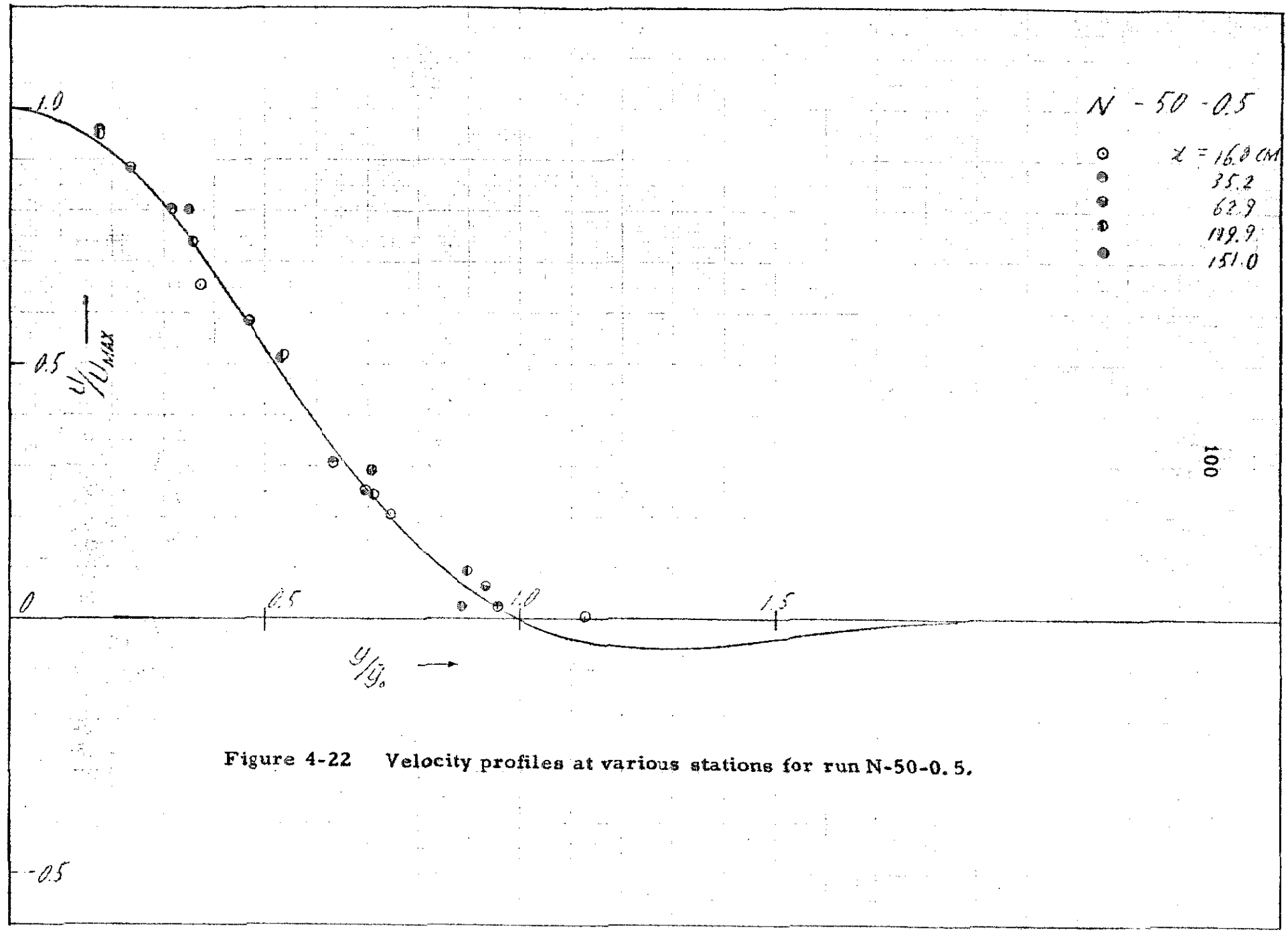

Figure 4-22 Velocity profiles at various stations for run N-50-0.5.

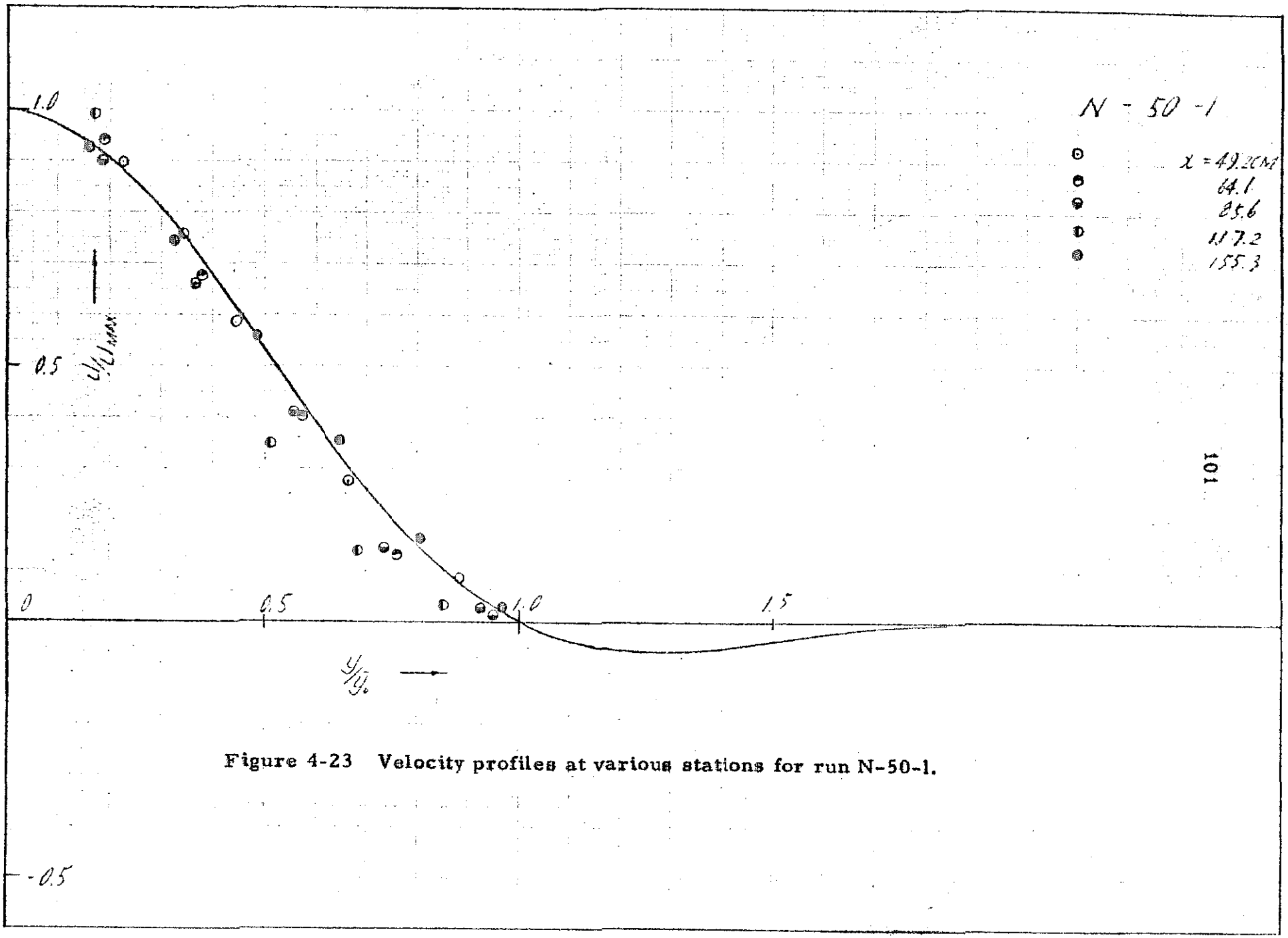

Figure 4-23 Velocity profiles at various stations for run N-50-1.

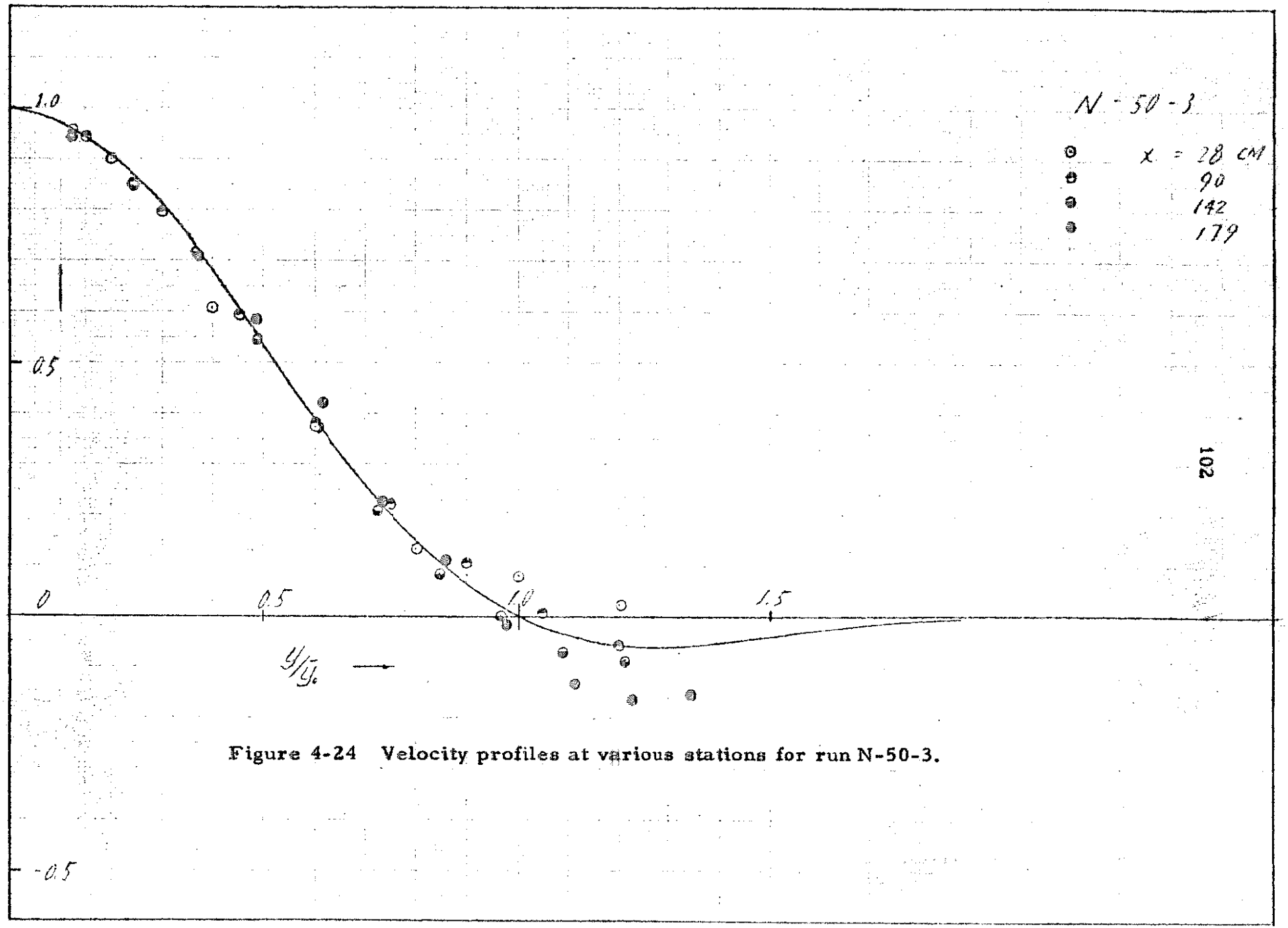

Figure 4-24 Velocity profiles at various stations for run N-50-3.

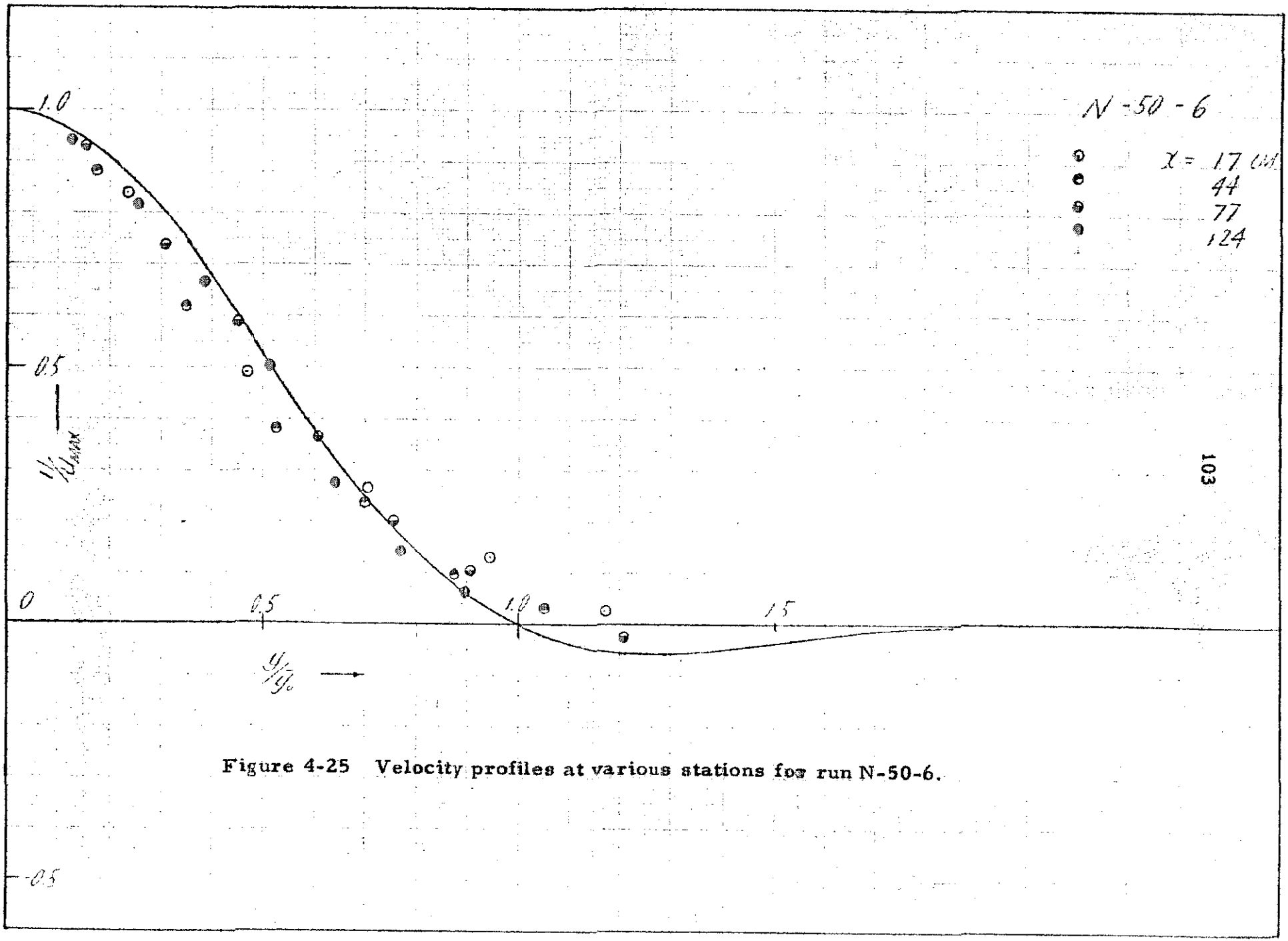

Figure 4-25 Velocity profiles at various stations for run N-50-6.

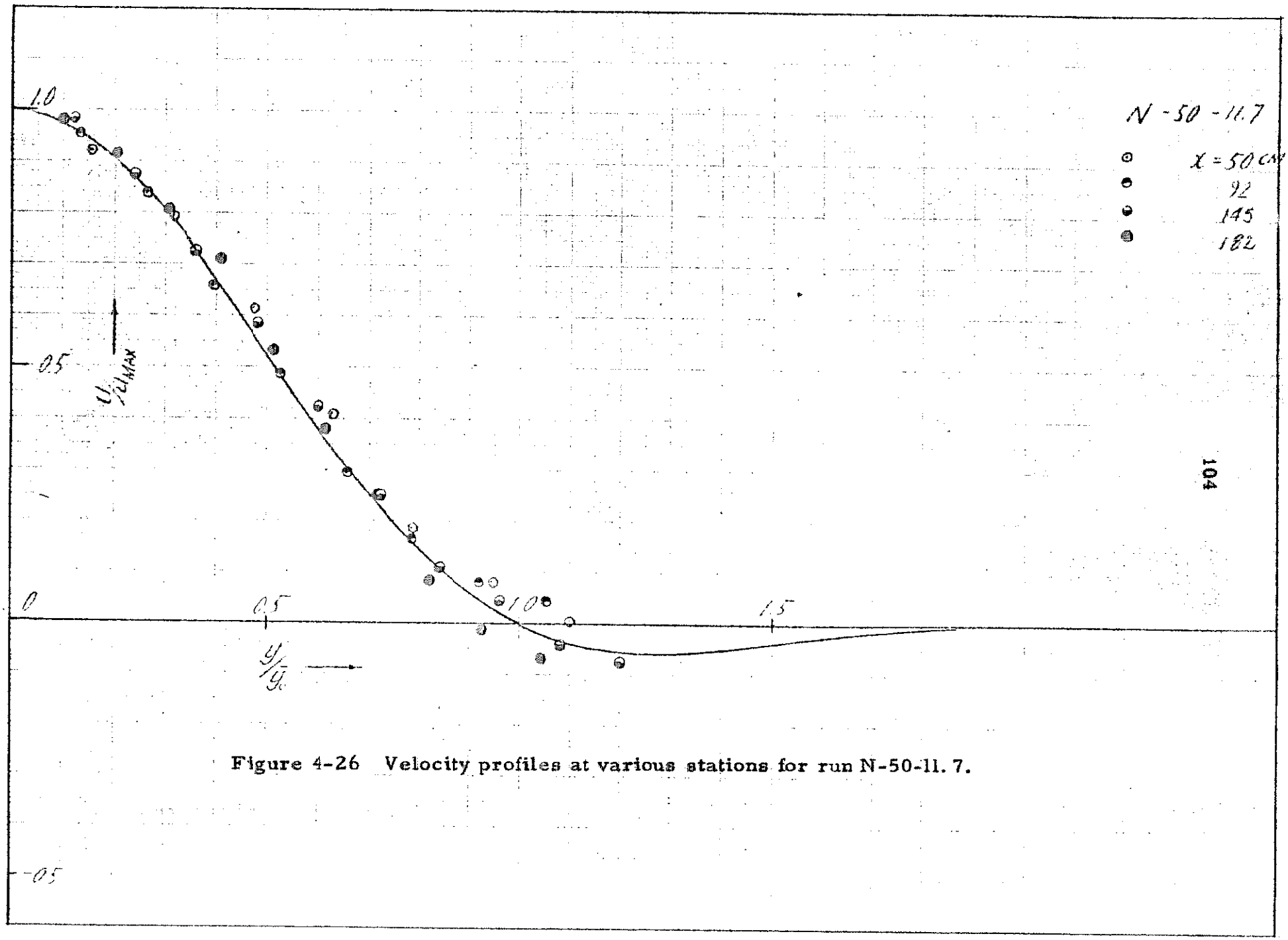

Figure 4-26 Velocity profiles at various stations for run N-50-11.7.

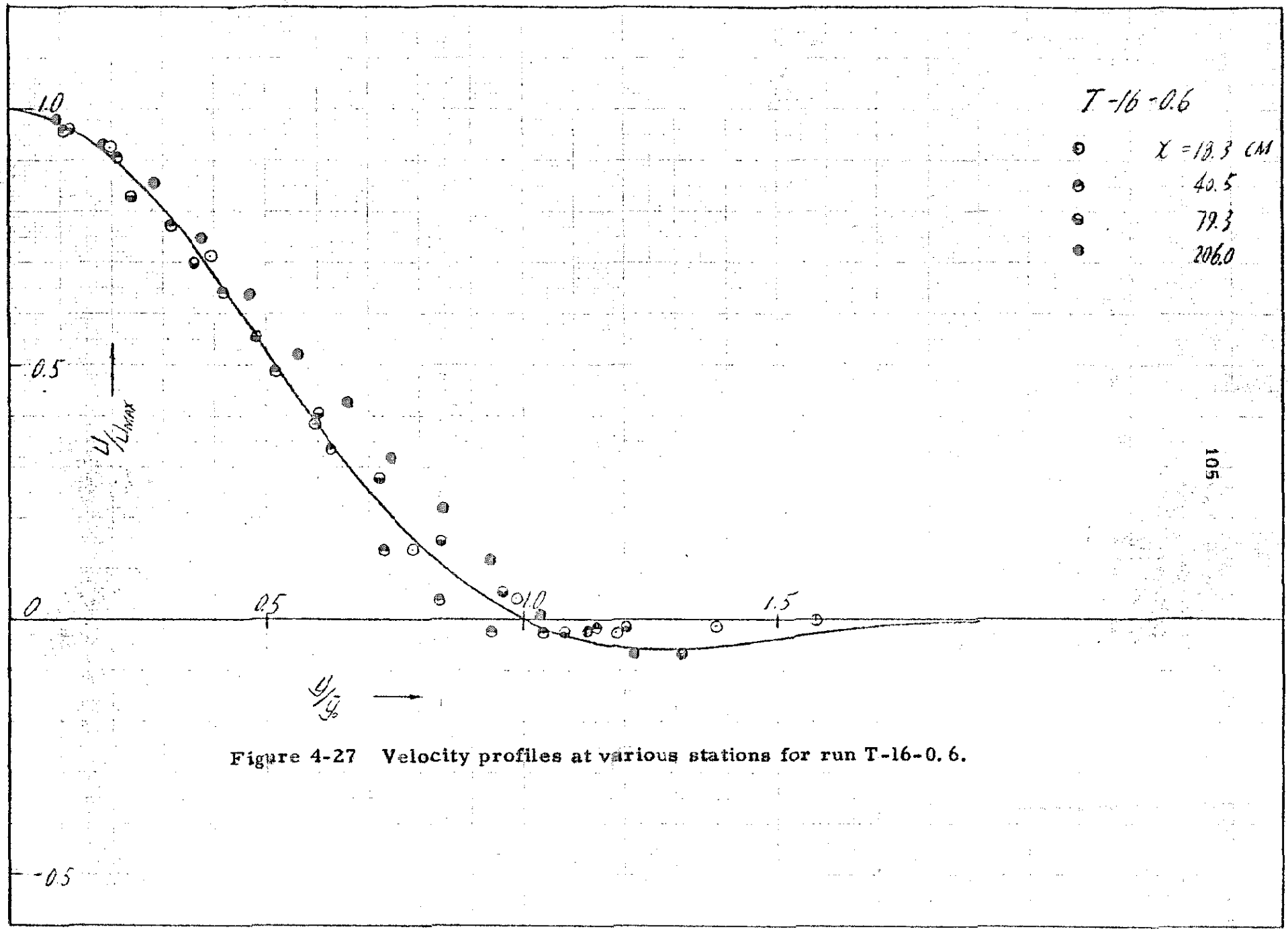

Figure 4-27 Velocity profiles at various stations for run T-16-0.6.

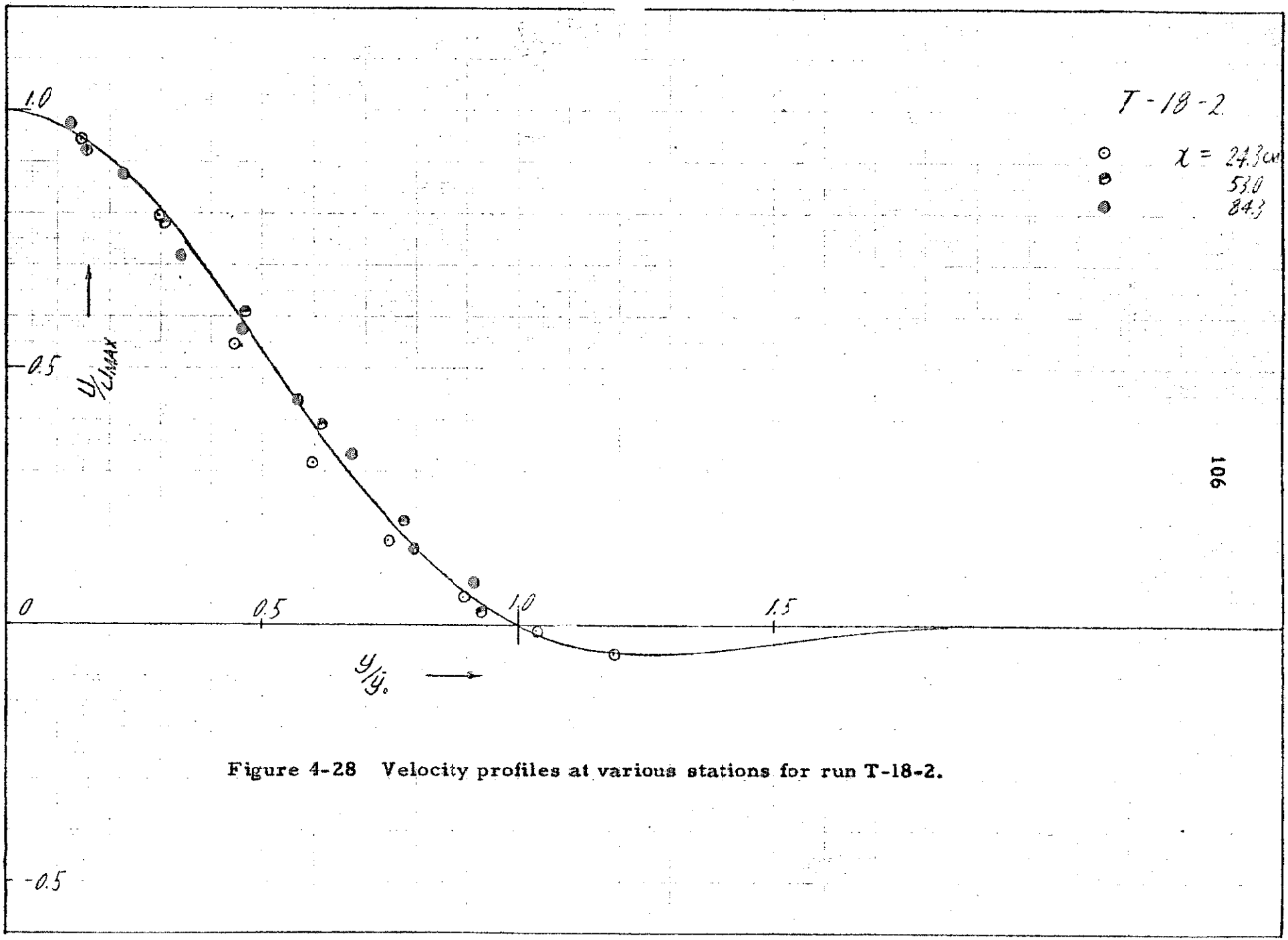

Figure 4-28 Velocity profiles at various stations for run T-18-2.

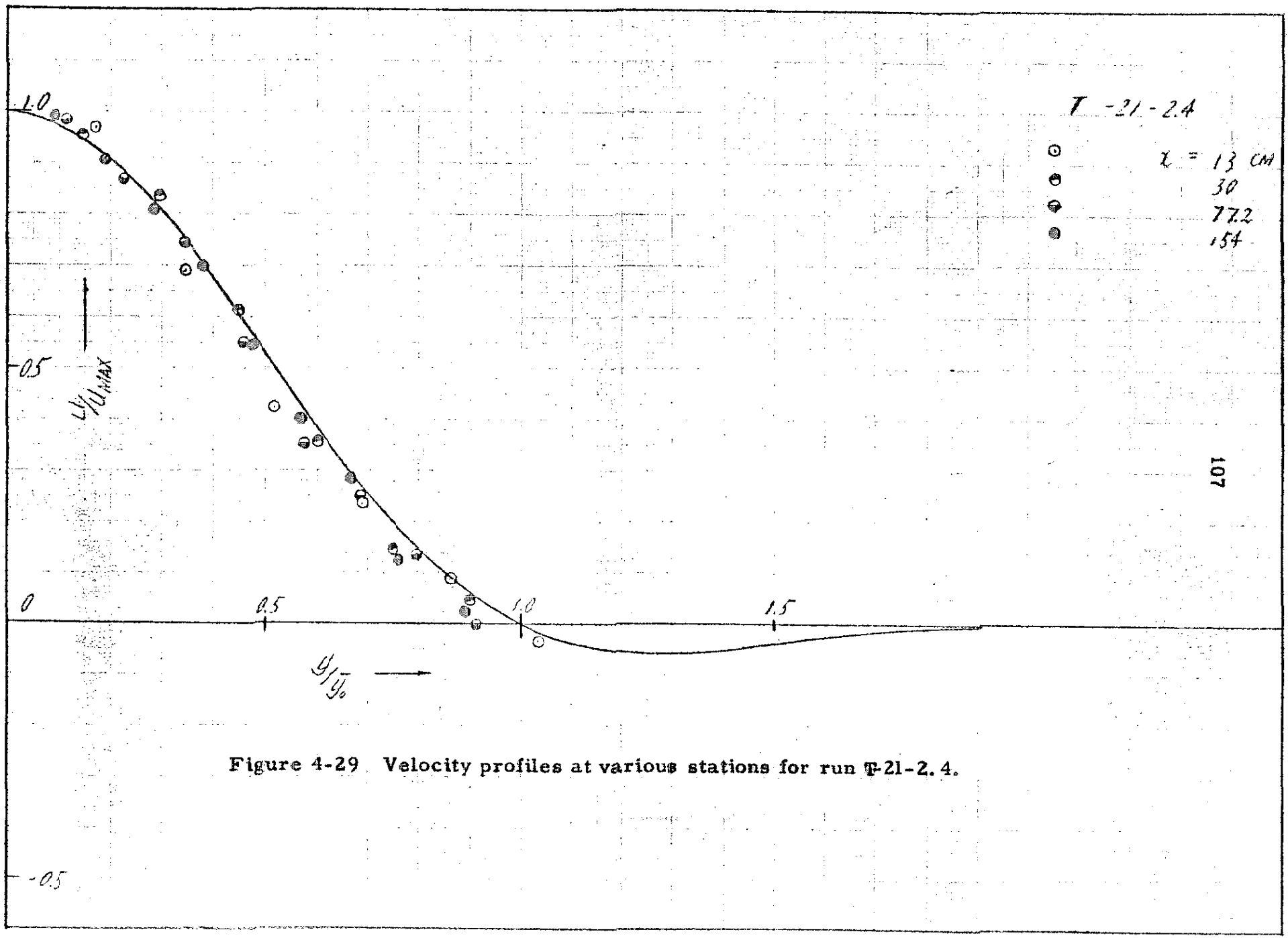

Figure 4-29 Velocity profiles at various stations for run T-21-2.4.

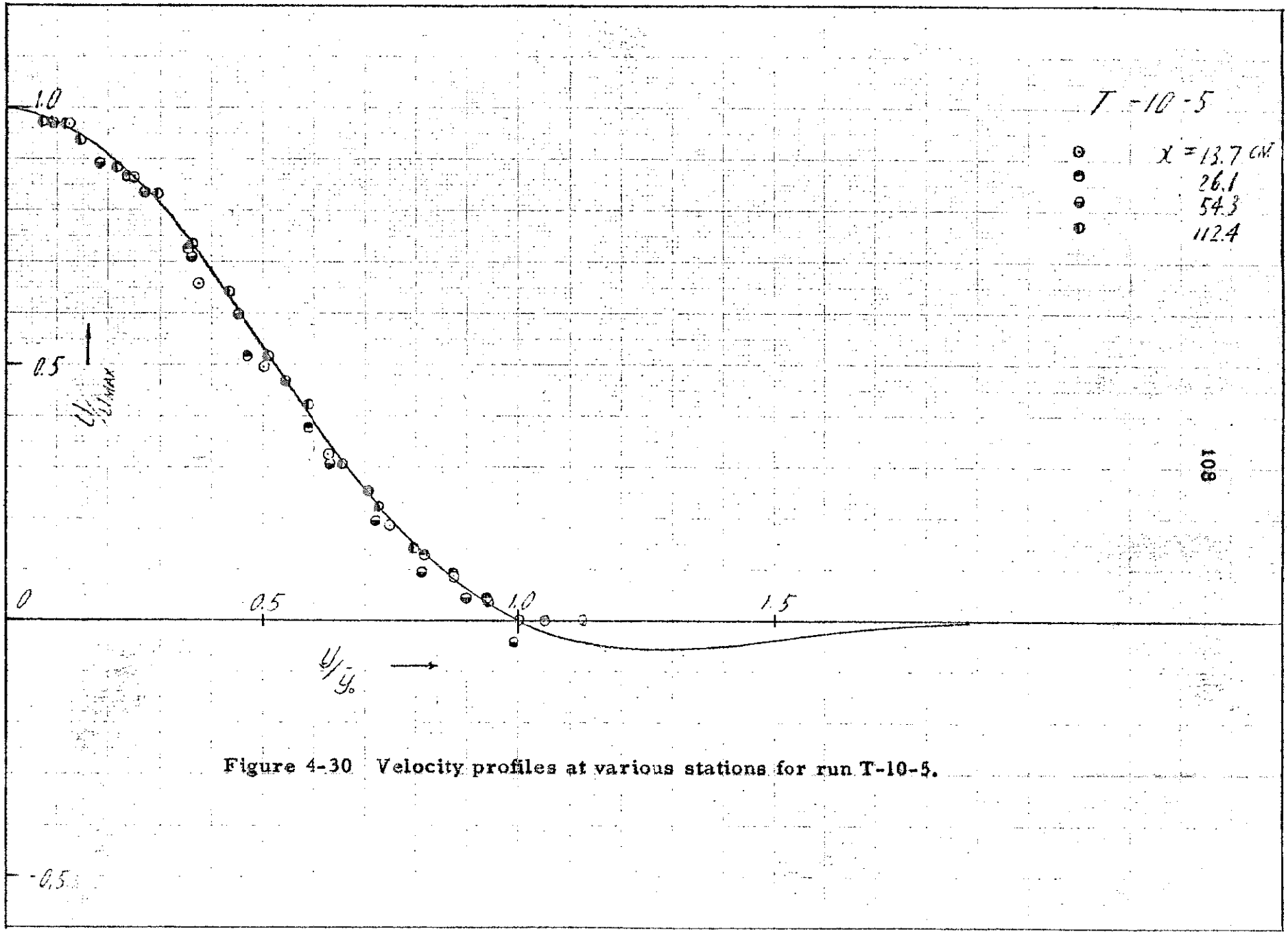

Figure 4-30 Velocity profiles at various stations for run T-10-5.

presented.

From these graphs it may therefore be concluded that the shape of the velocity profiles $u(y)$, obtained from the experiments, is the same as that predicted by the analysis presented in Chapter 2.

4-4 An Extension of the Zeroth Order Solution

In section 4-3 (equation 4-2), $\bar{y}_o$ was defined to be a length by which the vertical coordinate y was normalized so that the area under the curve would be constant. But there is another way that this length $\bar{y}_o$ may be interpreted which will have direct bearing on the conclusions which will be drawn from these experiments later.

In the zeroth order solution obtained in Chapter 2, the principal result is

$$u(x,y) = \frac{\alpha_o q}{x^{1/3}} f_o'\left(\frac{\alpha_o y}{x^{1/3}}\right) \quad , \tag{4-3}$$

where, as defined before, $\alpha_o = \left(\frac{\epsilon g}{\mathcal{D}\nu}\right)^{1/6}$. The function $f_o(\zeta)$ is tabulated and illustrated graphically in Chapter 2 (table 2-1 and figure 2-2). $f_o'(\zeta)$ is symmetrical about $\zeta = 0$ and hence

$$u_{max} = \frac{\alpha_o q}{x^{1/3}} f_o'(0) = -(0.284)\frac{\alpha_o q}{x^{1/3}} \quad , \tag{4-4}$$

where the number-0.284 is the value of $f_o'(0)$ as obtained in Chapter 2. In terms of q_f (as defined by equation 4-1), equation 4-4 may be rewritten

$$u_{max} = -(0.267)\frac{\alpha_o q_f}{x^{1/3}} \quad . \tag{4-5}$$

Now in equation 4-5, the only quantity which is not kinematic is α_o. The kinematic quantities u_{max}, q_f, and x may very simply be measured in the dye traces. Let one postulate that in cases when $q/\nu\alpha_o x^{2/3}$ is no longer small, the same zeroth order solution may be applied provided one allows the quantity α_o to vary. Hence define $\gamma = \alpha/\alpha_o$ where α is the value obtained from the experimental velocity profiles. Then

$$\gamma = \frac{\alpha}{\alpha_o} = \left\{ \frac{|u_{max}| x^{1/3}}{\alpha_o q_f (0.267)} \right\}_{measured} \quad (4\text{-}6)$$

There is, however, another way of obtaining γ, this time based on y_o, which is half the thickness of the withdrawal layer as measured from the dye lines. From the analytical solution in figure 2-2, for

$$f_o\left(\frac{\alpha_o y_o}{x^{1/3}}\right) = 0 \quad ,$$

we find

$$\frac{\alpha_o y_o}{x^{1/3}} = 3.57 \quad . \quad (4\text{-}7)$$

Now y_o and x may be measured and another γ may be computed by the formula

$$\gamma' = \alpha'/\alpha_o = \frac{3.57\, x^{1/3}}{\alpha_o y_o} \quad . \quad (4\text{-}8)$$

It turns out that $\gamma = \gamma'$ and $y_o = \bar{y}_o$ within experimental error. Thus, the zeroth order solution may be applied in all the cases obtained in the experiments provided one uses the appropriate value of α.

4-5 The Experimental Parameter $\chi = \alpha/\alpha_o$

As explained in the previous sections and as may be seen in figures 4-2 through 4-30, the zeroth order solution obtained in Chapter 2 is remarkably accurate provided the value of α_o is replaced by α, even though $q_b/D\alpha_o x^{2/3}$ and $q_b/\nu\alpha_o x^{2/3}$ are no longer small. It is therefore of the utmost importance to investigate how the value $\chi = \frac{\alpha}{\alpha_o}$ is related to the other physical parameters since once χ is known, the flow field is known. In these experiments, when $q_b/D\alpha_o x^{2/3}$, $q_b/\nu\alpha_o x^{2/3}$ are much smaller than unity, one expects χ to be unity since the zeroth order solution would then be directly applicable. The value χ as computed using the equation 4-6 was plotted against the variable $q_b/D\alpha_o x^{2/3}$. For each of the experiments separately they are as shown in figures 4-31 through 4-35. A straight line is drawn through each group of points and these lines are compiled in figure 4-36. The points representing the T-series runs are slightly displaced from those of the N-series runs. This is because the quantity D/ν was 1.25×10^{-3} for the N-series runs and 0.150 for the T-series runs. However, this displacement is not very large and is in fact within the experimental scatter. The experimental scatter may be attributed to several causes which will be described and discussed in Chapter 5.

4-6 Summary

The conclusions from the experiments may be summarized as follows:

i) When the conditions $\epsilon\delta$, $q_b/D\alpha_o x^{2/3}$, $q_b/\nu\alpha_o x^{2/3}$, $\delta/x \ll 1$ are satisfied ($q_b/D\alpha_o x^{2/3} < 1$ in the experiments), the zeroth order solution in Chapter 2 describes the flow field quite well (within approximately 10%).

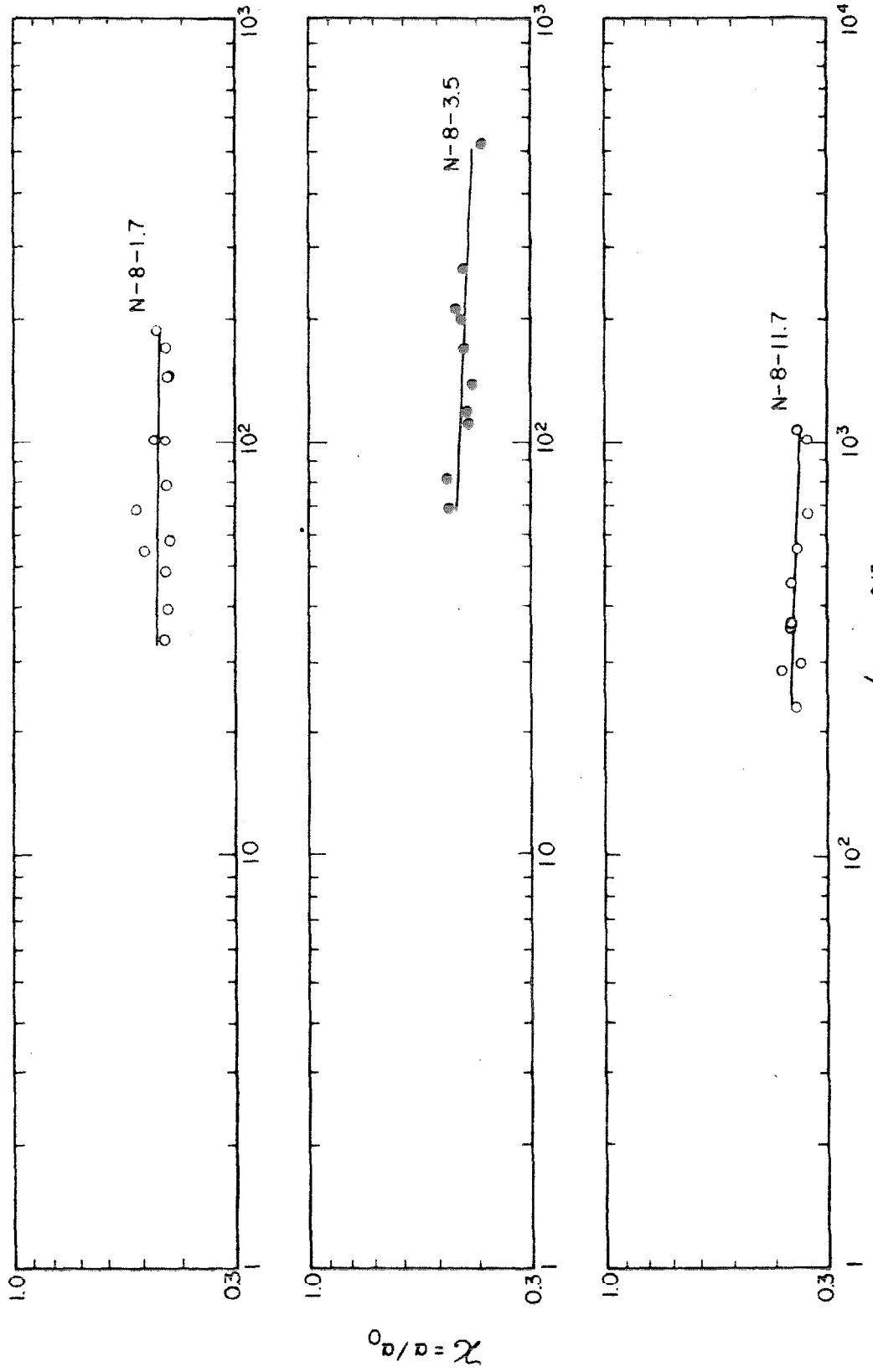

Figure 4-31 Variation of $\chi = \frac{\alpha}{\alpha_0}$ with $q_f/D\alpha_0 x^{2/3}$ for the N-8-series runs.

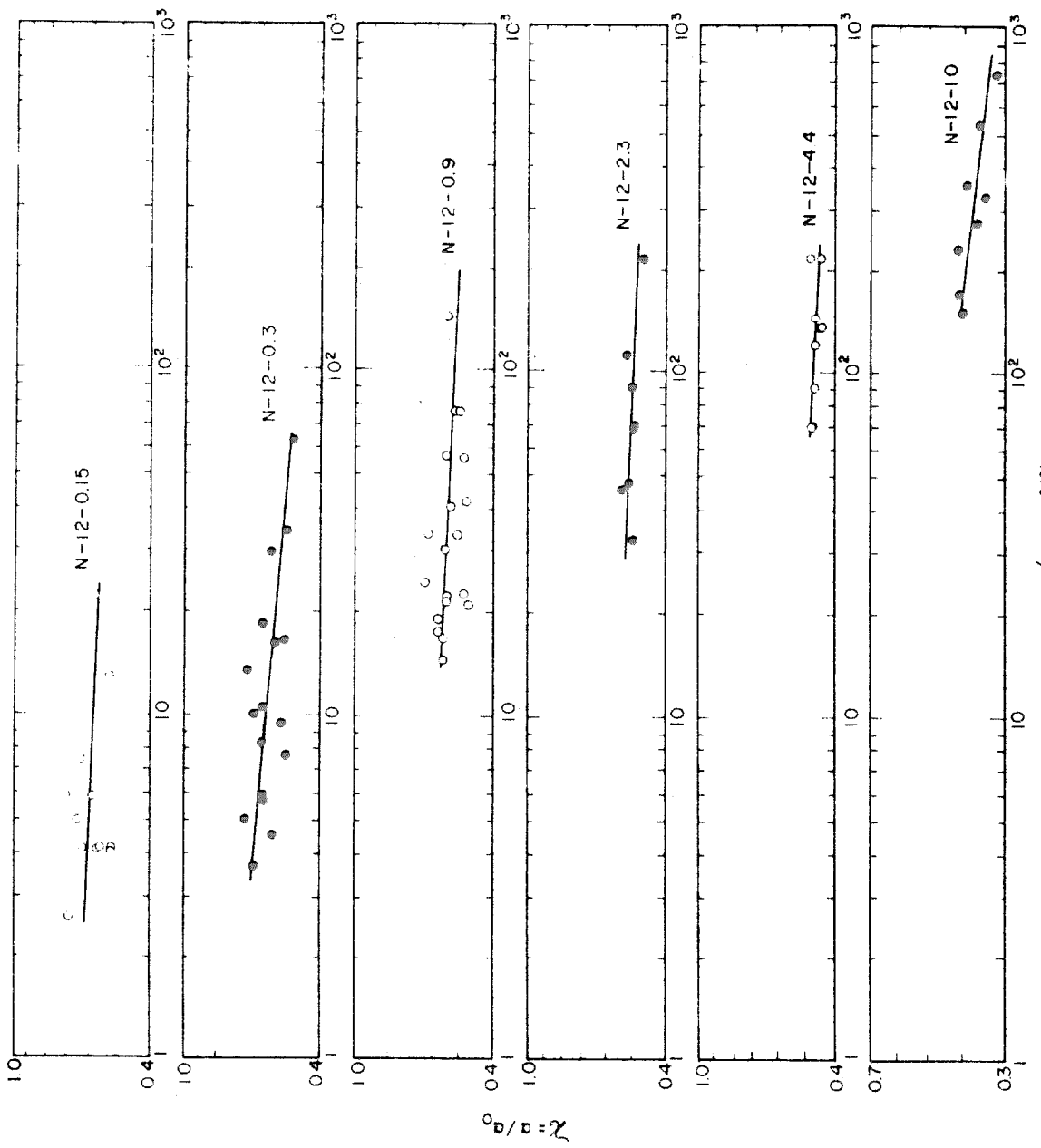

Figure 4-32 Variation of $\chi = \frac{\alpha}{\alpha_o}$ with $q_f/D\alpha_o x^{2/3}$ for the N-12-series runs.

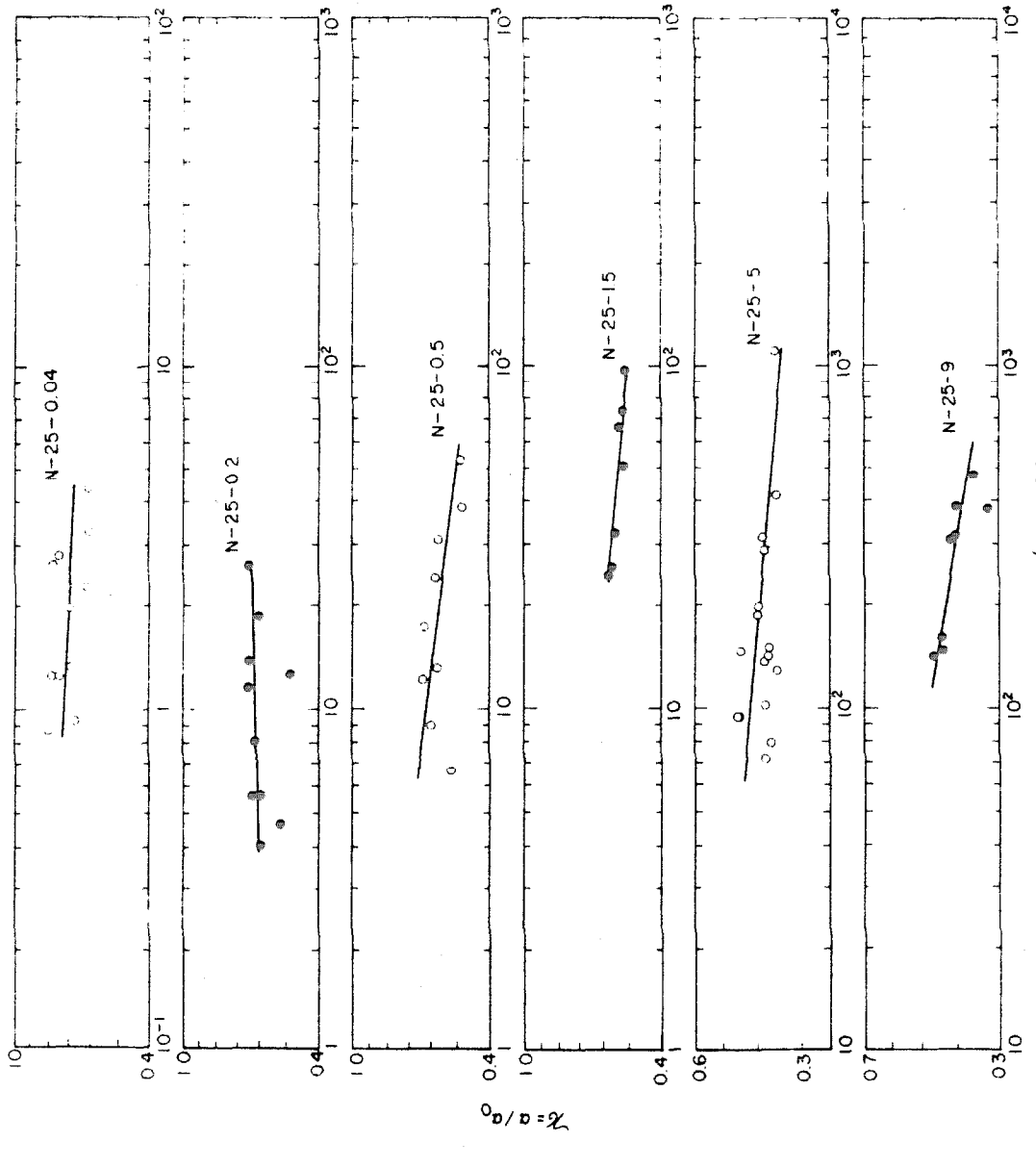

Figure 4-33 Variation of $\chi = \frac{\alpha}{\alpha_0}$ with $q_1/D a_0 x^{2/3}$ for the N-25 series runs.

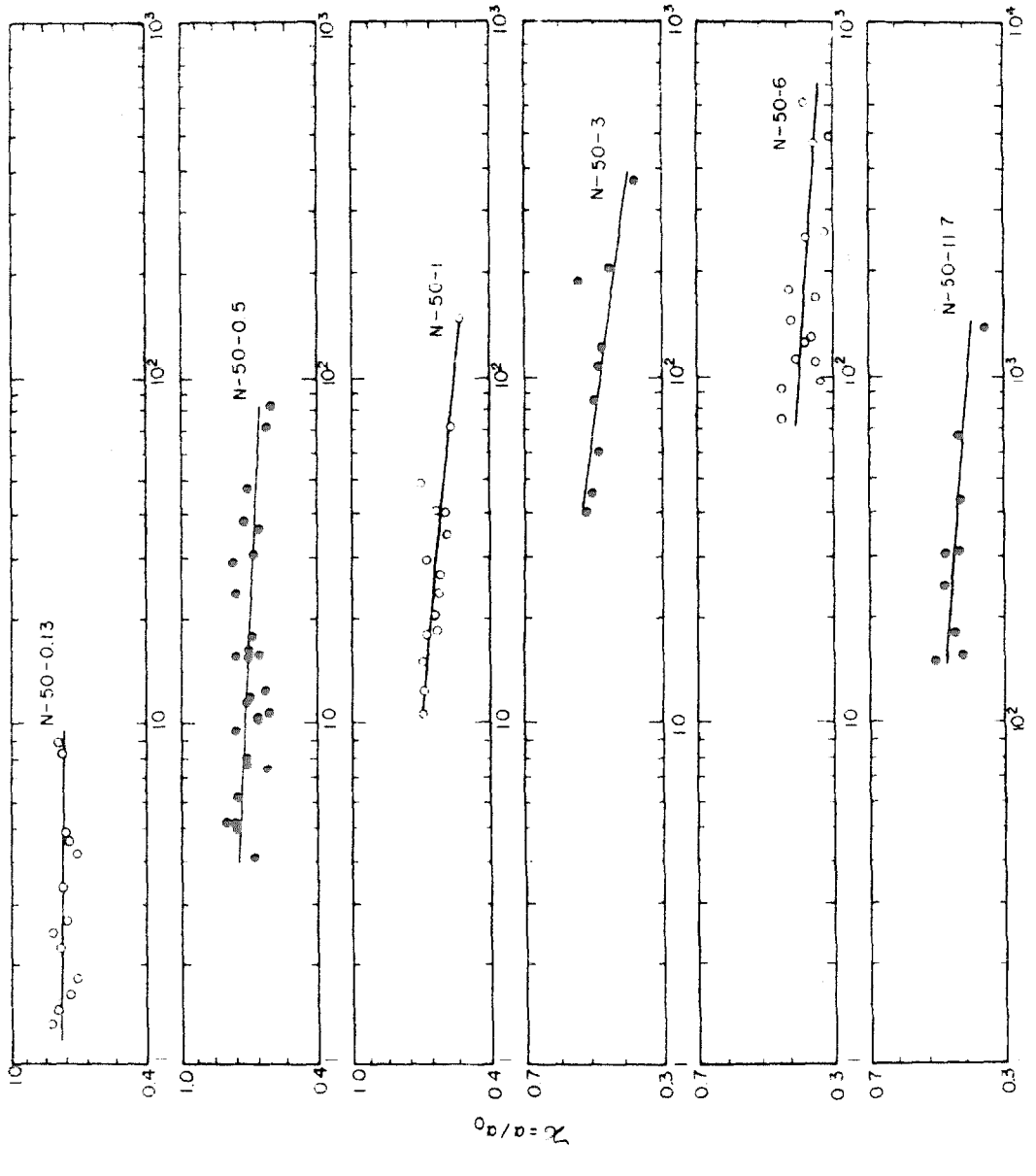

Figure 4-34 Variation of $\chi = \frac{\alpha}{\alpha_0}$ with $q_f/D a_0 x^{2/3}$ for the N-50-series runs.

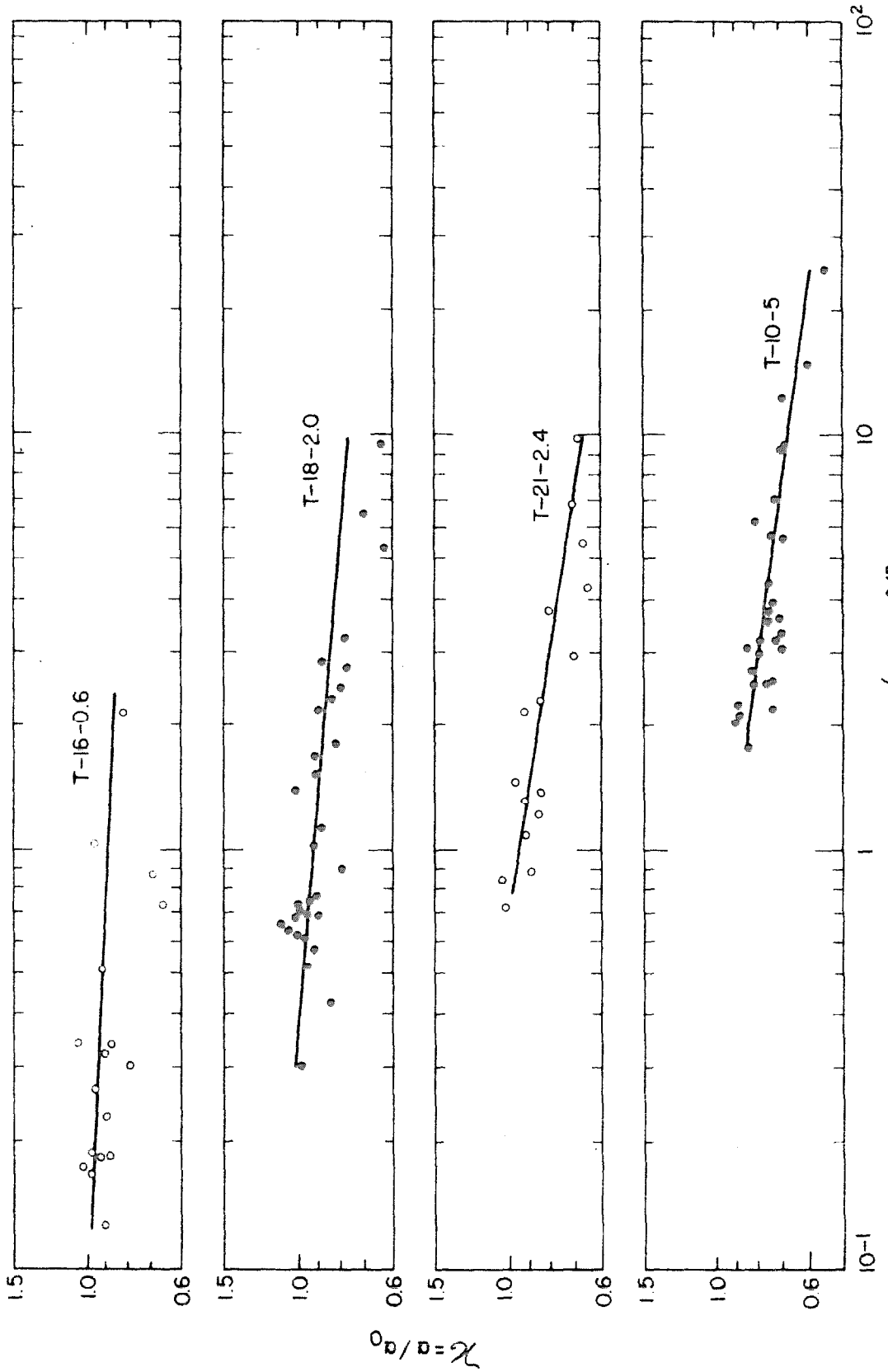

Figure 4-35 Variation of $\chi = \frac{\alpha}{\alpha_0}$ with $\frac{q_f}{D\alpha_0 x^{2/3}}$ for the T-series runs.

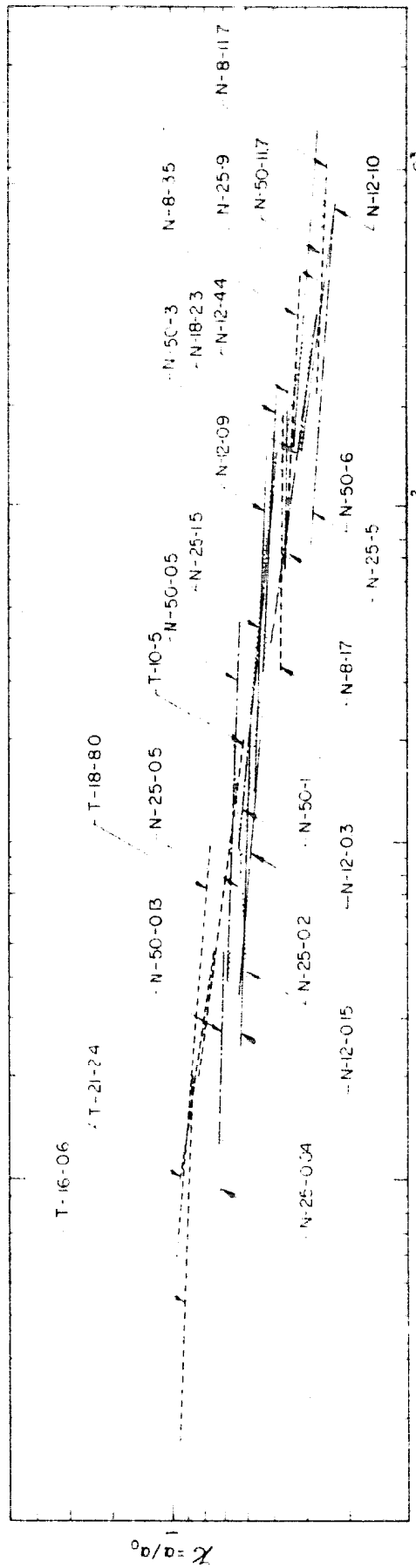

Figure 4-36 Variation of $\chi = \frac{\alpha}{\alpha_0}$ with $q_f/D\alpha_0{}^{2/3}$.

ii) When these conditions are not satisfied ($1 < \frac{q_f}{D\alpha_0 x^{2/3}} < 10^3$ in the experiments), the zeroth order solution may still be applied provided one now replaces α_0 by $\alpha(x)=\zeta\alpha_0$. ζ as a function of $\frac{q_f}{D\alpha_0 x^{2/3}}$ is presented in figure 4-36.

iii) In all the experiments, the velocity profiles are similar.

CHAPTER 5

DISCUSSION OF RESULTS

In Chapter 2 an analysis was presented based on the assumptions that the parameters $\epsilon\delta$, $\frac{\delta}{x}$, $\frac{q}{D\alpha_0 x^{2/3}}$, and $\frac{q}{\nu\alpha_0 x^{2/3}}$ are small. The fluid was assumed to be linearly stratified, and to extend to infinity. In Chapters 3 and 4, a series of experiments have been described. In these experiments, an attempt was made to duplicate the geometric conditions assumed in the analysis, but, of course, the fluid region in the tank is not infinite in extent. Also, because of the inherent difficulty in recirculating a miscible stratified fluid, the flow was not steady. These various effects will be discussed individually in greater detail in this chapter.

A discussion of the errors involved in the measurements of the various quantities will also be included in this chapter. The technique of the dye-streak tracer is the only reasonable one to use in this series of experiments since it was necessary to measure the velocity field (vertical velocity profiles at various horizontal stations) in a short time (about 20 minutes).

Discussions of the theoretical solution, its validity, its relation to Kao's solution, and its applicability are also presented.

5-1 Discussion of the Finite Length and Depth of the Experimental Tank

In this section it will be demonstrated that the errors due to the finite length and depth of the tank are secondary and that the experimental reservoir is an adequate one for the range of experiments performed. It was both assumed in the analysis and observed in the

experiments that the bulk of the flow is confined to a thin layer of thickness $\delta(x)$. One may, therefore, neglect the effect of the finite depth in the experiments if δ is much smaller than the depth. This was observed to be the case in almost all the experiments, as the largest value of δ observed was about 15 cm (in Run N-8-11.7) compared to the total depth of about 45 cm. Since 45 cm is the maximum depth possible, no experiment was performed especially to investigate the depth effect. In all the runs and for each velocity trace, there always exist two finite regions, one near the water surface and the other at the bottom where the dye traces did not substantially move. This may be seen clearly in figure 3-1. Thus, it is believed that the depth effect is secondary.

The length of the tank is also finite. Since the flow was simply drained out, the water surface in the reservoir dropped progressively during each experiment. This had an effect of varying the discharge along the length of the tank. If $q(x)$ = unit discharge at station x, h = depth of water in the tank, x = distance along the tank measured from the sink and t = time, then from continuity,

$$\frac{dh}{dt} = \frac{dq}{dx} = -\frac{Q}{C} = \text{constant} \,, \tag{5-1}$$

where Q = total discharge and C = total surface area of the tank. The effective total length of the tank is 500 cm but ninety percent of the velocity profiles were taken between 15 and 175 cm. Thus the total variation of q in the experimental section was roughly 30%. In calculating the experimental results, the local unit forward discharge, q_f, obtained by integrating the positive portion of the velocity profiles, was

always used.

A typical case of the variation of unit discharge is presented in figure 5-1, where q_f is plotted against x, the distance along the tank. It may be seen that most of the values are above the value of the unit discharge q measured at the outlet. This is because of a nearly parabolic velocity distribution in the horizontal plane across the width of the tank due to the sidewall effect which will be discussed in the next section. A line is also drawn so as to best fit the points and to extrapolate to zero at $x = 500$ cm. It may be seen that this fits fairly well indicating that most of the dye particles have been dropped in the same plane. A few of these points which fall well below this line must have been dropped close to the side walls. Within a small region of x, (say $x = 20$ to 30 cm, or $x = 100$ to 120 cm) the variation of q_f is small. Thus it is reasonable to assume that the flow is quasi-steady and the tank is quasi-infinite in length in the sense that the flow at a certain station x with the local unit forward discharge q_f in this experimental tank is the same, or nearly the same, as the flow in an infinitely long tank with uniform unit forward discharge q_f.

5-2 The Effect of the Finite Width; the Sidewall Effect.

Although the flow in the laboratory tank was intended to represent a two-dimensional flow, obviously it was not, because of the wall effects. Since the flow was laminar, and since there was no density variation across the tank (in the z-direction,) it is expected that there would be a parabolic velocity distribution in the z-direction. Moreover, there might be some cross flow, i.e. w, the velocity component in the z-direction may not be zero. To investigate the extent of this, time

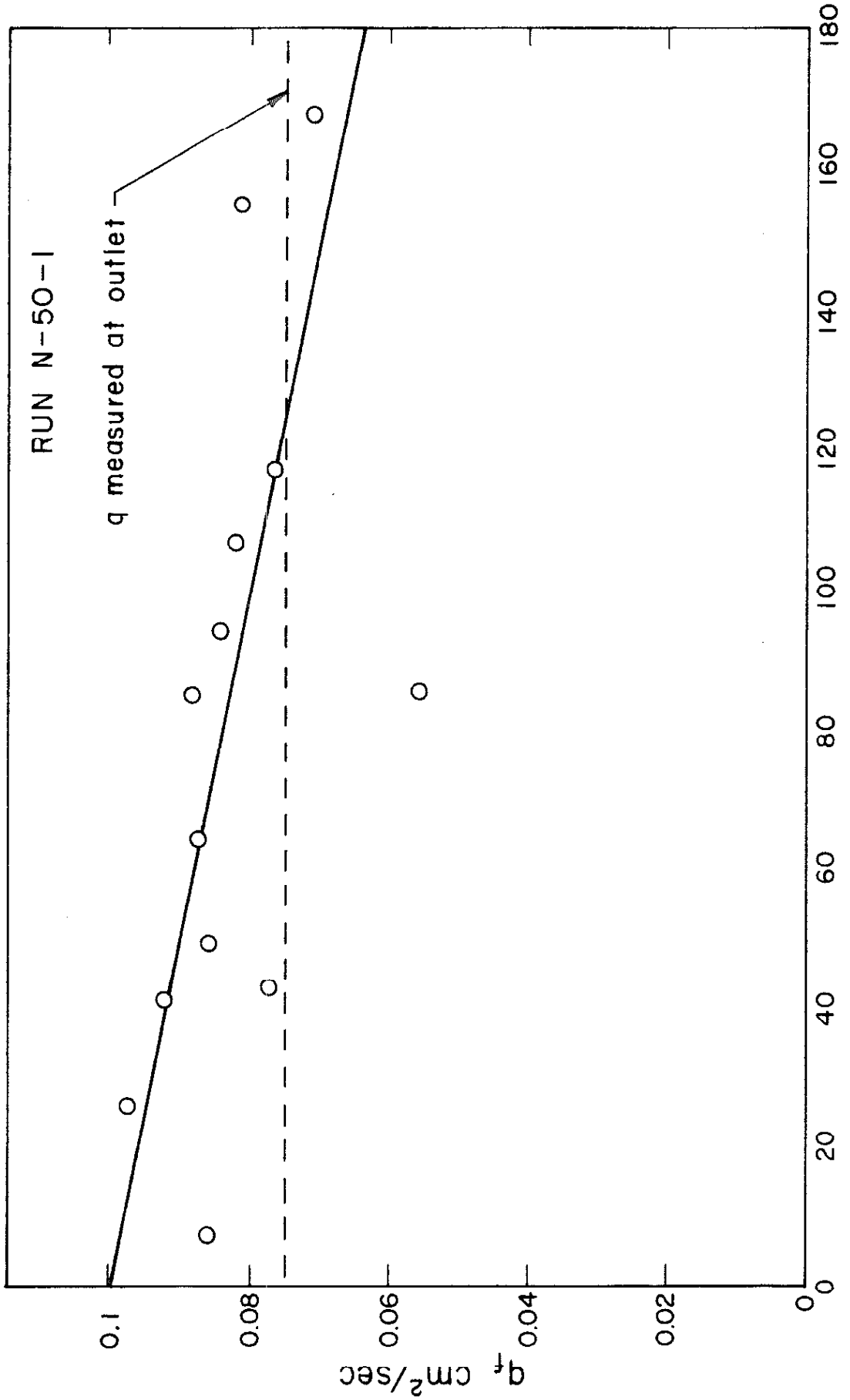

Figure 5-1 Typical variation of local unit forward discharge q_f with x.

lapse photographs were taken from atop the tank after dye particles were dropped in at various locations across the tank (various distances from the wall). This was done for only one case (ϵ = 0.000336 1/cm, $\nu \cong 10^{-2}$ cm^2/sec, q = 0.227 cm^2/sec) at three stations (x = 50, 115, 150 cm). In this way, the velocity distribution in the z-direction for the plane y = 0, the plane of the sink, may be obtained from the time lapse photographs, The velocity profiles are plotted in figure 5-2. It was checked by measuring the derivatives that these are nearly parabolas.

Figure 5-3 shows a photograph taken in the time lapse sequence. Since the dye streaks are parallel to the side walls, it may be concluded that there is no cross flow, i.e. w= 0.

The effect of the velocity distribution in the transverse or the z-direction is the introduction of additional shear. This effect may most readily be seen by returning to the basic equations. On the right hand side of equation 2-24, instead of simply $\mu_o \frac{\partial^2 u}{\partial y^2}$, one must now put $\mu_o \left(\frac{\partial^2 u}{\partial y^2} + \frac{\partial^2 u}{\partial z^2} \right)$. The values of $\frac{\partial^2 u}{\partial z^2}$ were computed for the three profiles measured and they are tabulated as follows:

y cm	x cm	$\partial^2 u / \partial z^2$ (cm-sec)$^{-1}$
0	50	0.0019
0	115	0.0023
0	150	0.0022

The values for $\partial^2 u / \partial y^2$ may be obtained from the corrected theory (inasmuch as the vertical velocity profile could not be measured simultaneously with the horizontal):

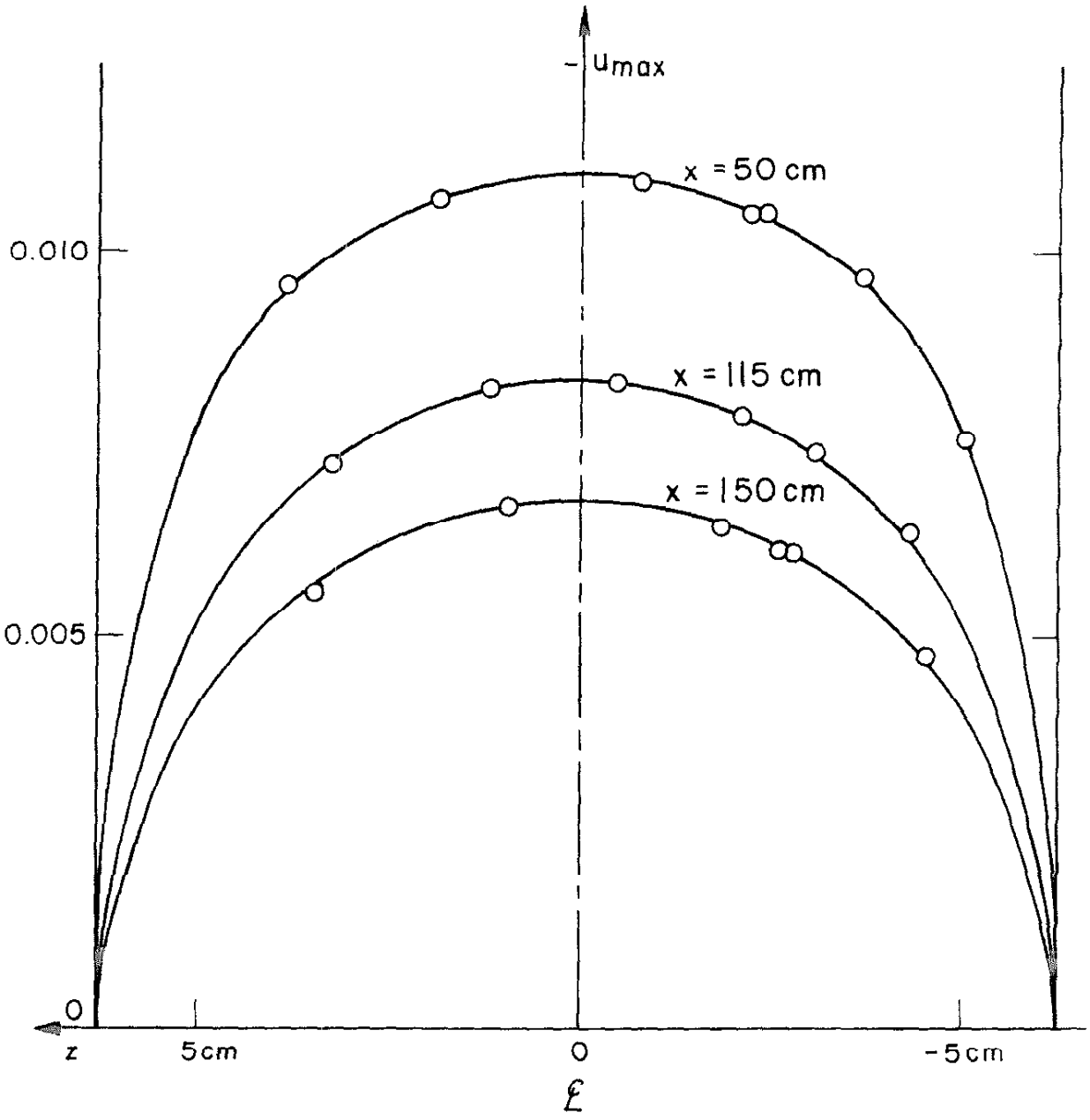

Figure 5-2 Velocity distribution in the z-direction for the investigation of the sidewall effect.

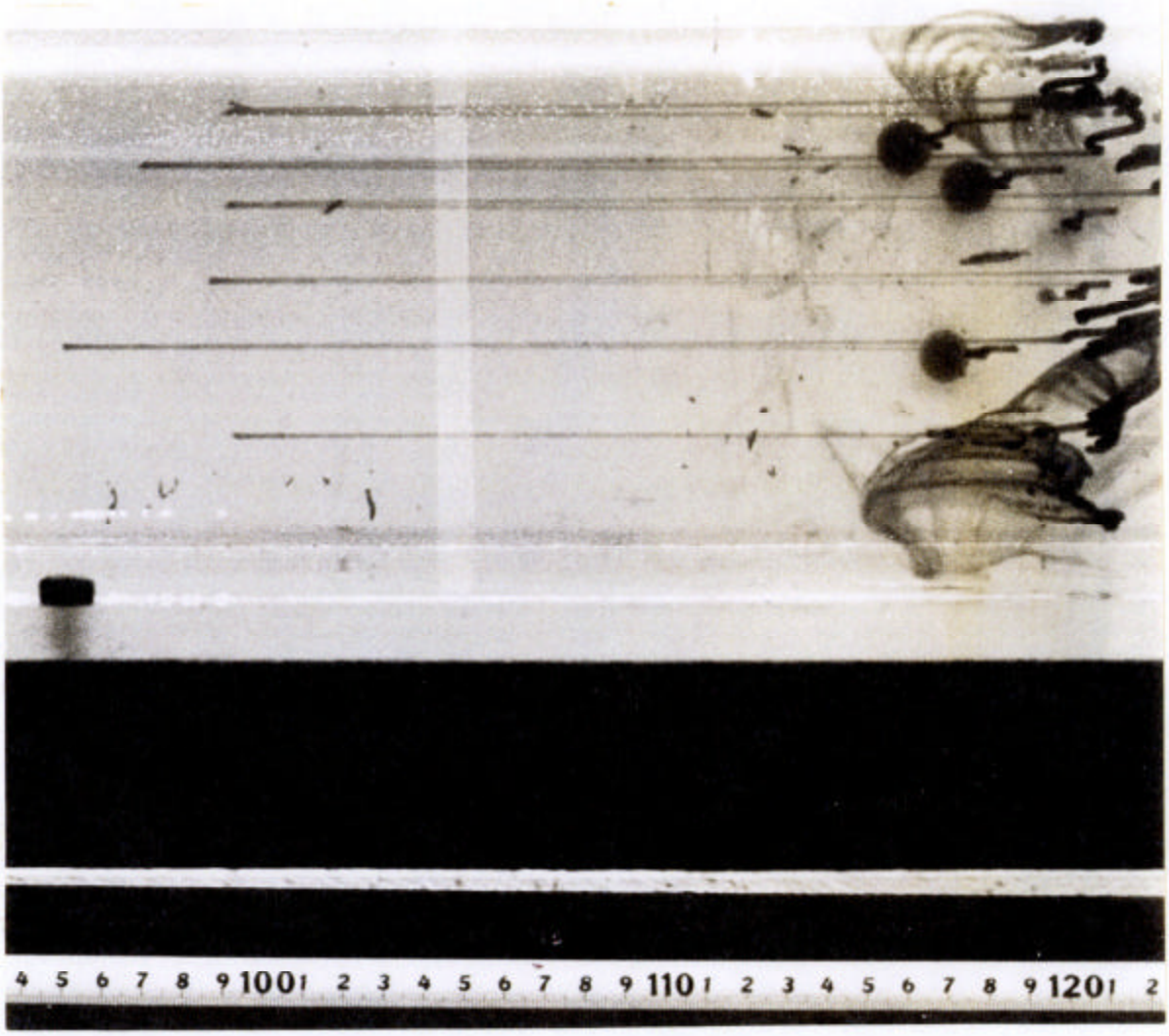

Figure 5-3 Photograph taken from atop the reservoir showing the dye lines for the investigation of the side wall effect.

$$\frac{\partial^2 u}{\partial y^2} = \frac{\alpha^3 q}{x} f_o'''(\zeta)$$

$$= \chi^3 \frac{\alpha_o^3 q}{x} f_o'''(\zeta) \quad .$$

In this case, $\nu \cong 10^{-2}\,cm^2/sec$, $D \cong 1.25 \times 10^{-5}\,cm^2/sec$, $q = 0.227\ cm^2/sec$, $\epsilon = 0.000336\ cm^{-1}$, and $g = 981\ cm/sec^2$. Hence

$$\alpha_o = \left(\frac{\epsilon q}{D\nu}\right)^{1/6} = 11.8\ cm^{-2/3} \quad .$$

Thus $q/D\alpha_o x^{2/3}$ = 50 to 100. Hence χ = 0.5 from figure 4-36. *Therefore,*

$$\frac{\partial^2 u}{\partial y^2} \cong \frac{50}{x} f_o'''(\zeta) \quad .$$

The function $f_o'''(\zeta)$ is plotted in figure 5-4. It is seen that for $\zeta = 0$, i.e. on the level of the sink, $|f_o'''(0)| \cong 0.1$ so that $\partial^2 u/\partial y^2 \cong 0.1,\ 0.04,\ 0.03\ (cm\text{-}sec)^{-1}$ respectively for the present case at x = 50, 115, and 150 cm. These are about 20 times the measured values of $\partial^2 u/\partial z^2$.

Away from the y = 0 plane, $f_o'''(\zeta)$ becomes smaller but so does $\partial^2 u/\partial z^2$. A good assumption is to take $\partial^2 u/\partial z^2$ away from the y= 0 plane to be proportional to $f_o'(\zeta)$. Thus,

$$\frac{\partial^2 u}{\partial z^2} \cong 0.002\ \frac{f_o'(\zeta)}{f_o'(0)} \quad .$$

To compare $\partial^2 u/\partial z^2$ with $\partial^2 u/\partial y^2$ in this example, it therefore suffices to compare

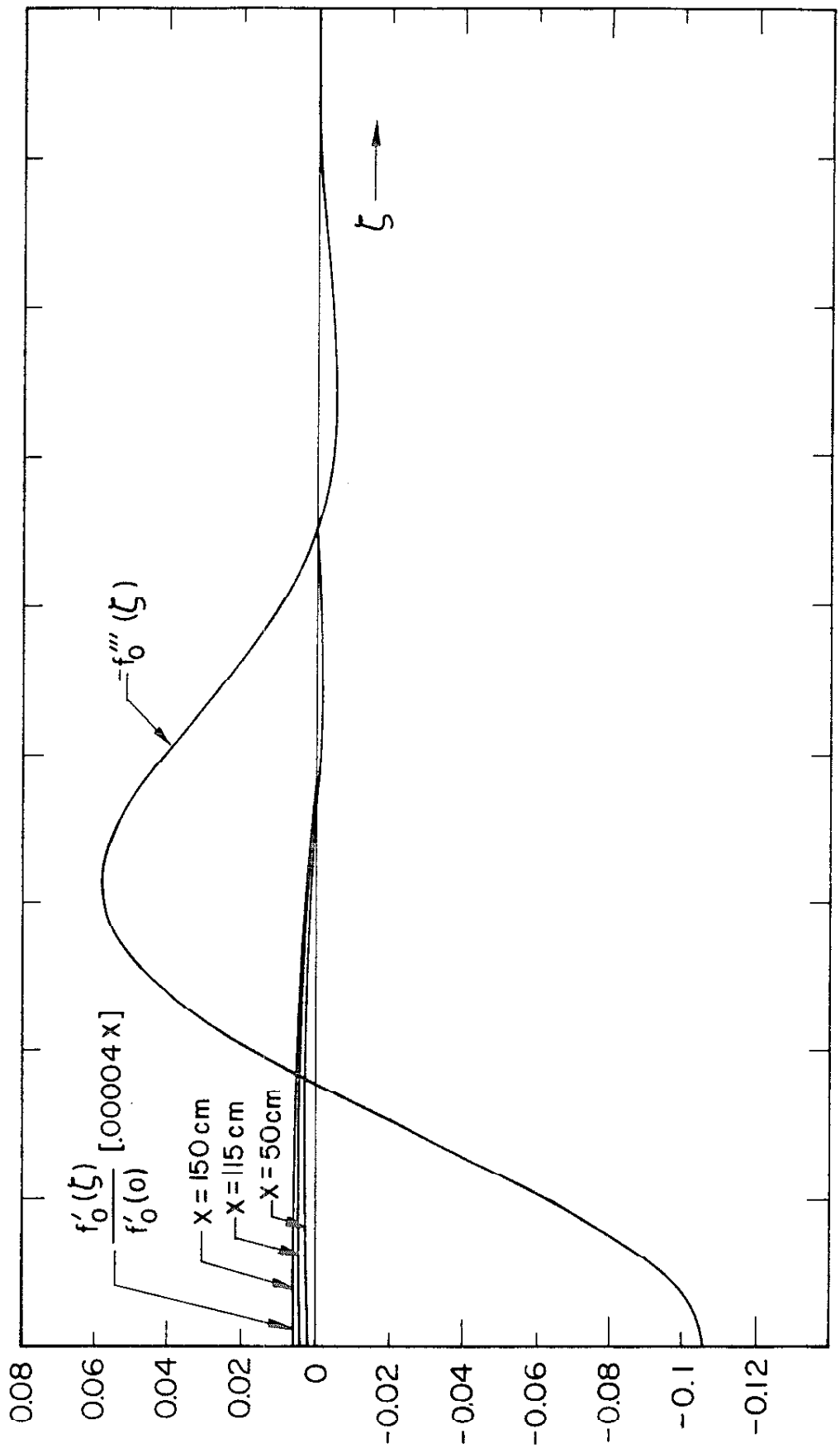

Figure 5-4 Comparison of $\partial^2 u / \partial y^2$ with $\partial^2 u / \partial z^2$ to demonstrate that sidewall effects are negligible.

$$(0.002)\ \frac{f_o'(\zeta)}{f_o'(0)} \qquad \text{with} \qquad \frac{50}{x}\ f_o'''(\zeta)\ ,$$

i.e.

$$(0.00004x)\ \frac{f_o'(\zeta)}{f_o'(0)} \qquad \text{with} \qquad f_o'''(\zeta)\ .$$

Lines of $(0.00004x)\ \frac{f_o'(\zeta)}{f_o'(0)}$ for x = 50, 115 and 150 are also drawn in figure 5-4. It may be seen from the figure that $\partial^2u/\partial z^2$ is much smaller than $\partial^2u/\partial y^2$, except in a small region around $\zeta = 1.75$, which is the inflection point of the vertical velocity profile. At $\zeta = 1.75$, $\partial^2u/\partial y^2 = 0$ since $f_o'''(1.75) = 0$. This does not mean that two-dimensionality is lost. It only means that both $\partial^2u/\partial y^2$ and $\partial^2u/\partial z^2$ are very small in this region. This comparison is done for the particular run performed especially to investigate the sidewall effect. It may be seen however that this is representative of all the experiments.

Therefore, one concludes that the only significant correction required by the sidewall effect is the apparent change in the unit discharge depending on the location of the plane in which the dye particle is dropped. In all the experiments, the dye particles were carefully dropped so that they were all within the central 30% of the width of the tank. Since the measured local unit discharge q_f was used throughout the calculations of the results, it is believed that the sidewall effect has been satisfactorily accounted for.

The three effects due to the finite size of the tank all point to the necessity of using a local discharge rather than the discharge measured at the outlet. The unit forward flowing discharge q_f, as discussed before in section 4-2, measured by planimetering the area

enclosed by time lapse images of dye traces, is the logical choice. These effects, though secondary, do contribute to errors in the experimental results, especially on x-dependent quantities. This will be discussed and summarized with all the other errors at the end of this chapter.

5-3 The Effect of the Transient.

Since the flow is not recirculated, it cannot be steady, although the experiments were supposed to represent a steady state case. Thus it was necessary to assume that the flow was at least quasi-steady and that the actual quasi-steady flow approximates the assumed steady flow. There is no way to truly and exactly investigate the effects of the transient without either the solution of the complete unsteady hydrodynamic equations or the performance of experiments where the fluid is recirculating and the flow steady. Either of these is by no means readily attainable. One is then left to do the next best thing.

In almost every experiment, (except N-25-5, the first one done) at least two sets of dye particles were dropped. The first set was dropped after a 5 or 10 minute period during which it was believed that steady state was achieved and the next set about 10 minutes after that. By a comparison of data obtained from these two sets, it was found that the transient had subsided. Run N-50-1, the same one used in figure 5-1 for the variation of q_f with x, is selected as a typical case. The graph of $\chi = \alpha/\alpha_0$ vs. $q_f/D\alpha_0 x^{2/3}$ is plotted for that run in figure 5-5 where the first and second sets of dye measurements are represented separately. It may be seen that the transient has died out sufficiently and the experiments do represent a quasi-steady case.

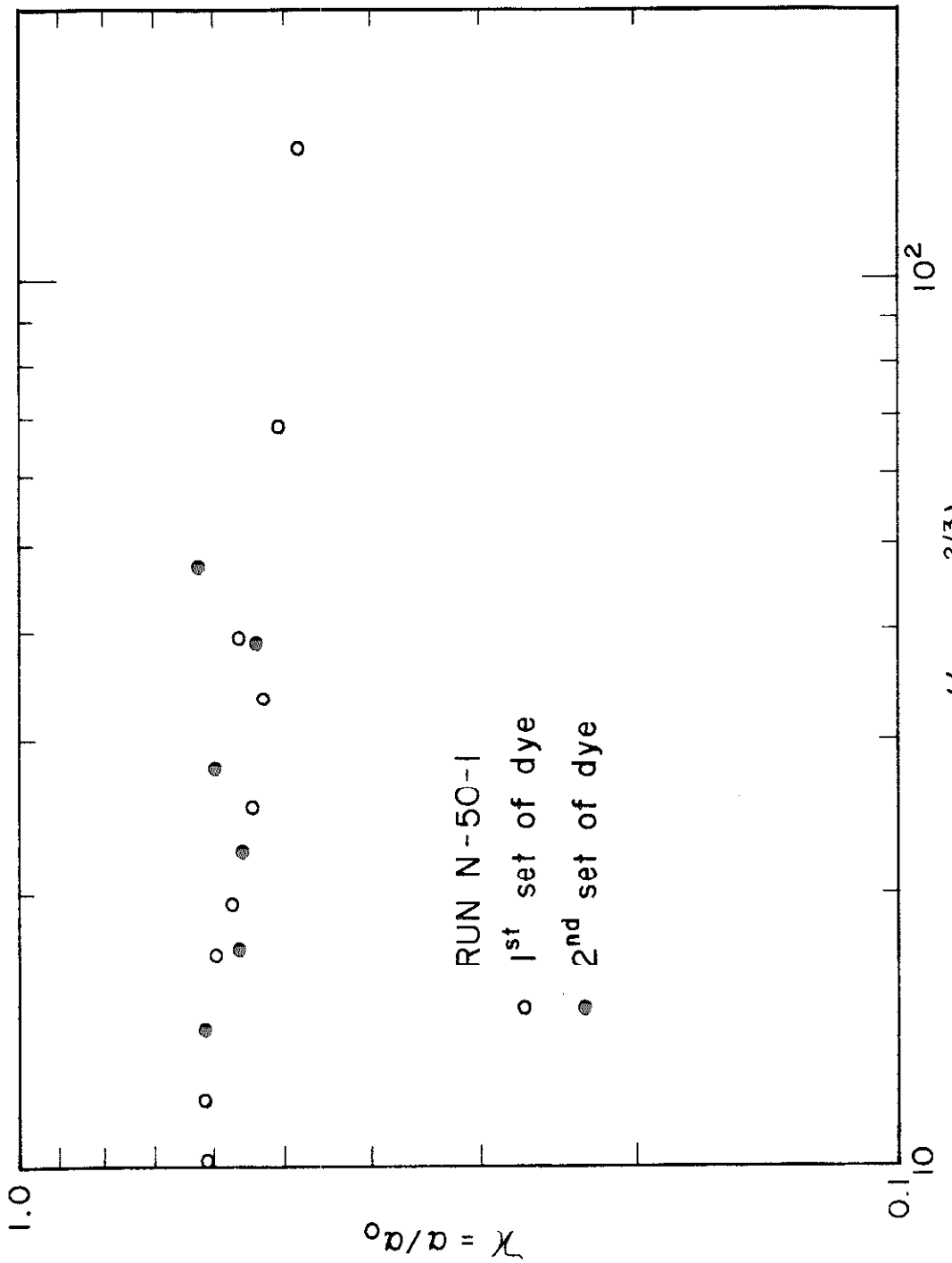

Figure 5-5 Comparison of first and second sets of dye line measurements to demonstrate that the transient has subsided.

5-4 Summary of Experimental Errors

It is seen from the previous sections in this chapter that these experiments are subject to quite a few errors, secondary as they may seem. The most significant errors should be in x-dependent results since the error producing items such as the length effect are x-dependent. Besides these systematic errors, there are, of course, random errors. A few of the more important ones will now be discussed.

In the measurements of the velocities by means of the dye traces the steps involved included the tracing of images from the negatives onto the paper. In so doing, the various images must first be aligned with aid of various reference crosses on the front side of the tank. Then the scale of the photograph had to be established by matching the scale in the photograph on the front side of the tank with a scale in the darkroom. Moreover, the distance in from the wall to various dye streaks was slightly variable making slight errors in the photographically measured lengths. It is believed that these errors together with the systematic errors discussed earlier are the cause of the scatter shown in figures 4-31 through 4-35 (roughly 15%).

5-5 Discussion of the Validity of the Theoretical Solution

The analytical solution presented in Chapter 2, (tabulated in tables 2-1 and 2-2 and shown graphically in figures 2-2 and 2-3, as the zeroth order solution), is valid provided the four quantities $\epsilon\delta$, δ/x , $q/D\alpha_0 x^{2/3}$, and $q/\nu\alpha_0 x^{2/3}$ are all much smaller than unity.

The first quantity $\epsilon\delta$ is the total relative change in density from the top to the bottom of the relevant flow field (in other words, the withdrawal layer). Since δ grows with x , the quantity $\epsilon\delta$ will be

small when ϵ is very small and δ not very large. This means that the solution should not be applied when x is too large since δ would then be too large. From the solution, $\frac{\delta}{x} \propto \frac{1}{\alpha_0 x^{2/3}}$. Thus, $\epsilon\delta \propto \frac{\epsilon x^{1/3}}{\alpha_0}$.

The second quantity δ/x, is, by virtue of the solution, the same order as $1/\alpha_0 x^{2/3}$ as seen in Chapter 2. For $\alpha_0 \neq 0$, this may be made very small when x is large.

The third and fourth quantities $q/D\alpha_0 x^{2/3}$, $q/\nu\alpha_0 x^{2/3}$ are very small when q is very small. The solution presented in Chapter 2 is taken to be the limiting solution when $q \to 0$. Thus, as long as D, ν, α_0, and x are not zero, these two parameters are truly negligible for small enough q.

Thus, to summarize the limitations imposed by the various assumptions on the validity of the theoretical solution: one may apply the zeroth order solution if ϵ is very small, x is neither small nor exceedingly large, and q very small. In a given problem in the stratified flow towards a line sink, one would be given ϵ, q, D, ν, and hence α_0. One can then calculate the quantities $1/\alpha_0 x^{2/3}$, $q/D\alpha_0 x^{2/3}$, $q/\nu\alpha_0 x^{2/3}$, and $\epsilon x^{1/3}/\alpha_0$ for various x. For those values of x where all these quantities are small, the zeroth order solution may be applied provided no further complications such as turbulence, nonlinear density distribution, and complicated geometry come into the problem. The validity of the theoretical solution is thus confined to a range of the variable x, that range within which the four quantities above are very small. In any given case, the extent of this region may be very large or there may not be any value of x at which the solution is valid. It all depends on the magnitude of the parameters q, D, ν, and ϵ.

5-6 The General Problem of Selective Withdrawal

It is enlightening now to examine the general problem of selective withdrawal and how the phenomenon may be divided into several regimes of flow depending on the relative magnitude and importance of the various flow parameters (i.e. inertia, gravity, viscosity, and diffusivity).

Assume first of all that gravity is of primary importance. It may be verified that if gravity were not included, then the flow of slightly stratified fluids is not very much different from the flow of homogeneous fluids. Thus most of the interesting cases of stratified flow and in particular, the phenomenon of selective withdrawal may be divided into the following three regimes:

i) Regime I, the inviscid regime. In this regime, viscosity and diffusivity are not important. Only the inertia and the gravity enters the problem. Selective withdrawal into a corner sink in this regime was solved by Kao (7). The solution is given by equation 1-9. In this case, q , a measure of inertia, and $g\epsilon$, a measure of gravity are the important quantities.

ii) Regime II, the general regime. In this regime, all the four effects (inertia, gravity, viscosity, and diffusivity) are important. Depending on the physical properties of the fluid and the agent causing the stratification, the diffusivity may be unimportant. The phenomenon of selective withdrawal in this regime has not been examined either analytically or experimentally for the continuously stratified case.

iii) Regime III, the viscous regime. In this regime, the inertia effect is unimportant (very slow motion, low Reynolds number) while the viscous forces may be quite large. The diffusive effects may be

important or unimportant depending on the properties of the fluid and agent of stratification. In the present thesis, the problem is solved in this regime assuming the diffusive effect is important. The solution is given in Chapter 2. It is conceivable that in certain cases, the diffusive effect may be neglected even though the viscous effect is important. This and the role of the diffusivity will be discussed in the next section.

With the notion of these regimes of flow, it is now possible to discuss the phenomenon of selective withdrawal. Assume that there is a large body of slightly stratified incompressible fluid with a density gradient $\epsilon = -\frac{1}{\rho_o}\frac{d\rho_o}{dy}$. A line sink withdraws fluid at the rate q . Very near the sink, the velocities are necessarily large. The inertia effect dominates and the flow is certainly in Regime I near the sink. Far away from the sink, where the vorticity has had a chance to diffuse outward, the velocities are necessarily small and the flow must be in Regime III. At intermediate distances from the sink, the flow would be in Regime II.

5-7 Discussion of the Role of Diffusion in the Theoretical Solution

The theoretical solution obtained in Chapter 2 is based on a viscous diffusive model for the fluid. The diffusion coefficient in equation 2-26 is multiplied by the highest order derivative. Thus transition from the present solution to the viscous non-diffusive case is a case of singular perturbation. The present solution is useless for that case. Yet it is physically reasonable to expect that in certain fluids with density stratifications due to certain causes, the flow should be adequately described by a viscous non-diffusive model.

To examine the viscous non-diffusive model, one must return

to the basic equations. Making exactly the same assumptions throughout as in the viscous diffusive model presented, but letting D = 0, equations 2-23 through 2-26 may be written

$$\frac{\partial u}{\partial x} + \frac{\partial v}{\partial y} = 0 \quad , \tag{5-2}$$

$$\rho\left(u\frac{\partial u}{\partial x} + v\frac{\partial u}{\partial y}\right) + \frac{\partial p}{\partial x} = \mu\frac{\partial^2 u}{\partial y^2} \quad , \tag{5-3}$$

$$\frac{\partial p}{\partial y} = -\rho g \quad , \tag{5-4}$$

$$u\frac{\partial \rho}{\partial x} + v\frac{\partial \rho}{\partial y} = 0 \quad . \tag{5-5}$$

Introducing the stream function ψ , eliminating the pressure p and neglecting the inertia terms gives

$$\frac{\mu}{g}\frac{\partial^4 \psi}{\partial y^4} + \frac{\partial s}{\partial x} = 0 \quad , \tag{5-6}$$

$$\frac{\partial \psi}{\partial y}\frac{\partial s}{\partial x} - \frac{\partial \psi}{\partial x}\left(\frac{ds_0}{dy} + \frac{\partial s}{\partial y}\right) = 0 \quad , \tag{5-7}$$

subject to the same boundary conditions as given by equations 2-42 and 2-43. It was not possible to find any simple similarity solution to this problem. Thus these equations must be solved as partial differential equations. This implies that one must now impose an upstream boundary condition which unfortunately is not known until the unsteady problem is solved. Equations 5-6 and 5-7 may be combined to give

$$\frac{\mu}{g}\frac{\partial^4 \psi}{\partial y^4} + \frac{d\rho}{d\psi}\frac{\partial \psi}{\partial x} = 0 \quad , \tag{5-8}$$

which is the fundamental equation for incompressible viscous non-diffusive stratified flow at low Reynolds numbers.

5-8 Discussion of the Practical Applicability of the Solution

The results of this investigation, both analytical and experimental, must be used with care when applying to actual cases in the field. In a natural reservoir, there is no reason to expect that the flow is laminar. In all probability, the flow is turbulent. The turbulence structure in a density stratified fluid is very different from that in a homogeneous fluid. The turbulence is necessarily non-isotropic since the vertical fluctuations are suppressed by the density stratification.

The problems of stability of viscous stratified flow, of the onset of turbulence in stratified flow and of the nature of turbulence in stratified flow all await investigation.

CHAPTER 6

SUMMARY OF CONCLUSIONS

A theoretical and experimental study of two-dimensional incompressible, steady viscous flow towards a line sink in a stably stratified fluid was made. The major conclusions will be summarized as follows:

1. The limiting solution applicable for very small discharge was obtained analytically by first making a boundary-layer-type assumption and then a perturbation based on the parameter $q_f/D\alpha_0 x^{2/3}$. It is a similarity-type solution, based on the similarity variable $\zeta = \frac{\alpha_0 y}{x^{1/3}}$. This solution is presented in Chapter 2.

2. According to this solution, the thickness of the withdrawal layer grows with distance x upstream like $x^{1/3}$ and is inversely proportional to the parameter $\alpha_0 = \left(\frac{\epsilon q}{D\nu}\right)^{1/6}$; the equation for δ is $\delta = \frac{7.14\, x^{1/3}}{\alpha_0}$.

3. Also according to this solution, the velocity field is given by $u(x,y) = \frac{\alpha_0 q}{x^{1/3}} f_0'\left(\frac{\alpha_0 y}{x^{1/3}}\right)$ where $f_0'(\zeta)$ is tabulated and shown graphically in table 2-1 and figure 2-2 respectively. For y = 0,

$$u = u_{max} = -(0.284)\frac{\alpha_0 q}{x^{1/3}} .$$

4. Twenty-five experiments were carried out where the range of variation of the parameter $q_f/D\alpha_0 x^{2/3}$ was 10^{-1} to 10^{3}. It was found that within the region of applicability of the analytical solution ($q_f/D\alpha_0 x^{2/3} < 1$ in the experiments), the experimentally determined velocity profiles agree within 10% with the analytical.

5. However, outside the range of direct applicability of the analytical solution, ($1 < q_f/D\alpha_0 x^{2/3} < 10^3$ in the experiments), experimental

observations show that the shape of the velocity profile is still the same as predicted. By varying α_0 to α by means of an experimentally determined coefficient $\chi = \alpha/\alpha_0$, these experimental results may also be made to fit the equations of the analytical solution. The coefficient χ was found to be a function of $q_f/D\alpha_0 x^{2/3}$ as given in figure 4-36.

6. For all the experiments, the local velocity profiles are similar in the sense that $u/u_{max} = f(y/y_0)$.

7. For all the experiments, using $\alpha(x) = \chi\alpha_0$, the formula for $\delta(x)$ is

$$\delta = \frac{7.14\, x^{1/3}}{\alpha(x)} .$$

APPENDIX

SUMMARY OF NOTATIONS

For simplicity, symbols of secondary importance which appear only briefly in the text are omitted from the following list.

The page numbers opposite the symbols refer to the page where the symbols first appear.

		Page
c	= concentration of solute in the stratified fluid	16
d	= depth of flow	8
D	= diffusion coefficient	16
$f_0(\zeta)$	= zeroth order non-dimensional stream function	30
$f_1(\zeta)$	= first order non-dimensional stream function	30
F	= $q/h_0^2\sqrt{ge}$ = Froude number	8
g	= gravitational acceleration	7
h_o	= depth of the flowing layer in Kao's solution	11
$h_0(\zeta)$	= zeroth order non-dimensional density function	30
$h_1(\zeta)$	= first order non-dimensional density function	30
K	= thermal diffusivity	17
$K_i(\zeta)$	= ith solution to the differential equation 2-50	34
p	= pressure	10
q	= unit discharge	1
q_f	= unit forward discharge	76
s_o	= non-constant part in hydrostatic density distribution $-$ $\rho_{hydrostatic} - \rho_o$	25
s	= density change due to motion = $\rho - \rho_o - s_o$	25

t	= time	16
T	= temperature	17
$\vec{u}$	= velocity vector	16
u	= velocity component in the x-direction	23
u_{max}	= maximum value of u for given x	76
v	= velocity component in the y-direction	23
w	= velocity component in the z-direction	121
x	= horizontal rectangular coordinate; distance from the sink	7
y	= vertical rectangular coordinate	7
y_o	= half the measured thickness of the withdrawal layer	76
$\bar{y}_o$	$= q_f / u_{max} \cdot (0.955)$ = half the thickness of the withdrawal layer, as predicted by the theory based on the measured q_f and u_{max}	78
z	= rectangular coordinate	121
α_o	$= (\epsilon g / D\nu)^{1/6}$ = dimensional stratification parameter	45
α	= experimentally determined value of α_o	110
β	$= (q_f^2 \nu \epsilon^3 / Dg)^{5/6}$	28
δ	= thickness of the withdrawal layer	22
ϵ	$= -\frac{1}{\rho_o} \frac{ds_o}{dy}$ = density gradient	8
ρ	= density of the fluid	1
ρ_o	= reference density	7
ψ	= stream function	7
φ	$= \psi / q_f$ = non-dimensional stream function	28
σ_o	$= \left(Dg / \epsilon^3 q_f^2 \nu\right)^{2/3} s_o / \rho_o$ = normalized s_o	28
σ	$= \left(Dg / \epsilon^3 q_f^2 \nu\right)^{2/3} s / \rho_o$ = normalized s	28

μ	= viscosity coefficient	21
μ_o	= reference viscosity coefficient	25
λ	$= \mathcal{D}/\nu$	32
ν	$= \mu_o/\rho_o$ = kinematic viscosity	28
$\bar{\alpha}$	$= \alpha/\alpha_o$	78
ξ	$= \frac{g}{9}\frac{\nu\epsilon^4}{}\, x$ = normalized x	28
η	$= \left[\frac{g^2\nu\epsilon^3}{\mathcal{D}g}\right]^{1/6} \epsilon y$ = normalized y	28
ζ	$= \eta/\xi^{1/3} = \alpha_o y/x^{1/3}$ = similarity variable	30
∇	= gradient	16
$\nabla\cdot$	= divergence	16
∇^2	= Laplacian	7

REFERENCES

1. Bell, H. S., "Stratified Flow in Reservoirs and its Use in Prevention of Silting," Misc. Publications No. 491, U. S. Dept. of Agriculture, Sept. 1942.

2. Harleman, D. R. F., "Stratified Flow", Chapter 26 in Handbook of Fluid Dynamics (Edited by V. L. Streeter), First Edition, McGraw-Hill, 1961.

3. Long, R. R., "Some Aspects of the Flow of Stratified Fluids II," Tellus, VI (1954), 2, pp. 97-115.

4. Long, R. R., "Some Aspects of the Flow of Stratified Fluids I," Tellus, V (1953), 1. pp. 341-357.

5. Yih, C. S., "Exact Solutions for Steady Two-dimensional Flow of a Stratified Fluid," J. Fluid Mech., 9, P. 2, (1962), pp. 161-174.

6. Yih, C. S., "On the Flow of a Stratified Fluid," Proceedings of the Third National Congress of Applied Mechanics, (1958).

7. Kao, T. W., "The Phenomenon of Blocking in Stratified Flow," Ph. D. Thesis, University of Michigan, (1963).

8. Debler, W. R., "Stratified Flow into a line Sink," Proc. Am. Soc. Civ. Engrs., J. of the Engineering Mechanics Division, Vol. 85, No. EM3, July 1959, pp. 51-65.

9. Gariel, P., "Experimental Research on the Flow of Non-homogeneous Fluids," La Houille Blanche, Jan.-Feb., 1949, pp. 56-64.

10. "Internal Density Currents Created by Withdrawal from a Stratified Reservoir," A cooperative study by the Tennessee Valley Authority and U. S. Corps of Engineers, Feb. 1962.

11. Long, R. R., "Velocity Concentrations in Stratified Fluids," Proc. Am. Soc. Civ. Engrs., J. of the Hydraulics Division, Vol. 88, No. HY 1, Jan. 1962, pp. 9-26.

12. Schlichting, H., Boundary Layer Theory, 4th. Edition, McGraw Hill Co., 1960.